Thermal transport, photoconduction and electrical switching in selected chalcogenide glasses exhibiting carrier type reversal

Thesis submitted to
COCHIN UNIVERSITY OF SCIENCE AND TECHNOLOGY
in partial fulfilment of the requirements for the award of the degree of
DOCTOR OF PHILOSOPHY

By

Rajesh R

Department of Instrumentation
Cochin University of Science and Technology
Cochin – 682 022

September 2001

CERTIFICATE

Certified that the work presented in this thesis is based on the bona fide work done by Mr. Rajesh R under my guidance in the Department of Instrumentation, Cochin University of Science and Technology, and has not been included in any other thesis submitted previously for the award of any degree.

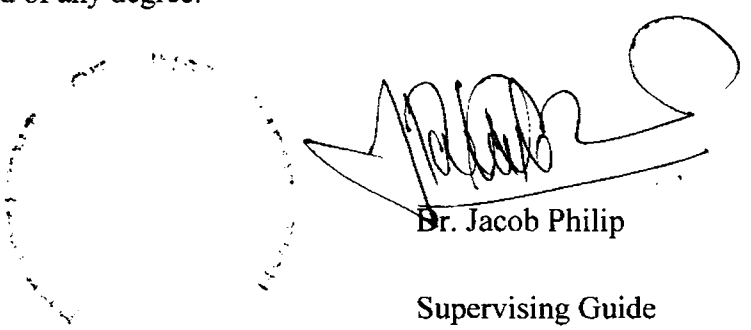

Cochin-682022 Dr. Jacob Philip

2nd September, 2001 Supervising Guide

DECLARATION

Certified that the work presented in this thesis is based on the original work done by me under the guidance of Dr. Jacob Philip, Professor, Department of Instrumentation, Cochin University of Science and Technology, and has not been included in any other thesis submitted previously for the award of any degree.

Cochin-682022 Rajesh R

2nd September, 2001

Contents

PREFACE

Non-crystalline or amorphous alloys form an important class of materials from the point of view of fundamental condensed matter research as well as technological applications. They differ from their crystalline counter parts by the absence of long-range order. Their interesting electrical, optical and magnetic properties along with the wide flexibility in preparation and composition make them unique in several applications. Like crystalline materials, non-crystalline materials can be ionic, covalent, metallic or van der Waals' bonded materials. Consequently, they can be insulating, semiconducting or metallic in nature.

Amorphous semiconductors can be generally classified into two groups as tetrahedrally coordinated semiconductors like a-Si, a-Ge etc. and chalcogenide semiconductors like Ge-Se, As-Se etc. Chalcogenide glasses contain one or more of the chalcogen elements, S, Se or Te of the sixth group of the periodic table. The four-fold coordination in Si leads to symmetrical bonding and the formation of rigid structures, while the two-fold coordination in chalcogens is highly asymmetrical and the structure gives rise to greater degree of flexibility for interatomic bonds. Like other glassy solids, these materials also possess only short-range order and because of this, the theories developed for crystalline materials cannot directly be applied to them.

Chalcogenide glasses form an important class of amorphous solids. They have very interesting physical properties and can be prepared in the bulk as well as thin film forms. One of the greatest advantages of these glasses is the composition dependent tunability of their properties, which enables one to design materials for

specific requirements. They have potential technological applications such as materials for threshold and memory switching, inorganic photoresist, xerography, IR detection and transmission etc. These materials are suitable for IR optical elements such as cell windows and prisms and as FIR beam condensers, splitters and other accessories, since they do not absorb IR radiation. Many of these glasses can be formed by the conventional melt quenching technique over a wide composition range making them suitable model systems for systematic studies on composition dependent properties.

In order to explain the features observed in the composition dependence of various properties of chalcogenide glasses, various models like random network models and topological models have been proposed. According to the chemically ordered covalent network (COCN) model, heteropolar bonding is maximized, there by favouring chemical order. Topological models use the concept of average coordination number Z and interpret the properties of chalcogenide glasses in terms of Z.

It has long been known that intrinsic chalcogenide glasses behave like p-type semiconductors and are insensitive to 'doping' in small amounts. This behaviour is attributed to the local valence saturation of the dopant atoms. Fermi level is considered to be pinned due to the equilibrium between positively and negatively charged defect states, known as valence alternation pairs (VAPs). The presence of a large number of defect states in the band gap makes them normally insensitive to impurity doping. However, of late, it has been found that the addition of heavy elemental metallic impurities like Pb or Bi to Ge-Se glasses or Pb to In-Se glasses can enter the network as charged species, alter the concentration of VAPs and

consequently change the conduction type from *p* to *n*-type at a certain composition. This discovery has led to extensive research on these materials and to a reconsideration of the existing theories of electronic structure of chalcogenide glasses. The *p* to *n*-type change over or carrier type reversal (CTR) gets reflected in electrical transport properties such as activation energy, thermoelectric power, Hall coefficient etc. We have measured the composition dependence of thermal parameters of Pb doped Ge-Se, Bi doped Ge-Se and Pb doped In-Se systems, which are reported to undergo *p* to *n* transition as Pb/Bi doping level is varied, using photopyroelectric (PPE) and photoacoustic (PA) techniques. Specifically, we have measured composition dependence of heat capacity and thermal conductivity across the transition composition. It is found that the thermal parameters show anomalous variations at compositions corresponding to the *p* to *n* transition or carrier type reversal. We have also studied the composition dependence of photoconductivity in these systems.

Electrical switching is an interesting property exhibited by certain Te based chalcogenide glasses. It is the rapid and reversible transition between a highly resistive OFF state and a conductive ON state driven by an external electric field and characterized by a threshold voltage. Depending on the material, switching can be of threshold type or memory type. In threshold type switching, the ON state persists only while the current flows, down to a certain holding voltage, whereas in memory type switching the ON state is permanent until a suitable reset pulse is applied. We have measured the variation of thermal parameters in In-Te glass system during electrical switching using PPE technique.

Ge-As-Se is a typical ternary chalcogenide glass system. It has got one of the largest glass forming regions. We have measured the thermal parameters of this system as a function of the average coordination number and studied the effect of various topological thresholds on them.

The thesis is divided into eight chapters. In the first chapter, an overall review of amorphous semiconductors is given. It includes an introduction to chalcogenide glasses, followed by a brief discussion on the important structural models proposed for chalcogenide glasses and their electrical and thermal properties. Photoconductivity, electrical switching and carrier type reversal in chalcogenide glasses are described in detail in this chapter.

Chapter 2 presents a description of the experimental techniques used in the present investigation. Brief description of the PA spectrometer is given. Photoacoustic measurement of thermal diffusivity is described. Simultaneous measurement of thermal conductivity and heat capacity employing photopyroelectric technique is also described. Details of photoconductivity and electrical switching experiments are also given in this chapter.

Pb-Ge-Se system forms homogeneous glass in two series (i) $Pb_{20}Ge_xSe_{80-x}$ (x = 17 – 24) and (ii) $Pb_yGe_{42-y}Se_{58}$ (y = 0 – 20). Both the series exhibit carrier type reversals; series I at $x \approx 21$, and series II at $y \approx 8$. We have measured the thermal parameters as a function of composition in this system. It is found that CTR gets reflected in these measurements. The results obtained are presented in chapter 3 of the thesis. The results are explained in terms of enhancement in carrier concentration during p to n transition.

Bi doped Ge-Se and Pb doped In-Se are two other systems which exhibit carrier type reversal. $Bi_xGe_{20}Se_{80-x}$ system exhibits CTR at $x \approx 7$, while $Pb_xIn_{25-x}Se_{75}$ system exhibits CTR at $x \approx 5$. We have measured the variation of thermal parameters as a function of composition in these systems, the results of which are discussed in chapter 4 of the thesis. The results are discussed in terms of the mechanism of CTR already outlined in chapter 3.

Chapter 5 deals with the photoconductivity measurements in Pb-Ge-Se and Pb-In-Se systems. It is found that the *p* to *n* transition gets reflected in these measurements. Temperature dependence of photoconductivity is also measured. The results obtained are analyzed in terms of the existing photoconductivity models, correlating them to the mechanism of *p* to *n* transition in these systems.

In chapter 6 we report the results of our electrical switching studies on In_xTe_{100-x} (x = 20-40) glass system that exhibit CTR. We have also measured the variation in thermal parameters of the samples during electrical switching.

Thermal parameters of Ge-As-Se system are reported in chapter 7 of thesis. We have measured the thermal parameters as a function of the average coordination number *Z*. The effects of various topological thresholds on thermal parameters are discussed in this chapter.

Chapter 8 is the concluding chapter incorporating overall conclusions of the work presented in earlier chapters. Further scopes for the work that can be done in this direction on other chalcogenide glass systems are also discussed.

Most of the results presented in this thesis have either been published or communicated for publication in the form of following papers/symposium proceedings.

1. Carrier type reversal in Pb-Ge-Se glasses: photopyroelectric measurement of thermal conductivity and heat capacity

   Applied Physics Letters **78** (2001) p. 745.

2. Photoconduction in Pb-Ge-Se semiconducting glasses exhibiting carrier type reversal

   Indian Journal of Pure & Applied Physics **38** (2000) 827.

3. Photopyroelectric determination of thermal parameters across p→n transition in Pb doped Ge-Se glasses

   Analytical Sciences **17** (2001) s99.

4 Thermal conductivity and heat capacity of certain chalcogenide glass systems exhibiting carrier type reversal (communicated).

5 Thermal properties across thresholds in Ge-As-Se glasses (communicated).

6 Thermal conductivity and heat capacity in In-Te glasses during electrical switching (communicated).

Symposium papers presented during the course of work

1. Photoconductivity properties around *p*→*n* transition in Pb-Ge-Se glasses

   Proc. DAE Solid State Physics Symposium, Vol.42 (1999) p.293.

2. Photopyroelectric determination of thermal parameters across *p*→*n* transition in Pb doped Ge-Se glasses

   Proc. XI International Conference on Photoacoustic and Photothermal Phenomena, Kyoto, Japan, June 25-29 (2000).

3. Carrier type reversal in Pb-In-Se glasses reflected in thermal transport measurements

   Proc. DAE Solid State Physics Symposium, Bilaspur, Dec 27-31, (2000).

4. Photoconductivity across *p* to *n* transition in Pb-In-Se semiconducting glasses

   National Seminar on Current Trends in Material Science, M. G. University, Kottayam, March 23-24 (2001).

5. Carrier type reversal in chalcogenide glasses: Some thermal facts and figures

   National Seminar on Current Trends in Material Science, M. G. University, Kottayam, March 23-24 (2001).

6. Thermal properties across thresholds in Ge-As-Se glasses

   DAE Solid State Physics Symposium, BARC, Mumbai, Dec 27-31 (2001) (communicated).

Acknowledgements

The work presented in this thesis have been carried out under the guidance and supervision of Dr. Jacob Philip, Professor, Department of Instrumentation, Cochin University of Science and Technology. I express my deep sense of gratitude for his able and inspiring guidance and constant encouragement at every stage of this work. I shall always cherish my days as a student under him.

I am grateful to Dr. Stephen Rodrigues, Head, Department of Instrumentation, Cochin University of Science and Technology and former Head, Dr. K. N. Madhusoodanan for providing necessary facilities to carry out this work. I thank all the faculty members of the Department of Instrumentation for their help and cooperation. Thanks are due to present and past Heads and faculty members of Department of Physics for extending help whenever needed.

I fondly recall all the timely help and support extended by all my lab mates and friends in the campus. Special mention to Alex Sir, Alex, Vasanth, Raghu, Vimala and Manjusha and to my seniors Dr. Gregorios Mathew, Dr. M. S. Kala, Dr. Sheenu Thomas, Dr. Johney Isaac, Dr. R. Sreekumar, Dr. A. A. Sudhakaran, Dr. Nelson Rodrigues, Dr. L. Godfrey and Dr. K. N. Nandakumar for their immense help and cooperation. Words can't express my gratitude to my dear friends, Aldrin and Alex for extending help whenever needed. All the help extended by Shaji, Sivakumar, Shibu, Manoj, Joseph, Taji, Shelly, Saji, Bindu and Deepthy are deeply acknowledged. I express deep sense of gratitude to all the research scholars of Physics and Photonics Departments for their cooperation.

I gratefully remember the help and cooperation of all the staff of our Departmental office and workshop. Thanks are due to. Mr. Murali, Mr. Gopi Menon, Mr. Sukumaran, Mr. K. V. Jose, Mr. Jose Jacob, Mr. Casimir Mr. Mohanan and Mr. Joshy for their timely help. The technical and library staffs of Physics Department also need a special mention for their help at various stages of my research.

I thank DST and Cochin University of Science and Technology for the financial support in the form of research fellowships.

I would like to thank Mrs. Radhika and Mr. V. M. Peter for their help at various stages.

I fondly recall the continuous encouragement and support given by my parents and family members throughout the course of this work. I owe my wife Preethy and our family a lot for their unstinting support and encouragement. As a true friend and partner, she has inspired and motivated me during my research life. She has provided me with the vital support without which this endeavor would not have had its successful culmination.

Finally, I convey my sincere thanks to all my well wishers and friends who have directly or indirectly helped me.

Rajesh R.

CHAPTER-1

Review of chalcogenide glasses

1.1 Introduction

A perfect crystal is a solid, in which the atoms or group of atoms are arranged in a pattern that repeats periodically in three dimensions to an infinite extent. An imperfect crystal is one, which possesses defects such as vacancies, interstitial foreign atoms or dislocations. Strictly speaking, most crystals are imperfect. On the other hand, non-crystalline or amorphous materials possess randomness or disorder in the arrangement of their atoms. Randomness or disorder can occur in several forms, of which topological (or geometrical), spin, substitutional and vibrational disorders are the most important. These types of disorders are illustrated in Fig. 1.1. Disorder is not a unique property. It must be compared with some standard, and that standard is the perfect crystal.

Topological disorder is that form of randomness in which there is no translational periodicity whatsoever (Fig. 1.1a). Certain amorphous materials have considerable short-range (or local) order, while others have little. However, both have no long-range order. So amorphous solids are therefore distinguished by their lack of periodicity and long-range translational order. This thesis deals with materials that possess topological disorder.

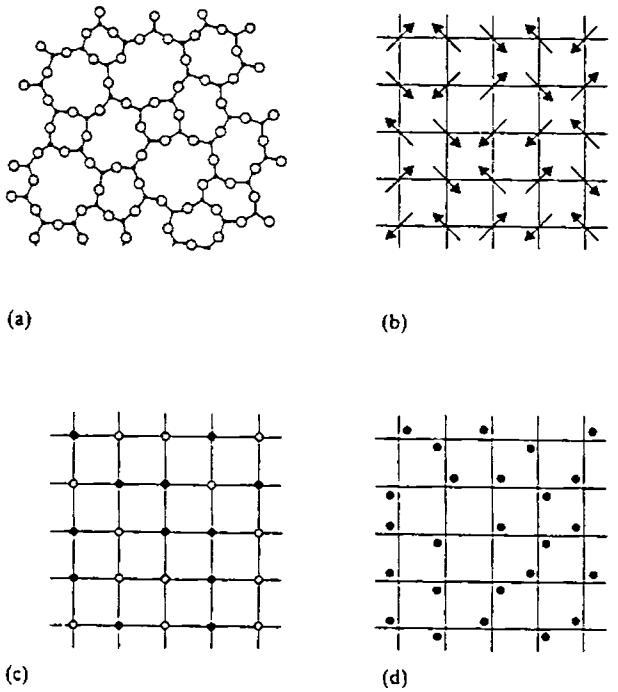

Fig. 1.1 Types of disorder

(a) topological disorder (b) spin disorder

(c) substitutional disorder (d) vibrational disorder.

Another variety of randomness is spin or magnetic disorder, in which the underlying crystalline lattice is preserved, but each atomic site possesses a spin or magnetic moment oriented randomly (Fig. 1.1b). Materials possessing randomness in spin are called spin glasses. A further kind of randomness is substitutional disorder in which, although the underlying crystalline lattice is preserved, the material is infact an alloy with one type of atom randomly substituting the other in the lattice (Fig. 1.1c). The final category of randomness is vibrational disorder of a crystalline lattice (Fig. 1.1d). The concept of a perfect crystal is only valid at absolute zero of temperature, and at any finite temperature, the random motion of atoms about their equilibrium positions destroys the perfect periodicity. However,

vibrational disorder is not another form of topological disorder, since although the atoms are vibrating, they do so about their equilibrium crystalline positions, which are not topologically disordered.

The terms amorphous and non-crystalline are synonymous and can be used interchangeably, whereas the term glass is more restricted. The definition of glass is that, it is an amorphous solid, which exhibits a glass transition, even though the term has conventionally been used for an amorphous solid prepared by quenching the melt. If the randomness in a liquid is frozen we get a solid, which is a glass. For a solid glass, the shear viscosity exceeds $10^{14.4}$ poise.

1.1.1 The glass transition

Materials that can be quenched from a melt to form an amorphous solid are represented by all the major types of bonding interactions found in solids viz., covalent, ionic, metallic, van der Waals' and hydrogen bonds. Consequently, they can be insulating, semiconducting or metallic in nature.

When a vapour is cooled, it forms a liquid and when the liquid is cooled further it solidifies. A liquid may solidify in the following two ways, (i) discontinuously to a crystalline solid or (ii) continuously to an amorphous solid. These are shown in Fig. 1.2. This figure should be read from right to left, since time runs in that direction during the course of temperature lowering. A sharp break or bend in *V(T)* marks a change of phase occurring with decrease of temperature The first occurs when the gas condenses to the liquid phase at the boiling temperature T_b. Continued cooling decreases the liquid volume in a continued fashion, the slope of the smooth *V(T)* curve defining the liquid's volume coefficient of thermal expansion. Eventually, when the temperature is bought low enough, a liquid → solid

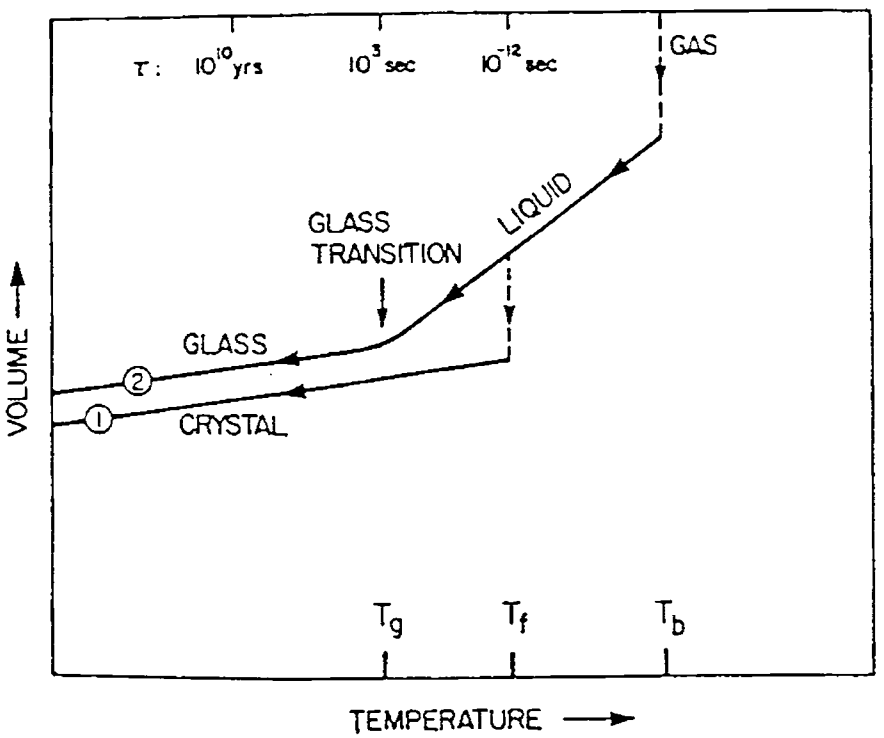

Fig. 1.2 The two general cooling paths by which an assembly of atoms can condense into the solid state. Route (1) is the path to the crystalline state. Route (2) is the rapid quench path to the amorphous solid state.

transition takes place following any one of the two ways cited above and as indicated in Fig. 1.2.

The liquid → crystal transition is marked by a discontinuity in $V(T)$, an abrupt contraction to the volume of the crystalline solid at temperature T_f. This is usually the route taken to arrive at the solid state if the quenching experiment is carried out at a sufficiently low cooling rate. But at sufficiently high cooling rates, it is found that most materials alter their behaviour and follow route (2) to the solid phase. Temperature T_f is bypassed and the liquid phase persists until a lower temperature T_g is reached. The liquid → glass transition occurs in a narrow temperature interval near T_g, the glass transition temperature. There is no volume

discontinuity as such; instead *V(T)* bends over to acquire a small slope characteristic of the low thermal expansion of a solid.

Experiments show that the observed glass transition temperature T_g depends upon the cooling rate at which the experiment is carried out. This dependence is very small in most solids. Typically, changing the cooling rate by an order of magnitude causes T_g to shift by a few degrees Kelvin. The reason that T_g shifts to lower temperatures when the cooling process is extended over longer times resides in the temperature dependence of a typical molecular relaxation time τ. The quantity $1/\tau$ characterizes the rate at which the molecular configuration (atomic scale structure) of the condensed system adapts itself to a change in temperature. This quantity varies enormously during the cooling process as indicated in Fig. 1.2. As soon as the temperature of the liquid is lowered to T_f, it may take route (1) to the solid state and crystallize. But crystallization takes time. Crystalline centres must form by nucleation and then grow by outward propagation of the crystal / liquid interfaces. With the liquid being cooled at a finite rate, the liquid may be taken below T_f along the *V(T)* trajectory, which smoothly continues the curve from higher temperatures. In the temperature interval between T_f and T_g, the liquid is referred to as supercooled liquid. If its temperature can be taken below T_g before crystallization has had time to occur, the liquid solidifies as the glass and remains in this form essentially indefinitely. Therefore, glass formation is a matter of bypassing crystallization.

The thermodynamic variables, volume, entropy and enthalpy are continuous through glass transition, but exhibit a change of slope there. This implies that at T_g, there should be a discontinuity in derivative variables such as coefficient of thermal

expansion, compressibility and heat capacity. This is indeed the case in all glasses. Even though a number of theories have been put forward to explain glass transition, it still remains a phenomenon, which is not yet completely understood.

1.2 Preparation and classification of amorphous solids

1.2.1 Preparation

The glass forming ability of solids vary considerably, but, in principle, all solids can be prepared in the amorphous state, provided the required necessary physical conditions are satisfied. Nearly all materials can, if cooled fast enough and far enough, be prepared as amorphous solids. Thus, the essential ingredient in the preparation of an amorphous solid is speed and the formation of amorphous state is a process of bypassing crystallization [1]. Usually cooling rates of 10^2-10^6 K sec^{-1} are required to freeze the disorder. For pure metals, cooling rates of 10^9 K sec^{-1} are required. Details of glass formation and related processes are discussed in many review articles [2-6].

There exists a number of ways for the preparation of materials in the amorphous state. Thermal evaporation, sputtering, chemical vapour deposition and melt quenching are the most commonly used techniques to prepare amorphous materials [7]. Amorphous thin films are usually prepared by vapour deposition or sputtering. Bulk glasses having a well-defined T_g are usually prepared by the melt quenching technique.

1.2.2 Classification

As already stated, amorphous solids are characterized by different kinds of bonding, and consequently they can be insulating, semiconducting or metallic in nature. Amorphous semiconductors can, in general, be divided into two groups as tetrahedrally coordinated silicon type materials and two-fold coordinated chalcogenide glasses [8]. Chalcogenide glasses contain one or more of the chalcogen elements, sulphur, selenium or tellurium of the sixth group of the periodic table. The distinction between these two classes can be well accounted for on the basis of chemical considerations. The four-fold coordination in Si leads to symmetrical bonding and the formation of rigid structures. In this case a continuous random network with tetrahedral bonds can be constructed with negligible density deficit and very little possibility for local reorganization of atoms. On the other hand, the two-fold coordination in chalcogens is highly asymmetrical and the structure gives rise to greater degree of flexibility. A major distinction comes from the fact that, in chalcogens, but not in Si, the valence band is formed from non-bonding lone pair p electrons and is very important when we consider the defect chemistry and various properties of chalcogenide glasses that differentiate it from Si type materials.

Out of these two classes of materials, chalcogenide glasses can be prepared in the bulk, as well as thin film forms, but a direct comparison of the properties of thin film and bulk glasses may not be possible. However, Si type materials cannot often be prepared in the bulk form by the melt quenching technique. These materials are usually prepared in the thin film form. The reason why certain materials can be prepared in the thin film as well as bulk forms, while others can only be prepared in the thin film form can be explained by the nature of chemical bonds present in these

materials. This difference has its origin in the mismatch between constraints and the number of degrees of freedom in three dimensions and the flexibility required to accommodate the mismatch. The flexibility of covalent bond angles is largest for the two-fold coordinated Se type materials and least for the tetrahedrally coordinated Si type materials. The reason for this is the greater variety of admixture from other atomic orbitals to the covalent bond when the coordination number is less than the number of valence electrons. Therefore, based on chemical considerations and the average coordination number Z, a classification of amorphous solids can be made as shown in Fig. 1.3. According to this, glasses are restricted to $3 \geq Z \geq 2$, and materials with higher connectivity, i.e., $4 \geq Z \geq 3$ are over constrained amorphous, while those with $Z < 2$ are under constrained amorphous. The average coordination number $Z = 4$ separates non-crystalline metals from semiconductors or insulators.

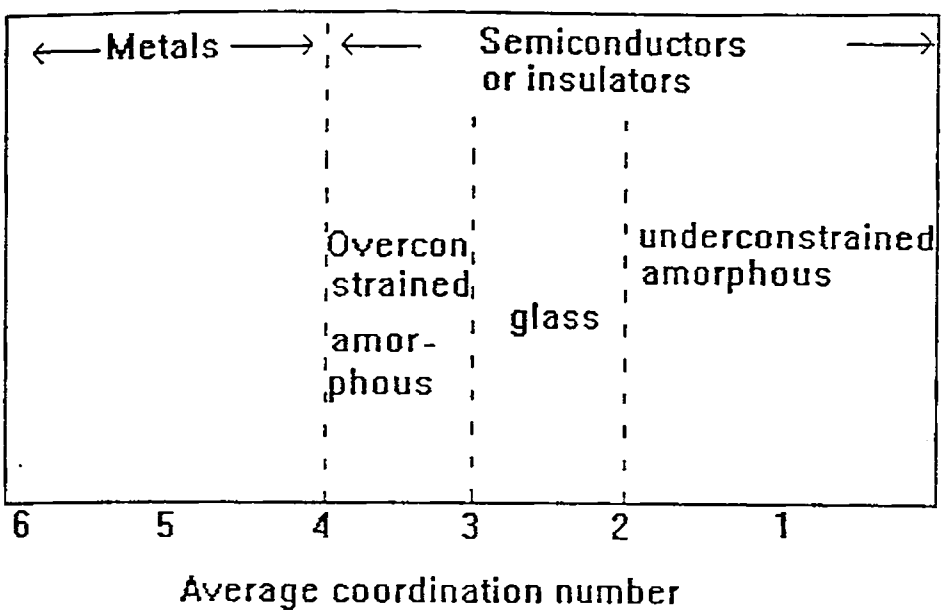

Fig. 1.3 Classification of non-crystalline solids based on the average coordination number.

1.3 Structural properties

Even though amorphous materials lack long-range periodicity of constituent atoms, the disorder is not complete on the atomic scale [9]. Short-range order similar to that present in crystalline materials is also present in these disordered materials. In chalcogenide glasses, the covalently bonded atoms are arranged in an open network with order extending up to 3^{rd} or 4^{th} nearest neighbours and they are also referred to as network glasses [10]. The semiconducting nature of chalcogenide glasses is however, a direct consequence of the covalent bonding that exists in these materials.

The structure of an amorphous solid can never be determined unambiguously. The absence of periodicity in a glass makes the unit cell concept invalid or one can consider unit cell is infinite which implies that the coordinate of each and every atom should be known. The uncertainty in the structure of an amorphous solid is compounded by the fact that the structure of a non-crystalline material, at both microscopic and macroscopic levels, often depends on the details of method of preparation. Furthermore, in general, more than one experimental structural probe must be used to obtain as complete a picture as possible of the structural arrangement in an amorphous solid. The best information one can get from the diffraction methods for a glass is the radial distribution function (RDF), which expresses the probability of finding another atom at a given distance from an arbitrary point.

In both amorphous and crystalline materials, the chemical forces holding the atoms together are the same. Therefore the amorphous state is always defined with reference to a crystalline state [7, 11]. From a comparison of radial distribution functions of amorphous and crystalline films of silicon, it has been revealed that

covalent glasses exhibit some ordering in their atomic structure. The structural ordering in covalent glasses can be classified into two types depending on their length scale [12, 13]. They are of short-range order in the range 2-5 Å and of medium-range order in the range 5-20 Å.

Since there is no unique structure for an amorphous material, structural modeling is very useful in determining the structure of amorphous solids. The structure of amorphous semicondonductors is developed by the repetition of one or more basic molecular units in a way that cannot be identified topologically with any known crystalline structure or with any periodic array. The atomic order within a molecular unit might be similar within small bond angle distortions in both crystalline and amorphous phases. This reveals the importance of short-range order in describing the structural behaviour of a non-periodic network. The most important aspects of the short-range order are the number and type of immediate neighbours, and their spatial arrangement about a given reference atom. Given the short-range order, with three parameters viz., the number of bonds, the bond length and the bond angle having well defined values in a narrow range, it is possible to construct a model for the amorphous structure. Such models are known as random network models. The continuous random network (CRN) model, the first model of an ideal glass proposed by Zachariasen [14] is the basis for all structural models. A number of structural models have been proposed to explain the various structure related properties of amorphous materials.

1.4 Structural models of amorphous solids

1.4.1. Network models

Covalent random network (CRN) model proposed by Zachariasen is more applicable for covalent glasses. He imposed some rules to be followed while building the model, based on the local similarity between crystalline and amorphous materials. A definite short-range order is imposed as each atom fulfills its chemical valence requirements according to Mott's (8-*n*) rule [15], where *n* is the number of valence electrons of the particular atom. The underlying principle of this model is that a closed outer shell of eight electrons is the most stable structure. Small variations introduced in bond lengths and bond angles lead to disorder in the glassy matrix. The variation in bond length is much less and they are within 1 % to those found in crystals. The major source of randomness comes from the variation in bond angles. The flexibility of covalent bond angles is largest for the two-fold coordinated chalcogens and least for tetrahedrally coordinated group IV elements. CRN model generates amorphous structure without taking into account structural defects such as dangling bonds and voids and it is not adequate to account for features observed in medium-range order.

The structure of chalcogenide glasses can be more appropriately described by the random covalent network (RCN) model or chemically ordered covalent network (COCN) model [16, 9].

Chalcogenide glasses can be prepared over a wide range of compositions. This means that glasses with non-stoichiometric compositions can also be prepared which will contain bonds between like atoms. It is essential to estimate the fraction

of different kinds of bonds present in a system, as it determines a number of physical properties. RCN and COCN models differ in their approach to the distribution of bonds.

Consider a simple binary system $A_x B_{1-x}$ where A and B atoms belong to say column 'a' and 'b' of the periodic table respectively and x is the normalized concentration variable. We have to estimate the fractions of A-A, B-B and A-B bonds present. RCN model estimates these fractions purely statistically, i.e., different types of bonds are considered to be equally probable and neglects the relative bond energies. The bond distribution is determined by the local coordinations of A and B and their concentration x. So A-A, B-B and A-B bonds are equally preferred at all compositions except at $x = 0$ and $x = 1$. On the other hand, in COCN model, bond energies are also taken into account. Thermodynamically, A-B bonds are preferred over A-A and B-B bonds. So at all compositions, A-B bonds are maximized first and then A-A and B-B bonds are favoured depending on the concentrations of A and B. So according to COCN model, there exists a critical composition defined by $x_c = \frac{Z_B}{Z_A + Z_B}$ where Z_A and Z_B are the coordinations of A and B atoms respectively. For example, in Ge_xSe_{1-x} system, the critical composition is $GeSe_2$, while in As_xSe_{1-x} system, the critical composition is As_2Se_3. At these compositions, anomalous variations are reported in many physical properties. The bond statistics obtained on the basis of RCN and COCN models for V-VI and IV-VI alloys are shown in Fig. 1.4.

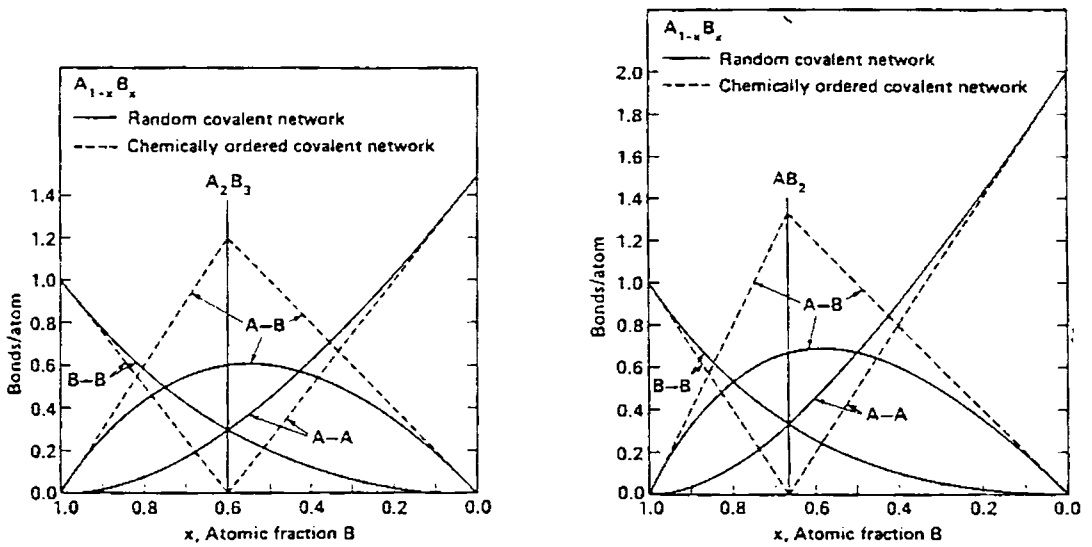

Fig. 1.4 Bond-counting statistics for (a) 3-2 network alloy (b) 4-2 network alloy.

1.4.2 Mechanical Threshold model

The models proposed by Phillips and Thorpe [17-20] and Tanaka [21] interpret the dynamical properties of chalcogenide glasses, in terms of the average coordination number Z. Phillips constraint model, also called mechanical threshold model, examines the constraints governing the random network structure of chalcogenide glasses which are covalently bonded. This model attempts to relate the glass forming tendency with the constraints acting on the network. The glass sructure is maximally optimized when the number of degrees of freedom (N_d) available for the atoms equals the number of constraints (N_c) in the network

i.e., $$N_c = N_d \qquad (1.1)$$

The total number of constraints acting on the system is the sum of bond stretching constraints and bond bending constraints. Consider a glassy network with N atoms of which N_Z atoms have Z bonds per atom. Then the total number of constraints acting on the system can be written as,

$$N_C = \left(\frac{Z}{2}\right) + (2Z - 3) \tag{1.2}$$

Here the first term $\left(\frac{Z}{2}\right)$ denotes the bond stretching constraints since a bond is shared between two atoms. The term $(2Z-3)$ represents the bond bending constraints. Two bonds with the central atom will have one bond angle constraint. For each of the remaining $(Z-2)$ bonds, two bond angles (one each with the two existing bonds) have to be specified. N_d can be 1, 2 or 3 for 1-dimensional, 2-dimensional or 3-dimensional space respectively. Phillips considered $N_d = 3$ for the cross-linked network structures. Now,

$$3 = \left(\frac{Z}{2}\right) + (2Z - 3) \tag{1.3}$$

This gives $Z = 2.41$. This is the critical average coordination number at which a floppy to rigid structural transition occurs. If $N_c > 3$, the structure is over constrained while if $N_c < 3$, the network is under constrained.

The transition from an under constrained to an over constrained network has been interpreted by Thorpe [19, 20] as the percolation of rigidity in an inhomogeneous medium containing both rigid and floppy regions. According to him, there are glassy regions (or islands), which are rigid and spread out in a soft or floppy region. This is shown in Fig. 1.5(a). As the average coordination number is increased, these regions grow in size and become interconnected. In other words, the

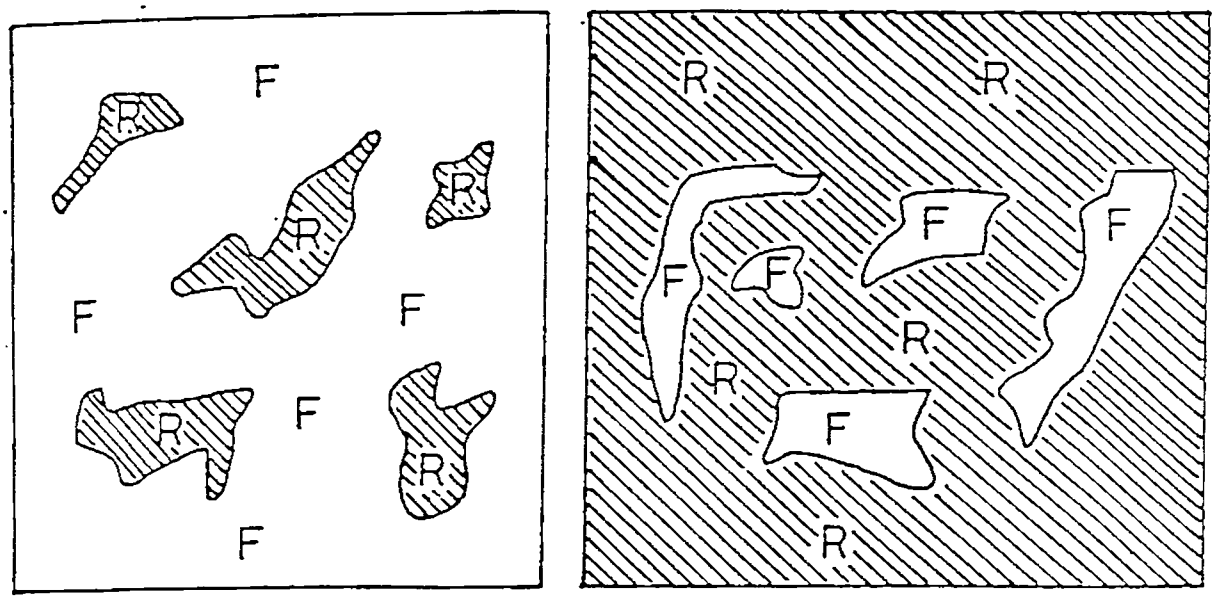

(a) (b)

Fig. 1.5 Rigid and floppy regions in the network of (a) polymeric glass and (b) amorphous solid.

rigid regions start percolating and at Z = 2.4, the system transforms into a mechanically rigid amorphous solid (Fig. 1.5(b)). The point at which this threshold occurs is termed mechanical or rigidity percolation threshold.

Tanaka modified the concept of Phillips and Thorpe, by arguing that medium-range order should also be considered in the constraints balancing conditions as evidenced by characteristic features in the composition dependence of certain physical properties at $Z = 2.67$ [21]. He assumed a hypothetical material

having a plane lattice laid in a 3-dimensional space. As per this modification, the bond bending term $(2Z-3)$ in Eq. (1.2) reduces to $(Z-1)$. Now Eq. (1.2) becomes.

$$N_C = \left(\frac{Z}{2}\right) + (Z-1) \qquad (1.4)$$

This gives Z = 2.67, i.e., the coordination number of glasses having stable layer structure becomes 2.67. This means a 2-dimensional glass possessing a layered structure appears to be stably fixed in a 3-dimensional space if the coordination number of the glassy network is 2.67.

The experimental reports on a wide range of physical properties of various binary glasses indicate the threshold behaviour at Z = 2.4 [22-32]. Some results have been reported, indicating a shift in Z value at which the threshold occurs. Photodarkening, molar volume, X-ray diffraction, elastic constants, optical band gap values etc. of ternary glasses show a threshold behaviour around Z = 2.67 [33-36].

1.5 Band Models

In a crystalline solid, the discrete energy levels of the atoms are broadened into bands of allowed energy levels, separated by forbidden energy regions. At very low temperatures, electrons will occupy the lowest possible energy levels and will exactly fill a certain number of bands. The highest of these occupied bands is known as the valence band and the empty band immediately above this is known as the conduction band. The separation between the top of the valence band and the bottom of the conduction band is called the energy gap (E_g). Experimental investigations reveal that many of the fundamental properties such as optical absorption spectra, Arrhenius nature of electrical conductivity etc. of amorphous semiconductors and

their crystalline counterparts look similar. The existence of different classes of materials (metallic, semiconducting and insulating) indicates that electronic structure of these materials should also possess energy gap similar to that of crystalline materials. This shows that these physical properties are largely associated with the short-range order rather than the translational periodicity. To account for these features, various models have been proposed.

According to Anderson's theory [37], the spatial fluctuations in the potential caused by the configurational disorder in amorphous materials, lead to the formation of localized tail states above and below the normal bands. These stats are localized in the sense that an electron in these regions will not diffuse away at zero temperature to other regions. Since localized and extended states cannot coexist at the same energy, a sharp boundary called 'mobility edge' separates the extended and localized states. All these models of the band structure of amorphous semiconductors use the concept of localized states in band tails and mobility edges.

The models tried to explain the features that are common to most of the glasses like the insensitivity of electrical conductivity to the added impurities, pinning of the Fermi level near the midgap etc.

1.5.1 Cohen-Fritzsche-Ovshinsky (CFO) model

This model [38] assumes that extensive tailing of the band edges occurs due to the compositional and topological disorders. The extensive tailing makes the conduction and valence band tails to overlap in the midgap, leaving an appreciable density of states (Fig 1.6a). As a consequence, there are filled states in the valence band that have higher energies than the unfilled states in the conduction band. A redistribution of charges takes place, forming negatively charged filled states in the conduction

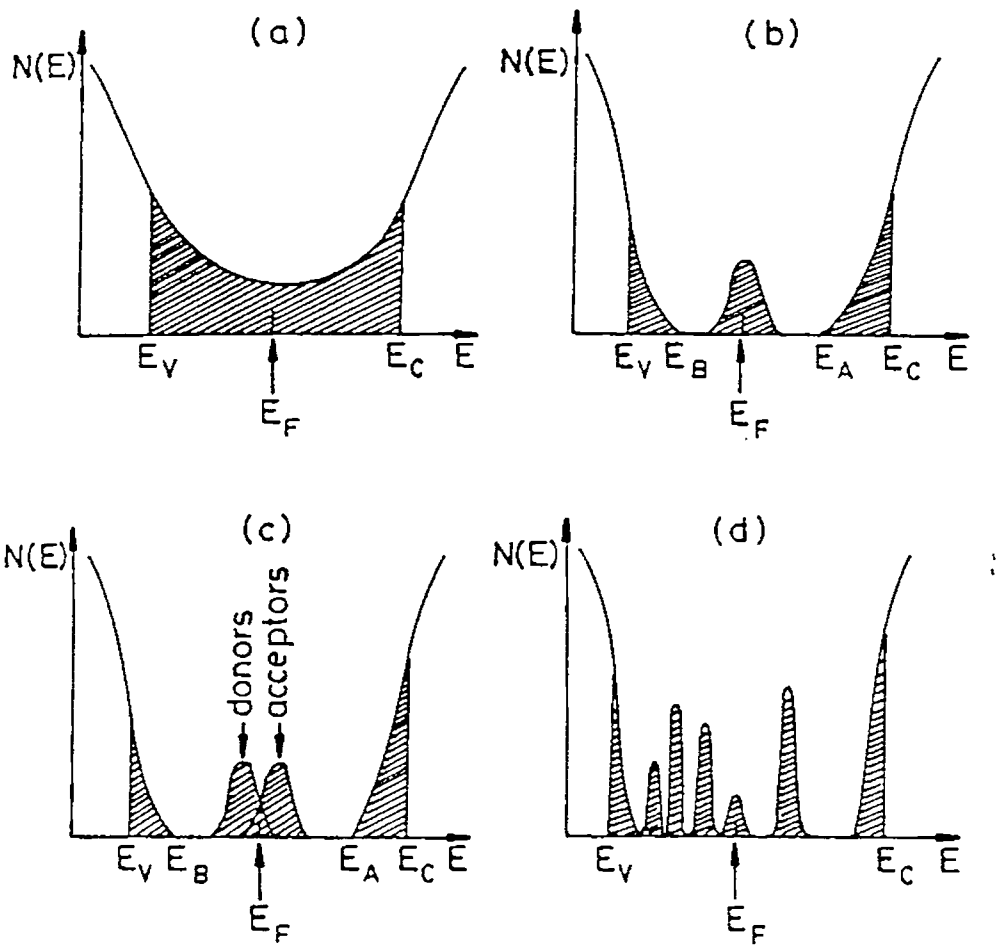

Fig. 1.6 Schematic density of states for amorphous semiconductors (a) CFO model (b) Davis-Mott model showing a band of compensated levels near the middle of the gap (c) modified Davis-Mott model (d) the 'real' glass with defect states.

band and positively charged empty states in the valence band. This ensures self-compensation and pinning of Fermi level near the mid gap as required by the experimental observations [39, 40]. The tail states will be localized due to disorder and are separated from extended states in the band at critical energies called the mobility edges, marked by E_c and E_v.

This model has certain drawbacks. According to this model, the elemental semiconductors like a-Si, a-Ge etc. should not have the extensive band tailing as they are free from compositional disorder [41]. The high transparency of amorphous chalcogenides below a well-defined absorption edge indicates that, the extent of tailing is only a few tenths of an eV into the gap [42].

1.5.2 Davis and Mott (DM) model

According to this model [41-43], the tails of the localized states should be narrow and extend a few tenths of an eV into the gap as shown Fig. 1.6b. A band of compensated levels exist near the middle of the gap originating from the defects in the random network like dangling bonds, vacancies etc. The gap states act as deep donors and acceptors with single and double occupancy conditions leading to two bands separated by an appropriate correlation energy. As a consequence of this, the Fermi level is pinned between the bands, which is an essential requirement. In the Figure, E_v and E_b represent the energies that separate the ranges where the states are localized and extended.

Transition from extended to localized states drops the mobility by several orders of magnitude producing a mobility edge. The interval between E_C and E_A act as a pseudo gap and is called the mobility gap. The model explains three processes, which deal with electrical conduction in amorphous semiconductors.

According to CFO and DM models, a large number of densities of unpaired electrons should exist. However, in chalcogenide glasses, no electron spin resonance has been observed [46, 47]. Also, there is no Curie paramagnetism [48, 50].

1.6 Properties of amorphous semiconductors

1.6.1 Electrical properties

The d.c. conductivity of amorphous semiconductors can be well understood within the framework of Davis-Mott model. The model predicts three regions of conductivity, (i) conduction in extended states, (ii) conduction in band tails and (iii) conduction in localized states at Fermi energy E_F.

Conductivity in extended states is characterized by large mobility that decreases sharply at the mobility edge. Assuming a constant density of states and constant mobility, the conductivity is shown to vary as

$$\sigma = \sigma_o \exp\left[-\left(\frac{E_C - E_F}{kT}\right)\right] \tag{1.5}$$

where the pre exponential factor σ_0 is given by

$$\sigma_o = eN(E_C)kT\mu_C \tag{1.6}$$

Here $N(E_c)$ is the density of states at the mobility edge E_c, and μ_c is the mobility. Electrons at and above E_c can move freely, while electrons below it can move through activated hopping [51]. Mobility in this region is of the order 10 $cm^2 V^{-1} S^{-1}$.

Conduction via band tails takes place by exchange of energy with a phonon. If the current is carried mainly by holes and conduction is by hopping, then conductivity

$$\sigma = \sigma_1 \exp\left\{\left(-E_F - E_B + \Delta W_1\right)/kT\right\} \tag{1.7}$$

where ΔW_1 is the activation energy for hopping and E_B is the energy at the band edge. σ_1 is expected to be less than σ_o by a factor of 10^2 to 10^4.

In the third region (conduction in localized states), carriers move between states located at E_F via phonon assisted tunneling process, which is analogous to impurity conduction observed in heavily doped and highly compensated semiconductors at low temperatures. Conductivity in this region is given by

$$\sigma_1 = \sigma_2 exp\left\{\frac{-\Delta W_2}{kT}\right\} \tag{1.8}$$

where $\sigma_2 < \sigma_1$ and ΔW_2 is the hopping energy of the order of half the width of the defect band shown in Fig. 1.7. As temperature is lowered, and the carries tunnel to more distant cites, conductivity behaves as,

$$ln\sigma = A - \frac{B}{T^{1/4}} \tag{1.9}$$

This variable range hopping at low temperatures is one of the interesting properties of amorphous semiconductors. As one goes from extended to localized states, mobility decreases by a factor of 10^3. This drop in mobility is called the mobility shoulder.

The three mechanisms for charge transport that contribute to d.c current can also contribute to a.c conductivity. The first is due to carriers excited to extended states near E_c or E_v. Conductivity could be given by a formula of Drude type,

$$\sigma(\omega) = \frac{\sigma(o)}{1+\omega^2\tau^2} \tag{1.10}$$

where τ is the relaxation time. The second is due to transport by carriers excited to localized states at the edges of the valence or conduction bands. Since transport here is by hopping, conductivity increases with frequency as $\omega^{0.8}$. The third is transport by carriers with energies near the Fermi level. This again increases with frequency in the same manner as in the second case.

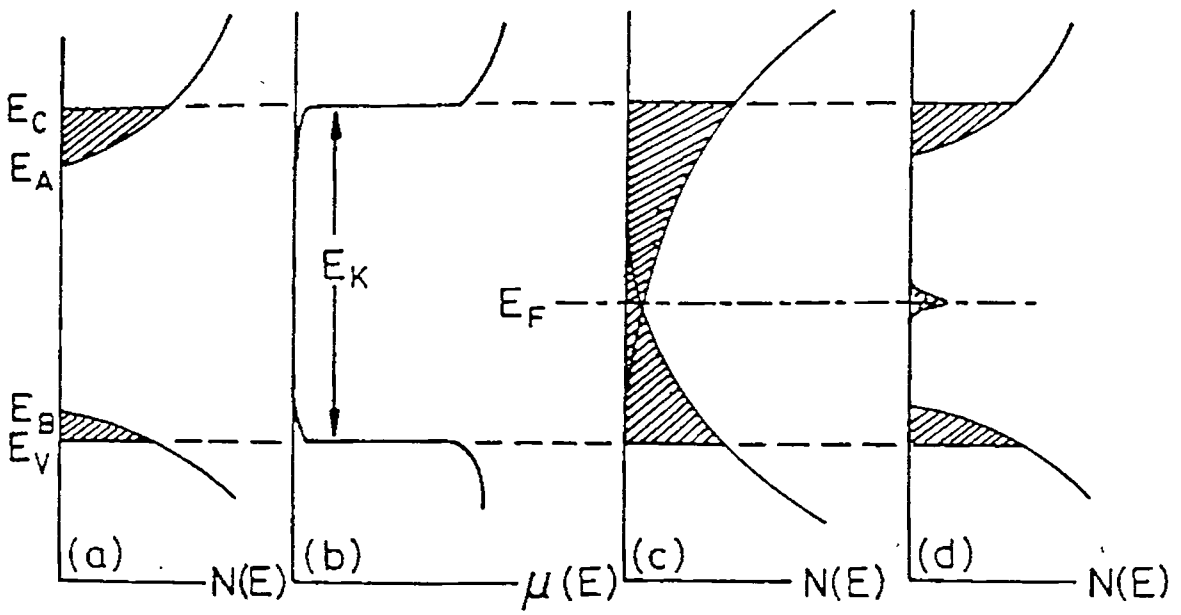

Fig. 1.7 Density of states and mobility as a function of energy in amorphous semiconductors.

Measurement of thermoelectric power as a function of temperature provides the most direct way of determining the temperature coefficient of activation energy for conduction. Measurement of thermoelectric power in chalcogenide glasses have shown the to be *p*-type in most cases. Hall measurements are used to determine the mobility of carriers. Hall coefficient yields a sign for carriers that is frequently in contradiction with thermoelectric power measurements, which are explained by the theory of Friedman [51].

1.6.2 Thermal properties

For amorphous materials, the phonon mean free path is shorter than that in crystals and correspondingly, thermal conductivity is low. At low temperatures, amorphous

materials exhibit a markedly different behaviour from their crystalline counterparts in phonon related properties such as heat capacity, thermal conductivity and acoustic absorption. The thermal properties of crystalline solids at low temperatures are well understood in terms of Debye's theory in which it is assumed that the distribution of phonons is cut off at some frequency to which a characteristic temperature Θ_D may be associated. The specific heat of glass decreases much more slowly with temperature than the Debye T^3 prediction at low temperatures (0K < T < 1K) [52, 53]. Thermal conductivity decreases slowly and monotonically with decreasing temperature [54, 55]. Near 10 K, thermal conductivity is only weakly temperature dependent, showing a plateau like region. Below 10 K, it shows a T^2 dependence. The magnitude of the temperature dependence appears to depend on the amorphous structure of the material, rather than the chemical composition. Hence, the thermal transport below 10 K is provided by phonons. Acoustic and dielectric absorption in amorphous solids is strongly enhanced at low temperatures and in many glasses large absorption peak is found around liquid nitrogen temperature. The anomalous features observed in specific heat, thermal conductivity, acoustic and dielectric absorption below 4 K etc. are interpreted using the two level system (TLS) model proposed by Phillips [56] and Anderson *et al.* [57]. At high temperatures, atoms forming the TLS change the configuration by means of thermally activated hopping over barriers while at low temperatures, tunneling through the barrier dominates.

The process of glass transition is another aspect that has been receiving continuous attention all the time. Glass transitions are always characterized by a phenomenological value T_g of the critical temperature and by a width ΔT_g of the so called glass transition around T_g. In this region, the diffusive motion of the melt

begins to freeze in before a glass structure is achieved, with viscosity values typical of solids. Both T_g and ΔT_g depend smoothly on cooling rate [51]. $\Delta T_g/T_g$ provides a rough estimate of the non-equilibrium effects occurring at glass transition; $\Delta T_g/T_g << 1$ is a necessary condition for any thermodynamic approach. For good glass formers this condition is fulfilled at relatively low cooling rates.

Non-isothermal heating studies such as differential scanning calorimetry (DSC) could provide great deal of information about thermal properties of glasses like kinetics of crystallization and thermal stability of glasses against crystallization, apart from being an indispensable characterization tool to investigate glass transition.

1.6.3 Optical properties

The sharp structure observed in the fundamental optical spectra of crystals, both vibration and electronic, can be interpreted by symmetry arguments based explicitly on the existence of long-range order. In the case of amorphous materials, no sharp features are present even at low temperatures. They lack any special directions associated with crystallographic axes and are optically isotropic. The spectral fine structure is a consequence of band structure of **k** conservation in the crystalline state. Translational periodicity demands that only **k** conserving transitions contribute to reflectivity spectra. Amorphous solids do not possess the long-range order and so do not show this fine structure in their comparatively blank spectra. Also the vibrational modes are no longer plane waves unlike in the case of crystalline solids in which they are plane waves. Though **k** is not a valid concept in glasses, the concept of vibrational density of states retains its validity.

Optical absorption in amorphous semiconductors can be separated into three regions, with absorption coefficient $\beta \geq 10^4$ cm^{-1}, 1cm^{-1} $< \beta <$ 10^4 cm^{-1} and $\beta \leq 1$ cm^{-1} as show in Fig. 1.8. Regions B and C are created by transitions within the fully coordinated system, perturbed to some extent by defects, while region A arises from transitions involving the defect states directly. The absorption edge has a defect induced tail at lower energies, an exponential region at intermediate energies and a power law region at higher energies. The defects occur in a number of ways like voids arising from preparation techniques, occurrence of like bonds, or occasional occurrence of coordination variation. In the high absorption region, the absorption is governed by a power law of the type

$$\beta = const.(h\upsilon - E_g)^{\rho} \qquad (1.11)$$

where ρ = 2 for amorphous semiconductors, under the assumption of parabolic bands and E_g defines the optical band gap. Amorphous semiconductors continue to absorb strongly beyond the fundamental absorption edge also. All pairs of extended states with energy difference hν can contribute to optical absorption, since the **k** conservation rule is relaxed. A plot of $\beta^{1/2}$ vs hν yields a straight line and the extrapolated hν at which $\beta^{1/2}$ tends to zero gives the value of E_g.

The exponential tail in β is associated with the intrinsic disorder in amorphous semiconductors in the intermediate range of absorption coefficient. It has been suggested that it is due to disorder induced potential fluctuations [58, 59] and strong electron-phonon interaction [60]. In chalcogenide glasses, defects due to coordination variation explain many of the optical properties. In the weak absorption region, the shape of the absorption tail is found to depend on the preparation, purity and thermal behaviour of the material [52]. The mobility gap in many amorphous

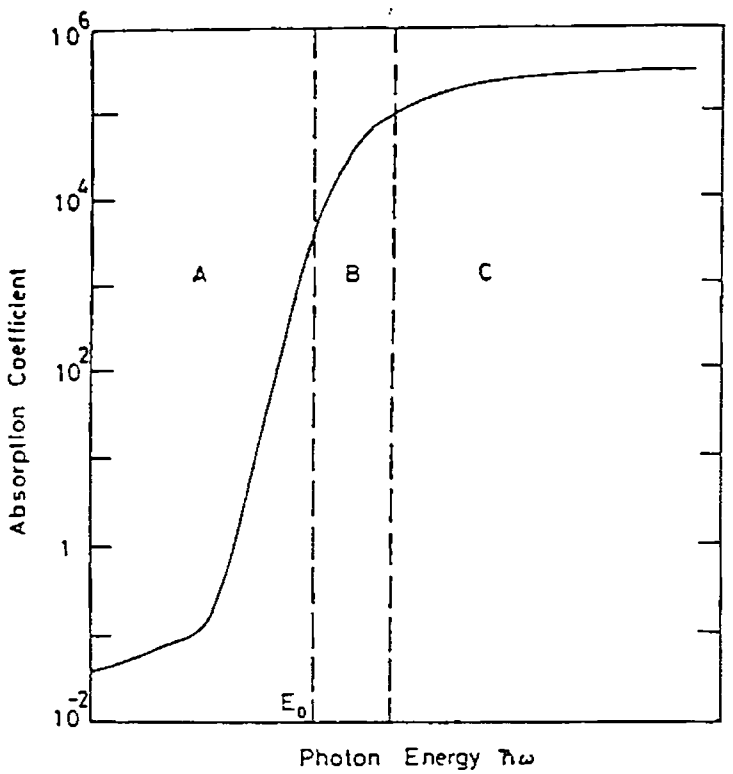

Fig. 1.8 Schematic representation of the absorption spectrum of amorphous semiconductors showing three different regions A, B and C.

semiconductors corresponds to a photon energy at which the optical absorption coefficient has a value approximately 10^4 cm^{-1}. Here the assumption is that the mobility gap is twice the activation energy for electrical conduction. From the measurements made using UV diffraction grating reflectometer, the optical constants can be derived from Kramers-Kronig analysis of reflectivity.

1.7 Photoconductivity in chalcogenide glasses

Photoconductivity is the enhancement in dark electrical conductivity of a material due to the absorption of electromagnetic radiation, especially in the visible region. This phenomenon was first observed by Willoughb Smith in 1873 with a selenium resistor. Thereafter, extensive research had been carried out on different materials to understand this phenomenon and use it for various applications. Different models were suggested to account for the characteristics of photoconductivity in materials [61-64]. In the dark under conditions of thermal equilibrium, the thermally generated carriers are distributed among the available energy states in accordance with Fermi-Dirac statistics. These electrons and holes occupying the conduction band determine the dark electrical conductivity of the material. When the sample is illuminated, a steady state is reached, in which the rate of photogeneration is balanced by the various recombination processes, through which the carriers tend to relax to the normal equilibrium distribution. Thus, the phenomenon of photoconductivity involves absorption, photogeneration, recombination and transport processes and an intimate relationship exists between them.

Amorphous solids have a disordered structure, and the disorder has profound effect on their photoelectronic properties. There are large densities of state within the band gap due to translational and compositional disorders. Due to this, the carrier lifetime and photosensitivity are greatly reduced. Also, carrier mobilities in amorphous solids are typically much smaller than those in crystalline state, reflecting reduced mean free paths.

In the discussion of photoconductivity, generally two simplifying assumptions are made,

(i) Conductivity is dominated by one of the carriers so that the contribution of the other can be neglected

(ii) The system remains electrically neutral during photoconduction process without a build up of appreciable space charge so that $\Delta n = \Delta p$. The excess conductivity due to the light absorption is given by,

$$\Delta\sigma = \Delta n \mu_n + \Delta p \mu_p \qquad (1.12)$$

where μ represents the mobility of corresponding carriers. The increase in conductivity is due to the increase in the densities of positively and negatively charged carriers compared to their values at thermal equilibrium. At low temperatures, the values of Δn and Δp may be considerably higher than the corresponding equilibrium densities n_o and p_o. Under steady state conditions, the excess densities are equal to the product of their generation rate g and lifetime τ. Generation rate is the number of carriers generated per unit time in unit volume. It is governed by the quantum yield η, which is the number of electron-hole pairs generated by the absorption of a photon.

The non-equilibrium charge carriers exist until they disappear by recombination of a free electron by a centre in which a hole is localized and capture of a hole by a centre in which there is a bound electron. In steady state, the rates of generation and recombination of carriers are equal. Since the band structure of a real amorphous semiconductor exhibits discrete energy levels associated with defect states, analysis of experimental data becomes complex. A variety of models have been proposed to explain different experimental findings satisfactorily [65-68]. Of these, the most important one is the ABFH model [69-72], outlined below.

1.7.1 The ABFH model for photoconductivity

Based on their photoconductivity behaviour, amorphous chalcogenides can be broadly divided into two groups namely, Type I and Type II. Type I photoconductivity has the following characteristics. (i) Photoconductivity shows a maximum at a temperatue T_m, and it has defined activation energies above (E^+) and below (E^-) the maximum. (ii) It shows a linear variation with light intensity and an exponential increase with $1/T$ at temperatures above T_m. (iii) It has a square root variation with light intensity at high intensities, a linear variation at low intensities and an exponential decrease with $1/T$ at low temperatures. (iv) Dark conductivity more than photoconductivity for $T > T_m$ and less for $T < T_m$. In the case of Type II photoconductors, the photoconductivity maximum is absent. Photoconductivity increases slowly and monotonically with increasing temperature, and in general, photoconductivity is much less than dark conductivity. Also, there are materials, which show an intermediate behaviour between Type I and Type II.

Although a number of models exist that try to describe this behaviour [65-68], the model proposed by Arnoldussen, Bube, Fagen and Holmberg [70-72], known as the ABFH model could describe this phenomenon adequately. The ABFH model incorporates the standard carrier recombination statistics applicable to semiconductors and a generalized distribution of localized states within the mobility gap of amorphous semiconductors. In addition to the traditional non-localized to localized state recombination transitions, localized to localized state recombination transitions are also included in this model, in order to establish consistency with experimental observations.

The basic energy parameter and transition processes are shown in Fig. 1.9. Here the localized states extend into the gap from the conduction and valence edges. With increasing energy above the valence edge, the density of effective recombination centres decreases sharply as the energy exceeds E_v^* for valence states and increases sharply as the energy exceeds E_c^* for conduction states.

Different types of possible electronic recombination transitions are shown in Fig. 1.9b. Transitions 1 correspond to electron (hole) capture by a positively charged valence state below E_v^* (negatively charged conduction state above E_c^*) with rate coefficient $C^+(C^-)$. Transitions 4 are similarly defined as capture of mobile electrons (holes) by a neutral conduction state above E_c^* (neutral valence state below E_v^*) with rate coefficient C^0.Transitions 2 correspond to recombination between electrons localized in conduction states above E_c^* and holes localized in valence states above E_v^*, with rate coefficient K. Transitions 3 represent recombination between an electron (hole) localized in a conduction state (valence state) above E_c^* (below E_v^*) and holes (electrons) localized at energies near the equilibrium Fermi level with rate coefficient K' (K''). In this model, it is assumed that for Type I photoconductors, transitions 1 or 2 dominate in the high temperature range. In the intermediate temperature range, transitions 2 dominate at high intensities and transitions 3 at low intensities and in the low temperature region, transitions 4 dominate. On the other hand, Type II photoconductivity can, in principle, be described under the assumption that transitions 3 dominate the photoconductivity over the whole measurable range without transforming to a transition 2 dominant region.

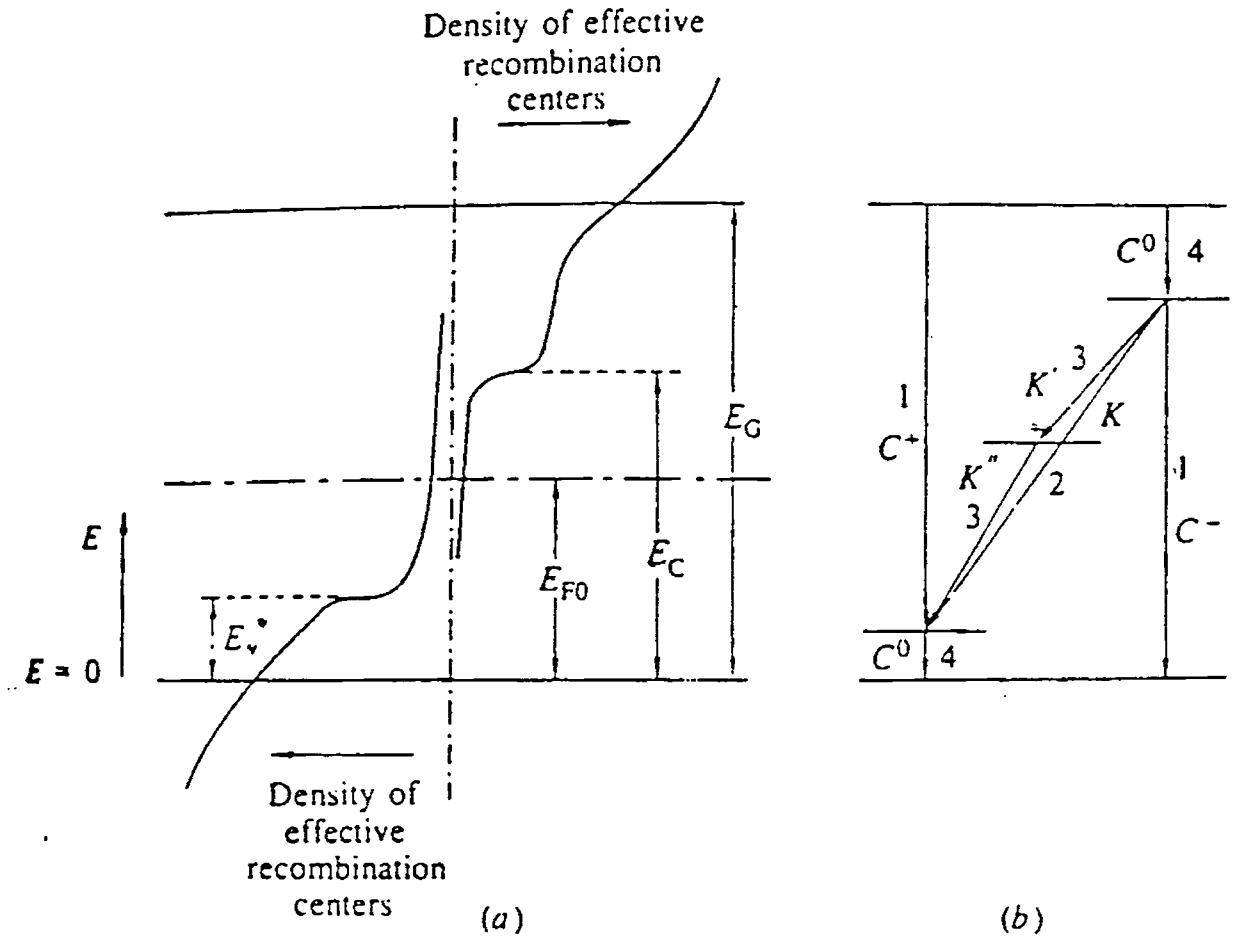

Fig. 1.9 Simple photoconductivity model for Type I photoconductivity in chalcogenide amorphous semiconductors, (a) schematic energy level diagram for the model (b) typical recombination transitions considered in the photoconductivity model.

.1.8 Electrical switching in chalcogenide glasses

Electrical switching is a very interesting phenomenon exhibited by certain chalcogenide glasses. It is the rapid and reversible transition between a highly resistive OFF state and a conducting ON state driven by an external electric field

and characterized by a threshold voltage. This has been an area of intense research, ever since Ovshinsky reported reversible switching in amorphous semiconductors [73-83]. Electrical switching could find applications in areas like information storage, electrical power control etc. Several tellurium containing chalcogenide glasses such as Cd-Te, Ga-Te, As-Te, As-Te-Se, Al-Ge-Te, Ge-As-Te etc. are reported to exhibit electrical switching [84-91].

While analyzing the OFF state *V-I* behaviour of a material possessing switching property, it can be seen that the *V-I* characteristics is linear only for a small region at low electric fields. Then the material goes into a quasi-equilibrium state where *V-I* behavoiur shows exponential dependence of the form $I \alpha V^n$ where $n > 2$. In this region, the material switches to a highly conductive state.

Electrothermal instability [92] seems to explain reasonably well the switching phenomenon in chalcogenide glasses. This is a combination of purely electronic and thermal effects. Electronic effect is caused by the deviation of the carriers from equilibrium by the electric field while the thermal effects are due to the lattice heating because of Joule effect. Joule heating causes the lattice temperature to rise locally above the ambient temperature, which could result in a large increase in conductivity owing to the thermal generation of carriers [93].

1.8.1 Threshold and memory switching

In general, there are two types of switching behaviour exhibited by chalcogenide glasses, (i) threshold switching and (ii) memory switching.

In threshold switching, the ON state persists only while a current flows, whereas in memory switching the ON state is permanent until a suitable reset pulse

is applied. The *V-I* characteristics of threshold and memory switchings are shown in Fig. 1.10. In threshold switching materials, the ON state requires a small holding current (I_H) and voltage (V_H) to sustain it. Once the switching current is removed, the material reverts back to the low conducting OFF state. On the other hand, in memory type switching, the ON state is permanent, even after the removal of the applied field. A suitable reset pulse has to be applied to bring it back to the OFF state. In both cases, switching occurs with a delay time reaching values of the order of 10^{-9} sec, when the voltage across the sample is about 50 % higher than the threshold voltage [74].

It is seen that the crystallization of glasses from the melt state is very important in determining the switching mechanism, rather than from the glassy state. Very easy glass formers may not exhibit switching under normal conditions, as they prefer to go to glassy state upon cooling. On the other hand, glasses that can be prepared only under high cooling rates, may exhibit switching [86, 87, 94-100].

1.8.2 Switching models

In order to account for the electrical switching process in chalcogenide glasses, different models have been proposed [96-98]. These models based on electronic, thermal and electrothermal mechanisms assume that threshold switching is electronic in origin, while memory switching is thermal in origin.

The model proposed by Adler and Petersen [101, 102] is one of the most successful explanations of threshold switching phenomenon in chalcogenide glasses. Chalcogenide glasses contain large densities (10^{18}-10^{19} cm^{-3}) of positively and negatively charged defect states called valence alternation pairs (VAPs) [103]. When sufficiently large electric fields are applied, carriers are excited and these defect

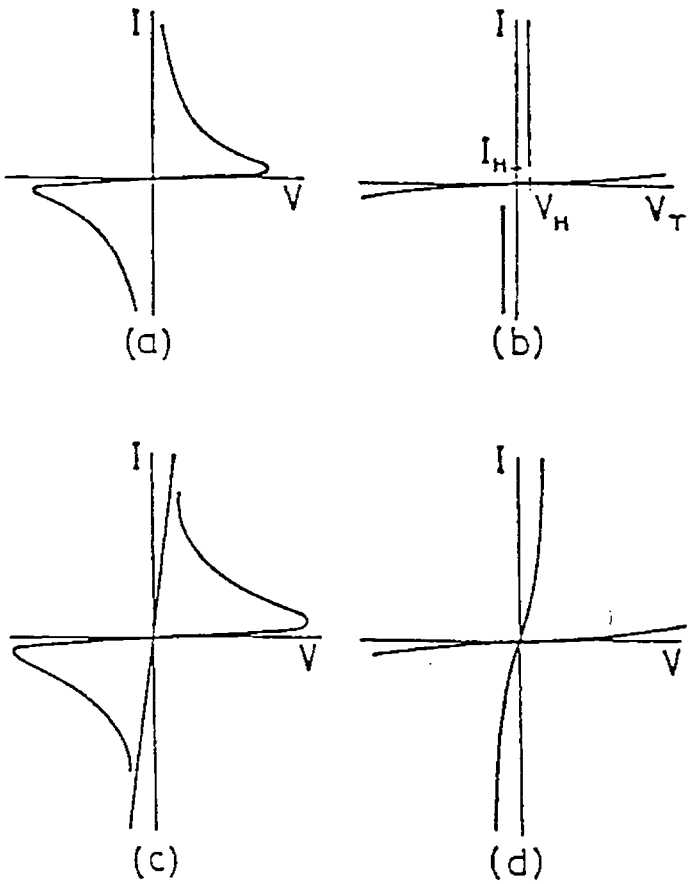

Fig. 1.10 The general classification of switching phenomenon exhibited by chalcogenide glasses, (a) negative resistance device (b) switching device (c) negative resistance device with memory (d) switching device with memory.

centers are filled. When all the traps are filled, the life time of the carriers increase sharply to a value, much larger than that needed to cross the thickness of the sample. This leads to a drop in the voltage and the associated switch to the conducting state. This process is clearly reversible.

In threshold type switching, a redistribution of charge carriers having very different mobilities and transition rates occur through the electrode interfaces. This gives rise to a space charge and field enhancement near one electrode and to a small

value for the holding voltage after switching (V_H). In general, the temperature being steady, the threshold voltage is not affected significantly upon the creation of high density of electron-hole pairs by photon or electron bombardment, even though current is considerably increased. However, with increase in temperature, threshold voltage is found to decrease with an increase in current [104-108].

It is believed that memory switching occurs in those chalcogenide glasses in which the cross-linking atoms are too few. Such glasses have lesser thermal stability [102] and consequently, crystallize easily when heated. It is proposed that memory switching phenomenon is caused by the phase transition of the material from the glassy to the crystalline state due to Joule heating [109]. In the crystalline state, conduction is higher compared to the non-crystalline state, since the disorder is significantly less. Clearly, this process is irreversible. The formation of a crystalline conducting channel in a memory glass during switching has been confirmed by electron microscope and optical reflectivity investigations [109].

According to Boer and Ovshinsky [98], electrothermal instability is the cause for electrical switching. They solved the thermal balance equation,

$$c\rho\frac{dT}{dt} = K\nabla^2 T + \sigma E_A^2 \qquad (1.13)$$

to calculate the break down temperature for switching [108, 110, 111], where c is the specific heat capacity, ρ is the density, K is the thermal conductivity, σ is the electrical conductivity and E_A is the applied electric field. According to them, the actual switching transition cannot be a simple thermal run away. It would require temperature in the current channel far in excess of those which can be reached without material destruction, and one should be able stabilize the transition with sufficiently large load resistor.

1.9 Carrier type reversal in chalcogenide glasses

It has been known for a long time that bulk chalcogenide glasses, prepared by the melt quenching technique are *p*-type semiconductors [42, 112, 113], with a positive Seebeck coefficient describing thermoelectric power. This is the case not only for chalcogenide elements themselves, but also for binary, ternary and multicomponent glass forming alloys of S, Se and Te with elements like Ge, As, Sb, Si, Sn etc. Further, addition of impurities to them does not alter the nature of conductivity.

In the case of chalcogenide glasses, the valence band is constituted by the chalcogen lone pair orbitals [114]. The effect of structural disorder is less on the lone pair band compared to that on the antibonding orbitals that constitute the conduction band [112]. Therefore, the range of localized tail states at the valence band edge is smaller in comparison to the localized states at the conduction band edge. As a consequence, the number of electrons excited above the conduction band mobility edge is less than the number of holes excited below the valence band mobility edge. This is one of the reasons for the *p*-type conductivity found is chalcogenide glasses.

As mentioned in the previous section, chalcogenide glasses contain a large number of positively and negatively charged defect states, known as valence alternation pairs (VAPs) [103]. During thermal excitation, the life time of free holes excited from the positively charged defect states are higher than the life time of free electrons from negatively charged defects, which also account for *p*-type conductivity of amorphous chalcogenides.

In general, chalcogenide glasses are insensitive to the addition of impurities. This is because of the fact that the Fermi level in these materials is pinned near the

middle of the band gap by valence alternation pairs [108, 115]. However, of late, it has been found that, the addition of certain heavy elemental metallic impurities like Bi or Pb could change the conduction to *n*-type in certain chalcogenide glass systems. These impurities enter the network as charged species, and change the ratio of valence alternation pairs to such as extent that the Fermi level gets unpinned. When the concentration of charged additives exceeds that of the valence alternation pairs, chalcogenide glasses can exhibit the phenomenon of carrier type reversal (CTR) or *p* to *n* transition.

This phenomenon was first observed in bismuth doped germanium selenide glass [116, 117]. $Bi_xGe_{20}Se_{80-x}$ system of glasses, where the subscript is the normalized concentration variable, exhibits CTR around $x \approx 8$. This discovery has led to extensive research on these materials [118-124] and to a reconsideration of the existing theories of electronic structure of chalcogenide glasses [125]. Since a significant amount of Bi has to be incorporated for CTR to occur, it is desirable to use the term 'chemical modification' rather than doping [126]. Continued efforts to understand CTR, led to the discovery of this phenomenon in other chalcogenide glassy systems like Pb-Ge-Se, Pb-In-Se, Pb-Ge-Se-Te, Bi-Ge-Te-etc [127-130]. Electrical transport measurements clearly show the occurrence of CTR at certain specific compositions. For example, $Pb_{20}Ge_xSe_{80-x}$ (x = 17-24) system shows CTR at $x \approx 21$, $Pb_yGe_{42-y}Se_{58}$ (y = 0-20) system exhibits CTR around $y \approx 8$, $Pb_xIn_{25-x}Se_{75}$ (x = 0-15) system exhibits CTR around $x \approx 5$, $Pb_xGe_{42-x}Se_{48}Te_{10}$ (x = 0-20) system exhibits CTR around $x \approx 8$, while $Bi_xGe_{20}Te_{80-x}$ (x = 0-6) system exhibits CTR around $x \approx 3.5$.

In all these systems, the sign of the thermo power changes from positive to negative at the respective critical compositions. In this thesis, we report the results of our measurements on Pb-Ge-Se, Bi-Ge-Se and Pb-In-Se systems. We have measured the thermal parameters viz., thermal diffusivity (α), thermal effusivity (e), thermal conductivity (k) and heat capacity (c_p) of these systems as a function of composition, using an improved photopyroelectric (PPE) technique [131]. It is found that the thermal parameters show anomalous variations at critical compositions [132, 133]. We also report the results of photoconductivity measurements on Pb-Ge-Se [134] and Pb-In-Se systems.

There is a vast scope for technological exploitation of the phenomenon of carrier type reversal observed in chalcogenide glasses such as preparation of a new class of p-n junctions [135] based entirely on glasses, since it offers several manufacturing advantages [136].

1.10 Applications of amorphous materials

Amorphous materials have got a wide range of applications. For many applications, they are more suitable than crystalline materials. Until recently, silicate glasses were the only type of amorphous materials commonly used. However, the relatively recent discovery that many other types of materials can be produced in the amorphous form, either as bulk glasses or as thin films has led to a rapid expansion in the use of such materials in electronic, magnetic and optical applications.

One of the main advantages of amorphous materials over crystalline materials is that, they are relatively easy to prepare. Large area homogenous

amorphous thin films can be prepared for solar cell applications. Bulk glasses can often be prepared easily by melt quenching technique.

A number of amorphous semiconductors are used as passive and active elements in electronic devices [137, 138]. These applications are in the fabrication of solar cells, thin film transistors and in electro photography. The ability of certain ions to diffuse readily in oxide or chalcogenide glasses in the presence of a concentration gradient or an electric field opens up a range of electrochemical applications such as solid state batteries, electrochemical sensors and electrochromic optical devices [139, 140]. The most wide spread use of an electrochemical sensor is in the so called 'glass electrode' commonly used to monitor proton activity.

Amorphous materials find applications in infrared optical communication systems also. They are extensively being tested and used for the fabrication of optical fibers, prisms and optical windows. Near the glass transition temperature, the material remains workable over a range of temperature, so that it can be easily fashioned into fibers. Further, amorphous materials, particularly bulk glasses, are often structurally homogeneous and isotropic over a macroscopic length scale, as a result of which their physical properties are also isotropic. Since these materials have ultra low optical loss characteristics in the IR region, they are extensively used for optical communication applications, both for long distance and local area networks. There have also been reports on active optical devices like LEDs [141, 142].

The phenomenon of electrical switching exhibited by certain tellurium rich glasses finds applications in switching devices. Switching materials find applications in electrical power control also. Amorphous semiconductor thin films are used as

storage targets in electron beam memory devices [143]. Chalcogenide glasses are also used as IR filters and in other IR optical elements [144]. This is possible because chalcogenide glasses have very good transmittance reaching up to the far IR region. Chalcogenide glasses have found several applications relating to their photoconducting property. Two major applications are in xerography and photo detection [144].

Another advantage of amorphous materials over crystalline materials is that, they can be prepared over a wide range of compositions, and not restricted to stoichiomertic values. Because of this, physical properties of such amorphous materials can often be varied continuously by varying the composition. This allows one to design materials for specific requirements.

References

1. D. Turnbull, Contemp. Phys. **10** (1969) 473
2. E. S. R. Gopal, *Proc. 30 Years' Comemmoration Saha Institute of Nuclear Physics*, Calcutta, India (1983) 37
3. D. Turnbull, *Undercooled Alloy Phases*, edited by E. W. Collings and C. C. Koch, (Metallurgical Soc. Warrendale PA, 1986) 3
4. F. Yonezawa, *Solid State Physics*, edited by H. Eherenreich and D. Turnbull, (45 Academic Press Inc-199)
5. R. B. Schwarz and W. L. Johnson, Phys. Rev. Lett. **51** (1983) 415
6. C. C. Koch, O. B. Cavin, C. G. McKamey and J. O. Scarbrough, Appl. Phys. Lett. **43** (1983) 43
7. S. R. Elliot, *Physics of Amorphous Materials*, 2nd edition, (Longman, London)
8. J. C. Phillips and M. F. Thorpe, Solid Satate Commun. **53** (1985) 699
9. G. Lucovsky and T. M. Hayes, *Amorphous Semiconductors*, edited by M. H. Brodsky, (Springer Verlag, Berlin, 1985)
10. R. Zallen, *The Physics of Amorphous Solids*, (John Wiley, 1983).
11. A. F. Ioffe and A. R. Regel, Prog. Semiconductors **4** (1960) 237
12. S. R. Elliot, Nature **354** (1991) 445
13. A. C. Wright, R. A. Hulme, D. I. Grimley, R. N. Sinclair, S. W. Martin, D. L. Price and F. L. Galeener, J. Non-Cryst. Solids **129** (1991) 213
14. W. H. Zachariasen, J. Amer. Chem. Soc. **34** (1932) 3841
15. N. F. Mott, Adv. in Phys. **16** (1967) 49
16. R. M. White, J. Non-Cryst. Solids **16** (1974) 387

17. J. C. Phillips, Phys. Today (February, 1982) 27

18. J. C. Phillips, J. Non-Cryst. Solids **43** (1979) 153

19. M. F. Thorpe, J. Non-Cryst. Solids **57** (1983) 355

20. J. C. Phillips and M. F. Thorpe, Solid State Commun. **53** (1985) 699

21. K. Tanaka, Phys. Rev. B **39** (1989) 270

22. R. Ota, T. Yamate, N. Soga and M. Kunugi, J. Non-Cryst. Solids **29** (1978) 67

23. K. Murase, K. Yakushiji and T. Fukunaga, J. Non-Cryst. Solids **59-60** (1983) 855

24. M. Bensoussan, Rev. Phys. Appl. **12** (1977) 753

25. K. S. Gilroy and W. A. Phillips, Phil. Mag. B **47** (1983) 655

26. K. N. Madhusoodanan and J. Philip, Phys. Stat. Solidi (a) **108** (1988) 775

27. A. Denewville, J. P. Keradec, P. Gerrad and A. Mini, Solid State Commun. **14** (1974) 341

28. K. N. Madhusoodhan, J. Philip, G. Parthasarathy, S. Asokan and E. S. R. Gopal, Phil. Mag. B **50** (1983) 123

29. K. E. Peterson, U. Birkholz and A. Adler, Phys. Rev. B **8** (1973) 1453

30. S. Asokan, G. Parathasarathy and E. S. R. Gopal, Phys. Rev. B **35** (1987) 8269

31. K. N. Madhusoodhanan, J. Philip, S. Asokan, G. Parthasarathy and E. S. R. Gopal, J. Non-Cryst. Solids **109** (1989) 255

32. K. N. Madhusoodhanan, K. Nandakumar, J. Philip, S. S. K. Titus and E. S. R. Gopal, Phys. Stat. Solidi (a) **114** (1989) 525

33. K. Tanaka, T. Nakagawa and A. Odajima, Phil. Mag. B **54** (1983) L3

34. K. Tanaka, Y. Kasanuki and A. Odajima, Thin Solid Films **117** (1984) 251

35. K. Tanaka, Solid State Commun. **60** (1986) 295

36. K. Tanaka, Phys. Rev. B **39** (1989) 1270

37. P. W. Anderson, Phys. Rev. **109** (1958) 1492

38. M. H. Cohen, H. Fritzsche and S. R. Ovshinsky, Phys. Rev. Lett. **22** (1969) 1065

39. H. Fritzsche in *Electrical and Structural Properties of Amorphous Semiconductors*, edited by P. G. Le Comber and J. Mort (Academic Press, London, 1973) 55

40. H. Fritzsche in *Amorphous and Liquid Semiconductors*, edited by J. Tauc (Plennum Press, New York, 1974) 221

41. D. Adler, Naturwissenschaften **69** (1982) 574

42. N. F. Mott and E. A. Davis, *Electronic Processes in Non-Crystalline Materials*, (Clarendon Press, Oxford, 1979)

43. E. A. Davis and N. F. Mott, Phil. Mag. **22** (1970) 903

44. N. F. Mott, Phil. Mag. **26** (1972) 505

45. N. F. Mott, Contemp. Phys. **26** (1985) 203

46. S. C. Agarwal, Phys. Rev. B 7 (1973) 685

47. J. Tane, F. J. Disalvo, G. E. Peterson and S. L. Wood, *Proc. Symp. on Amorphous Magnetism* (Detroit, Michigen, 1972)

48. S. G. Bishop, U. Strom and P. C. Taylor, Phys. Rev. Lett. **34** (1975) 1346

49. S. G. Bishop, U. Strom and P. C. Taylor, Phys. Rev. Lett. **36** (1976) 543

50. S. G. Bishop, U. Strom and P. C. Taylor, Phys. Rev. B **15** (1977) 2278

51. P. Nagels in *Amorphous Semiconductors*, edited by M. H. Brodsky (Spinger Verlag, Berlin 1985) 113

52. R. C. Zeller and R. O. Pohl, Phys. Rev. B **4** (1971) 2029

53. Stephens, Phys. Rev. B **13** (1976) 852

54. R. Berman, *Proc. R. Soc. London* A **208** (1951) 96

55. W. A. Phillips in *Amorphous Solids: Low Temperature Properties*, (Springer Verlag, 1981) 65

56. W. A. Phillips, J. Low Temp. Phys. **7** (1972) 351

57. P. W. Anderson, B. I. Halperin and C. M. Varma, Phil. Mag. **25** (1972) 1

58. J. Tauc, Mat. Res. Bull. **5** (1970) 721

59. J. D. Dow and D. Redfield, Phys. Rev. B **5** (1972) 594

60. R. A. Street, Solid State Commun. **24** (1977) 363

61. R. H. Bube, *Photoelectronic Properties of Semiconductors*, (Cambridge University Press, 1992)

62. R. H. Bube, *Photoconductivity of Solids*, (Krieger Publ. Co., New York, 1978)

63. J. Mort and D. M. Pai, *Photoconductivity and Related Phenomena*, (Elsevier, New York, 1976)

64. K. Weiser, R. Fisher and M. H. Brodsky, *Proc. of the 10th Int. Semiconductors Conf.*, (Cambridge, US, AEC, Oak Ridge, 1970)

65. E. A. Fagen and H. Fritzsche, J. Non-Cryst.Solids **4** (1970) 480

66. J. G. Simmons and G. W. Taylor, J. Non-Cryst. Solids **8-10** (1972) 947

67. J. G. Simmons and G. W. Taylor, J. Phys. C **6** (1973) 3706

68. G. W. Taylor and J. G. Simmons, J. Phys. C **7** (1974) 3067

69. T. C. Arnoldussen, R. H. Bube, E. A. Fagen and S. Holmberg, J. Non-Cryst. Solids **8-10** (1972) 933

70. T. C. Arnoldussen, R. H. Bube, E. A. Fagen and S. Holmberg, J. Appl. Phys. **43** (1972) 1798

71. T. C. Arnoldussen, C. A. Menzer, Y. Nakagawa and R. H. Bube, Phys. Rev. B **9** (1974) 3377

72. R. H. Bube, J. E. Mahan, R. T. S. Shiah and H. A. van der Plas, Appl. Phys. Lett. **25** (1974) 419

73. S. R. Ovshinsky, Phys. Rev. Lett. **21** (1968) 1450

74. S. R. Ovshinsky and H. Fritzsche, IEEE Trans. on Electron Devices **20** (1973) 91

75. R. Neale and J. A. Aseltine, IEEE Trans. on Electron Devices **20** (1973) 195

76. S. R. Ovshinsky and H. Fritzsche, Met. Trans. **2** (1971) 641

77. M. H. Cohen, R. G. Neale and A. Paskin, J. Non-Cryst. Solids **8-10** (1972) 885

78. A. G. Steventon, J. Non-Cryst. Solids **21** (1976) 319

79. K. Nakashima and K. C. Kao, J. Non-Cryst. Solids **33** (1979) 189

80. D. Adler, H. K. Henisch and N. F. Mott, Rev. Mod. Phys. **50** (1978) 209

81. D. Adler and S. C. Moss, J. Vac. Sci. & Technol. (1972) 1182

82. A. E. Owen and J. M. Robertson, IEEE Trans. on Electron Devices **20** (1973) 105

83. J. Bicerano and S. R. Ovshinsky, J. Non-Cryst. Solids **75** (1985) 75

84. G. A. Denton, G. M. Friedman and J. F. Schetzina, J. Appl. Phys. **46** (1975) 3044

85. J. Vazquez, E. Marquez, P. Villares and R. G. Jimenez, Materials Letters **4** (1986) 60

86. R. L. Hargraves, P. R. Mason and J. C. Anderson, J. Phys. D: Appl. Phys. **7** (1974) 85

87. S. S. K. Titus, R. Chaterjee, S. Asokan and A. Kumar, Phys. Rev. B **48** (1993) 1460

88. S. Prakash, S. Asokan and D. B. Khare, Semicond. Sci. Technol. **9** (1994) 1484

89. J. A. Savage, J. Non-Cryst. Solids **11** (1972) 121

90. R. Aravinda Narayanan and A. Kumar, Phys. Rev. B **60** (1999) 11859

91. R. Aravinda Narayanan, S. Asokan and A. Kumar, Phys. Rev. B **54** (1996) 4413

92. M. P. Shaw and N. Yildrim, Adv. Electr. Electron Phys. **60** (1983) 307

93. N. Klein, Thin Solid Films **100** (1983) 335

94. A. C. Warren, J. Non-Cryst. Solids **4** (1970) 613

95. C. F. Drake and I. F. Scanlan, J. Non-Cryst. Solids **4** (1970) 234

96. W. D. Buckley and S. H. Holmberg, Solid State Electronics **18** (1975) 127

97. H. K. Henisch, E. A. Fagen and S. R. Ovshinsky, J. Non-Cryst. Solids **4** (1970) 538

98. K. W. Boer and S. R. Ovshinsky, J. Appl. Phys. **41** (1970) 2675

99. Z. U. Borisova, *Glassy Semiconductors*, (Plenum, New York, 1985)

100. D. F. Weirauch, Appl. Phys. Lett. **16** (1970) 72

101. K. E. Petersen and D. Adler, J. Appl. Phys. **47** (1976) 256

102. D. Adler, Sci. Amer. **236 (5)** (1977) 36

103. M. Kastner, D. Adler and H. Fritzsche, Phys. Rev. Lett. **37** (1976) 1504

104. K. Subhani, M. S. Shaw and D. Adler, *Proc. Int. Conf. on Amorphous Semiconductors*, edited by W. E. Spear, (Univ. of Edinburgh, 1977)

105. M. P. Shaw, S. C. Moss, S. A. Kostylev and L. H. Slack, Appl. Phys. Lett. **22** (1973) 114

106. K. Homma, Appl. Phys. Lett. **18** (1971) 198

107. H. K. Henisch, W. R. Smith and W. Wihl, *Amorphous and Liquid Semiconductors*, edited by J. Stuke and W. Brenig, (Taylor and Francis, London, 1974)

108. D. Adler and C. J. Yoffa, Phys. Rev. Lett. **36** (1976) 1197

109. H. Fritzsche in *Amorphous and Liquid Semiconductors*, edited by J. Tauc (Plenum, London, 1974) 313

110. S. K. Shinakawa, Y. Inagaki and T. Arizumi, Jap. J. Appl. Phys. **12** (1973) 1043

111. G. C. Vezzoli and I. M. Pratt, Thin Solid Films **12** (1972) 161

112. S. D. Baranovskii et al., Fiz. Tekh. Poluprovodn **18** (1984) 1016 (Sov. Phys. Semicond. **18** (1984) 633)

113. A. V. Kolobov, J. Non-Cryst. Solids **198-200** (1996) 728

114. M. Kastner, Phys. Rev. Lett. **28** (1972) 355

115. N. F. Mott, Adv. Phys. **16** (1967) 49

116. N. Tohge, Y. Yamamoto, T. Minami and M. Tanaka, Appl. Phys. Lett. **34** (1979) 640

117. N. Tohge, T. Minami and M. Tanaka, J. Non-Cryst Solids **38-39** (1980) 283

118. S. Kumar, S. C. Kashyap and K. L. Chopra, J. Appl. Phys. **72** (1992) 2066

119. P. Kounavis and E. Mytilineou, J. Non-Cryst. Solids **201** (1996) 119

120. L. Tichy, H. Ticha, A. Pacesova and J. Petzlt, J. Non-Cryst. Solids **128** (1991) 191

121. V. K. Bhatnagar, K. L. Bhatia, V. Yadav and N. Kishore, Phys. Rev. B **39** (1989) 11203

122. K. L. Bhatia, D. P. Gosain, G. Parthasarathy and E. S. R. Gopal, Phys. Rev. B **34** (1986) 8786

123. J. C. Phillips, Phys. Rev. B **36** (1987) 4265

124. A. K. Agnihotri, A. Kumar and A. N. Nigam, J. Non-Cryst. Solids **93** (1987) 267

125. S. R. Elliot in *Disordered Semiconductors*, edited by M. Kastner, G. A. Thomas and S. R. Ovshinsky, (Plenum, New York, 1987) 219

126. S. R. Ovshinsky in *Amorphous and Liquid Semiconductors*, edited by W. L. Spear, (University of Edinburgh, Edinburgh, 1977) 519

127. N. Tohge, H. Matsuo and T. Minami, J. Non-Cryst. Solids **95-96** (1987) 809

128. R. M. Mehra, Sandeep Kohli, Amit Pundir, V. K. Sachdev and P. C. Mathur, J. Appl. Phys. **81** (1997) 7842

129. S. Murugavel and S. Askon, Phys. Rev. B **58** (1998) 4449

130. K. L. Bhatia, G. Parthasarathy, A. Sharma and E. S. R. Gopal, Phys. Rev. B **38** (1988) 6342

131. C. Preethy Menon and J. Philip, Meas. Sci. & Technol. **11** (2000) 1744

132. J. Philip, R. Rajesh and C. Preethy Menon, Appl. Phys. Lett. **78** (2001) 745

133. J. Philip, R. Rajesh and C. Preethy Menon, Analytical Sciences **17** (2001) s99

134. R. Rajesh and J. Philip, Indian J. of Pure & Appl. Phys. **38** (2000) 827

135. N. Tohge, K. Kanda and T. Minami, Appl. Phys. Lett. **48** (1986) 1739

136. P. Kounavis, E. Mytilineou and M. Roilos, J. Appl. Phys. **66** (1989) 708

137. Hamakawa in *Non-Crystalline Semiconductors*, edited by M. Pollak, Vol. I, (CRC Press, 1987)

138. A. Madan and M. P. Shaw, *The Physics and Applications of Amorphous Semiconductors*, (Academic Press, 1988)

139. J. Gabona, *Glass: Current Issues*, 1985

140. G. Eisenman, *Glass Electrodes for Hydrogen and other Cations-Principles and Practice*, Marcel Dekker (1967)

141. T. Miya, Y. Terunuma, T. Hosaka and T. Miyashita, Electronic Lett. **15** (1979) 106

142. H. Weber, Wiss ZutschrFriedrich-Schiller Univ. **32** (1987) 239

143. A. C. M. Chen, A. M. Dunham and J. M. Wang, J. Appl. Phys. **44** (1973) 1436

144. Z. Cimple and F. Kosek, J. Non-Cryst. Solids **90** (1987) 577

CHAPTER 2

Experimental techniques

2.1 Introduction

This chapter deals with the details of the various experimental techniques used for the investigations of different physical properties of the selected chalcogenide glass samples. Photoacoustic and photopyroelectric techniques have been used to determine various thermal parameters viz., thermal diffusivity (α), thermal effusivity (e), thermal conductivity (k) and heat capacity (c_p) of the samples. Photoconductivity studies are done on selected systems. Variations of thermal parameters during electrical switching are studied on In-Te system. UV-Vis-NIR spectrophotometer is used to study the optical absorption of the samples. Details of these techniques are described in the following sections of this chapter. The results presented in chapters 3, 4, 5, 6 and 7 have been obtained by carrying out measurements using the above techniques.

2.2.Photoacoustic spectroscopy

Optical spectroscopy is one of the most powerful and effective techniques to study the physical properties of matter. It is based on the interaction of light with matter at atomic or molecular levels. Conventional optical spectroscopic methods are either transmission type or reflection type. In transmission type, the intensity of the transmitted light beam through the medium is measured, while the reflection type

involves the measurement of intensity of radiation reflected or scattered from the sample. However, these techniques fail in the case of weakly absorbing samples, highly light scattering samples like powders, amorphous materials etc. or opaque materials. Several techniques have been developed to overcome these difficulties and the most common of these are diffuse reflectance [1], attenuated total reflection (ATR) and internal reflection spectroscopies [2] and Raman scattering [3]. Even-though such techniques have been very useful, they suffer from several limitations. Each method is applicable only to a limited category of materials, each is useful only over a limited wavelength range, and the data obtained are often difficult to interpret.

The photoacoustic spectroscopy has evolved over the past two-three decades as a powerful method to study those materials that are unsuitable for study by conventional spectroscopic techniques [4-7]. This technique is based on the photoacoustic effect, originally detected by Alexander Graham Bell in 1880 [8, 9]. It possesses some unique features, mainly due to the fact that, even though the incident energy is in the form of photons, the interaction of these photons with the sample is studied not through the subsequent detection and analysis of some of the photons, but through a direct measurement of the energy absorbed by the material as a result of its interaction with the incident photon beam

The photoacoustic (PA) effect is the generation of an acoustic signal when the sample under investigation, placed inside an enclosed chamber, is irradiated by an intensity modulated beam of light. In case of gaseous or liquid samples, the sample fills the entire volume of the cell and acoustic signals are detected by a microphone or a piezoelectric transducer. In the case of solids, the samples fill only

a portion of the cell and the remaining volume of the cell is filled with a non-absorbing gas like air. The PA signal is detected using a sensitive microphone suitably placed inside the cell. The absorption of the incident radiation will excite the internal energy levels of the sample and upon subsequent deexcitation, all or part of the absorbed photon energy is converted into heat through non-radiative deexcitation processes. In the case of gas and liquid samples, which fill the entire volume of the sample chamber, this internal heating causes pressure fluctuations having the same frequency as that of the modulation frequency of the incident radiation and can be detected using an acoustic transducer kept in intimate contact with the sample. In the case of solid samples which fill only a portion of the sample chamber, the periodic heating of the sample results in a periodic heat flow from the interior of the sample to the surrounding non-absorbing gas medium, which in turn produces pressure fluctuations in the gas and are detected as acoustic signal by a microphone suitably placed in the chamber. It is also possible to measure the heat generated in a bulk solid sample through the subsequent pressure or stress variations in the sample itself by means of a piezoelectric detector in intimate contact with the sample. Even though the sensitivity in this case is better, it is not always possible to employ a piezoelectric detector due to the limitations imposed by the nature of the sample. Also, the use of piezoelectric transducers is very difficult for PA measurements that involve variations of the sample temperature over a wide range.

Photoacoustics is essentially a combination of optical absorption spectroscopy and calorimetry. From the calorimetric viewpoint, the heat input into the sample is supplied indirectly by the incident beam of light and the rise in temperature is detected by another indirect method using an acoustic transducer

instead of a thermal detector. For a typical solid sample, using gas-microphone detection system, temperature rise of the order of 10^{-6} °C can be detected. This acoustic detection has several advantages over conventional thermal detection using temperature sensors such as thermistors or thermopiles in terms of sensitivity, detector rise time and the speed at which measurements can be made. The advantages of photoacoustics as a form of spectroscopy are evident from the very nature of the technique. Since absorption of optical or electromagnetic radiation is essential for the generation of the PA signal, light that is transmitted or elastically scattered by the sample does not interfere with the inherently absorptive PA measurements. This enables one to work with essentially transparent media or highly light scattering materials such as powders, amorphous solids, gels and colloids. On the other hand, since the technique does not depend upon the detection of photons, it is possible to obtain optical absorption spectra of materials that are completely opaque to transmitted light. Thus, the advantages offered by photoacoustics over other conventional spectroscopic techniques are due to the following two basic aspects viz., the insensitivity to the non-absorbed light and the non-dependence on the detection of photons.

Spectroscopy is however, only one of the several applications of PA effect. In the spectroscopic regime itself, photoacoustics can be used to measure the absorption and excitation spectra, the life time of excited states and the quantum yield of radiative processes. In addition to this, the calorimetric or thermal aspects associated with the PA effect offers a wide range of applications to study the thermal and elastic properties of materials. In such studies, the calorimetric or acoustic aspect of photoacoustics plays the dominant role, while the optical part is simply a

convenient mechanism for heat generation. Such applications include measurement of thermal parameters, thermal wave imaging and study of phase transitions in solids.

2.2.1 Theory of Photoacoustic effect in solids

A number of theoretical explanations of PA effect have been put forward in the 19th century itself. But the present understanding of the PA effect in solids is based on modern theories developed during 1970's. The first attempt to develop a proper theory of PA effect in solids was carried out by Parker [10] in 1973 in order to give a quantitative explanation for the PA signal emanating from cell windows while performing PA measurements on gases. The general theory of PA effect in solids formulated by Rosencwaig and Gersho [11, 12] has been found to be very successful in interpreting most of the experimental observations. The Rosencwaig-Gersho theory states that in a gas-microphone PA cell, the signal depends on the generation of an acoustic pressure disturbance at the sample-gas interface and is caused by the periodic heat flow from the sample, which is governed by thermal diffusion equations. This theory gives an exact equation for the magnitude and phase of the PA signal as a function of the optical, thermal and geometrical properties of the sample, the cell and the gas within the cell. Although the thermal part of the theory has been treated exactly, the acoustic part is treated in an approximate heuristic manner, which is, however, valid for most experimental conditions.

The Rosencwaig-Gersho (R-G) theory is a one-dimensional analysis of the production of photoacoustic signal in a simple cylindrical cell as shown in Fig. 2.1. The cell has a diameter D and length L. It is assumed that the length L is small compared to the wavelength of the generated acoustic signal.

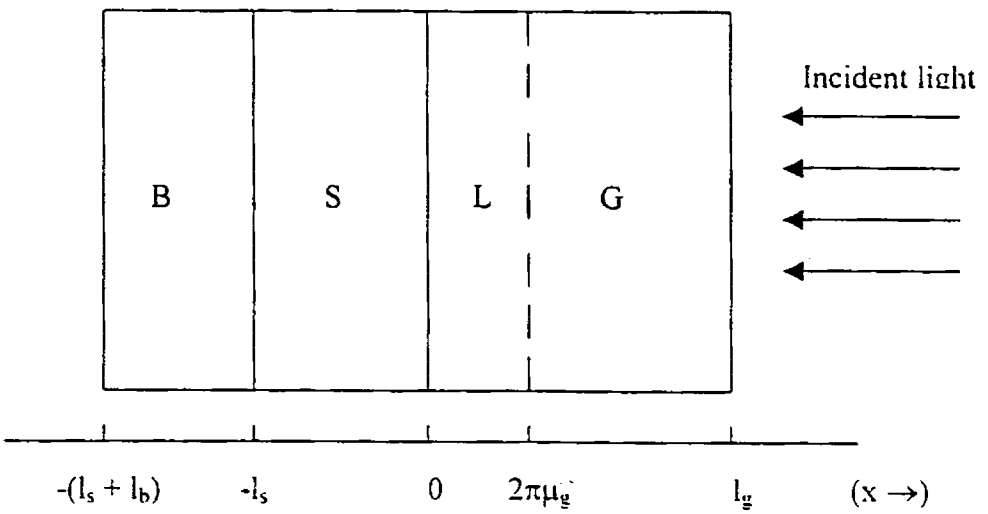

Fig. 2.1 Cross-sectional view of a simple cylindrical photoacoustic cell

B, S, L and G represent backing material, sample, boundary layer of gas and gas medium respectively

A microphone (not shown in figure) detects the average pressure produced in the cell. The solid sample is considered to be in the form of a disc of diameter D and length l_s. The back surface is against a poor thermal conductor of thickness l_b. The length of the gas column in the cell is l_g. It is also assumed that, the gas and the backing material do not absorb light. The parameters, which are important in the theoretical formulation, are defined below.

K = thermal conductivity (cal $cm^{-1}s^{-1}K^{-1}$)

ρ = density (g cm^{-3})

c = specific heat capacity (cal g^{-1} K^{-1})

$\alpha = \frac{K}{\rho c}$ = thermal diffusivity (cm^2 s^{-1})

$a = \left(\frac{\omega}{2\alpha}\right)^{1/2}$ = thermal diffusion coefficient (cm^{-1})

$\omega = 2\pi\upsilon$, where υ is the modulation frequency of the light beam

$\mu = 1/a$ = thermal diffusion length (cm)

According to R-G theory, it is seen that, when a sinusoidally modulated beam of light with wavelength λ and intensity I_o is incident on the sample, the complex envelope of the sinusoidal pressure variation Q is given by [6],

$$Q = \frac{\beta I_0 \gamma P_0}{2\sqrt{2} T_0 K_s l_g a_g \left(\beta_s^2 - \sigma_s^2\right)} x \left[\frac{(r-1)(b+1)e^{\sigma_s l_s} - (r+1)(b-1)e^{-\sigma_s l_s} + 2(b-r)e^{-\beta_s l_s}}{(g+1)(b+1)e^{\sigma_s l_s} - (g-1)(b-1)e^{-\sigma_s l_s}} \right] \tag{2.1}$$

Here,

γ = ratio of specific heats of the gas medium in front of the sample

P_0 = ambient pressure

T_0 = sum of ambient and d.c. temperature at the surface

β = optical absorption coefficient

$$b = \frac{K_b a_b}{K_s a_s} \tag{2.2}$$

$$g = \frac{K_g a_g}{K_s a_s} \tag{2.3}$$

$$\sigma = (1+i)a \tag{2.4}$$

$$r = \frac{(1-i)\beta_s}{2a_s} \tag{2.5}$$

The subscripts s, b and g denote the sample, backing and gas medium respectively.

Special cases

The difficulty in interpreting Eq. (2.1) can be reduced by examining various special cases. The special cases are determined by the relative magnitudes of the optical absorption length $l_\beta = 1/\beta$, the thermal diffusion length μ and thickness l of the sample respectively. Also, it is convenient to define

$$Y = \frac{\gamma P_0 I_0}{2\sqrt{2}\, T_0 l_g} \tag{2.6}$$

which always appears as a constant factor in the expression for Q.

We consider the case of optically opaque solids, which is relevant in our case. In this case, most of the light is absorbed within a distance that is small compared to l_s and essentially no light is transmitted.

Case (a) Thermally thin solids ($\mu_s >> l_s$, $\mu_s >> l_\beta$)

Using the approximations $e^{-\beta_s l_s} \approx 0$, $e^{\pm\sigma_s l_s} \approx 1$ and $|r| >> 1$, we get

$$Q \approx \frac{(1-i)}{2a_g}\left(\frac{\mu_b}{K_b}\right) Y \tag{2.7}$$

In this case, the signal is independent of β_s. This would be the case for a very black absorber such as carbon black. The signal is quite strong, depends on the thermal properties of the backing material and varies as ω^{-1}.

Case (b): Thermally thick solids ($\mu_s < l_s$, $\mu_s > l_\beta$)

Setting $e^{-\beta_s l_s} \approx 0$, $e^{-\sigma_s l_s} \approx 0$ and $|r| > 1$,

$$Q = \frac{(1-i)}{2a_g}\left(\frac{\mu_s}{K_s}\right)Y \qquad (2.8)$$

Eq. (2.8) is similar to Eq. (2.7), except that the thermal parameters of the backing material are now replaced by those of the sample. Here also, the signal is independent of β and varies as ω^{-1}.

Case (c): Thermally thick solids ($\mu_s << l_s$, $\mu_s < l_\beta$)

Setting $e^{-\beta_s l_s} \approx 0$, $e^{-\sigma_s l_s} \approx 0$ and $|r| < 1$

$$Q \approx \frac{i\beta\mu_s}{2a_g}\left(\frac{\mu_s}{K_s}\right)Y \qquad (2.9)$$

This is a very interesting and important case because even though the sample is optically opaque, it is not photoacoustically opaque, as long as $\mu_s < l_\beta$ i.e., acoustic signal is proportional to β. The signal is also dependent on the thermal properties of the sample and varies as $\omega^{-3/2}$.

2.2.2 Thermal diffusivity measurement using photoacoustic technique

Thermal diffusivity is of direct importance in thermal transport properties as it determines the rate of periodic or transient heat propagation through a medium. It is defined as $\alpha = \frac{K}{\rho c}$ where, K, ρ and c are thermal conductivity, density and heat capacity of the medium. Two kinds of techniques have been commonly used to determine thermal diffusivity: Transient heat flow methods [13] and periodic heat flow methods [14]. In the transient heat flow method, an addition or removal of thermal energy from the sample induces a transitory temperature change and α is

determined from a measurement of the temperature as a function of time at one or more points along the sample. In periodic heat flow methods, the thermal energy supplied to the sample is modulated at a fixed period. Consequently, the temperature at all points in the sample vary with the same period and α is then determined from the amplitude and phase of the thermal wave in the sample.

The photoacoustic technique [7], which belongs to the periodic heat flow method, is an effective method for determining thermal parameters of various materials, when the PA signal is measured as a function of modulation frequency. The method enables one to measure indirectly, and with high sensitivity, the surface temperature of the sample by non-contact means. The PA technique has been used to measure the thermal diffusivities of a wide variety of samples [15-21].

One of the parameters which determines the amplitude of the PA signal is the thermal diffusion length μ given by, $\mu = \left(\frac{\alpha}{\pi f}\right)^{1/2}$, where α is the thermal diffusivity of the sample and f is the modulation frequency. In the thermally thick regime ($\mu_s < l_s$, where l_s is the sample thickness), the PA signal is independent of the thermal properties of the backing material on which the sample is mounted, where as in the thermally thin regime ($\mu_s > l_s$), the PA signal gets modified by the thermal properties of the backing material as well. For an appropriate sample thickness, one can obtain a cross over from a thermally thin regime to a thermally thick regime by increasing the modulation frequency. The amplitude versus modulation frequency plot then shows a change in slope at the characteristic frequency f_c at which the cross over takes place. According to R-G theory, the characteristic frequency f_c is related to the thermal diffusivity of the sample as,

$$f_c = \frac{\alpha}{l_s^2} \qquad (2.10)$$

Once f_c is determined, thermal diffusivity can be obtained from Eq. (2.10) as,

$$\alpha = f_c l_s^2 \qquad (2.11)$$

Thermal diffusivity α, although a derived characteristic of a substance, is of direct importance in heat flow studies as it determines the rate of periodic or transient heat propagation through the medium. It has got dimensions $(\text{length})^2\ (\text{time})^{-1}$.

We have used a modified PA phase lag technique [22] for the determination of thermal diffusivity in our experiments. In this technique, a single beam PA cell that can be rotated through 180^0 about a vertical axis is used. PA signal is measured with front and rare surface illuminations of the sample, one after the other. If ψ_F and ψ_R denote the PA signal phases during front surface and rear surface illuminations respectively, it can be shown that [22],

$$\tan\Delta\psi = \tan(\psi_F - \psi_R) = \tanh(a_s l_s)\tan(a_s l_s) \qquad (2.12)$$

Thermal diffusivity can be calculated from the above expression using the relation, $a_s = \left(\frac{\pi f}{\alpha}\right)^{1/2}$. A schematic diagram of the experimental setup is shown in Fig. 2.2. A He-Cd laser of wavelength 442 nm and intensity ≈ 120 mW is used as the source of light. A mechanical chopper (Model SR540) is used to modulate the light beam. An electret microphone is used to detect the acoustic signal, the output of which is fed to a dual phase lock-in amplifier (Model SR830). The advantage of this technique is that measurement at only a single modulation frequency is enough to determine thermal diffusivity.

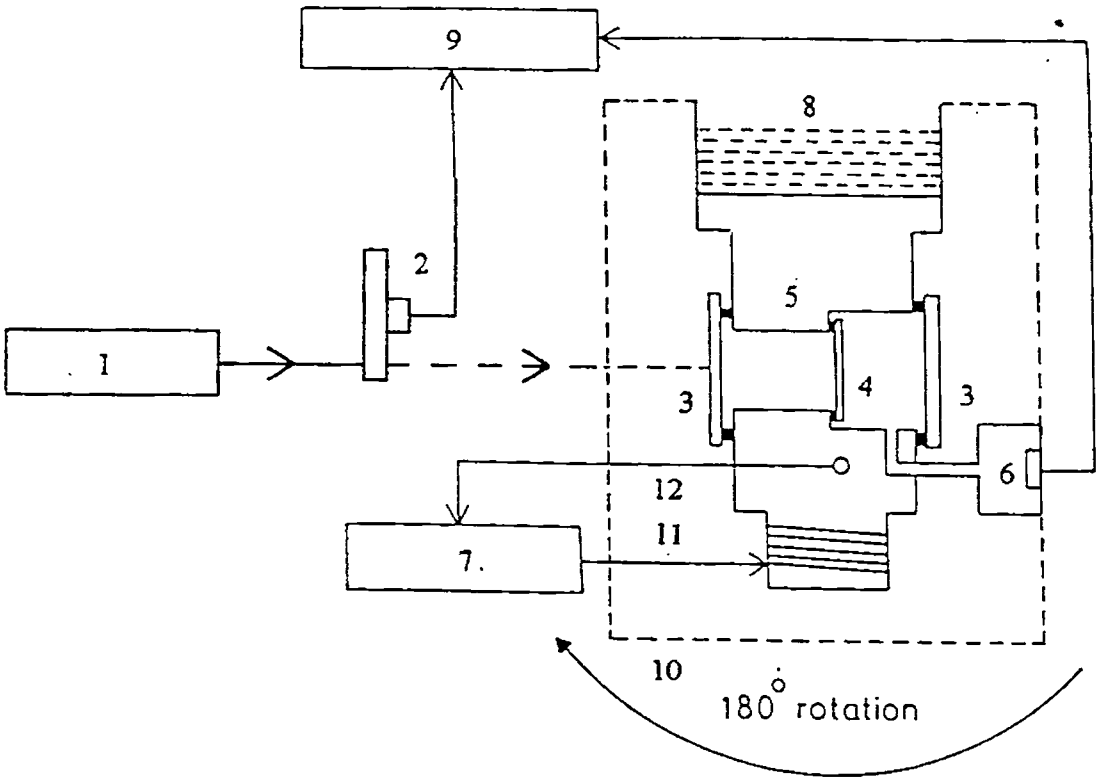

Fig. 2.2 Schematic diagram of the PA set up for measuring thermal diffusivity 1. laser 2. chopper 3. cell windows 4. sample 5. sample holder 6. microphone 7. temperature controller 8. liquid nitrogen chamber 9. lock-in amplifier 10 outer chamber 11. heater 12. temperature sensor

2. 3 Photopyroelectric Spectroscopy

Photothermal techniques have proved to be very useful in various fields such as spectroscopy, thermal characterization and non-destructive evaluation. Like the photoacoustic technique, the single beam photopyroelectric (PPE) technique is a well established photothermal method used for spectroscopic and thermal characterization of various materials as well as for studies of thermophysical properties of gases [23-31]. The basic principle of the single beam PPE technique is

that, when a periodically modulated energy from a source impinges on the surface of a sample, the sample absorbs some of the incident energy, and in turn, produces a localized temperature increase following a non-radiative deexcitation process. This periodic temperature variation in the sample can be directly detected with a pyroelectric transducer, which is in contact with the sample. The transducer is made of a thin film pyroelectric material [e.g. polyvinylidene difluoride (PVDF)]. The PPE signal from the pyroelectric transducer is due to a temperature dependent change in polarization of the pyroelectric material [23-25].

The PPE technique is the only photothermal technique based on the direct detection of photothermal heating, i.e., on the temperature changes. Therefore, it has a number of advantages over other detection schemes involving secondary mechanisms [32, 33], since each conversion step in the signal generation degrades the overall signal to noise ratio, sensitivity and band width performance and complicates the theoretical interpretation of results. A PPE experiment is rather simple to design and the specimen needs no special preparation. The materials that can be investigated range from weakly absorbing solids like thin films [24, 34-36] or liquids [37], semiconductors [38], surfaces and absorbates [32, 35, 39, 40] to strongly absorbing solids [41] and liquids [42, 43] or diffusing materials [23].

Mandelis and Zver in 1985 [30] put forward a one-dimensional analysis of the photopyroelectric model of a solid sample in intimate contact with a pyroelectric thin film, supported on a backing material. They were successful in deriving a general expression for the pyroelectric voltage developed in the detector due to light absorption in the sample. The calculations showed that the photopyroelectric voltage is governed by the interplay between the optical absorption in the sample and in the

pyroelectric transducer itself. These theoretical calculations helped to establish photopyroelectric spectroscopy as a valid spectroscopic technique with high promise in the realm of non-destructive probing of samples with minimal preparation. These features set this technique ahead of photoacoustic and photothermal deflection spectroscopies in certain respects.

In 1989, Chirtoc and Mihailiscu [27], generalized the theory by Mandelis and Zver, to understand the role played by finite reflectance at the sample pyroelectric interface and the mechanism responsible for the peak inversions observed in the reflection mode PPE spectroscopy [42, 44], since these questions have found no satisfactory answers in the frame work of the former theory. It is seen that, the assumption of an arbitrary value for reflectance, completely changes the physical nature of the PPE effect, featuring simultaneous optical absorption and transmission characteristics. Also, it creates very diverse experimental opportunities for optical and thermal investigations of solid, liquid and gaseous substances.

Complete characterization of a material requires the determination of thermal transport properties such as thermal conductivity and heat capacity. Conventional techniques used to measure thermal conductivity include the well known steady state and transient methods. Comparatively large size samples, typically of size $5mm^3$ or higher are needed while using these techniques to avoid boundary effects. Moreover, large temperature rise often becomes necessary to obtain a reasonable signal-to-noise ratio, leading to considerable temperature gradient being setup in the sample. However, techniques for high resolution measurements of specific heat capacity are well established [45, 46].

It has been shown that the photothermal techniques allow the simultaneous measurement of specific heat capacity c_{ps} and thermal conductivity K_s [47]. The photoacoustic technique has been used for the simultaneous determination of thermal diffusivity, thermal conductivity and heat capacity of liquid crystalline compounds [48], but some restrictions are imposed on this technique, because considerable complications arise in the design of the cell due to the presence of a coupling fluid. Marinelli *et al.* [47] were quite successful in developing a technique for determining thermal diffusivity, thermal conductivity and heat capacity simultaneously at low temperatures with the pyroelectric detector kept in vacuum. The boundary conditions involved in the theory of this method are not easy to satisfy at temperatures above room temperature. We have used a photopyroelectric technique for the simultaneous determination of thermal conductivity and heat capacity of samples in which the pyroelectric transducer is in contact with a thermally thick backing medium [49]. The advantage of a thermally thick backing medium is that there will be sufficient heat exchange between the heated pyroelectric detector and the backing so that, signal fluctuations can be reduced to a minimum.

2.3.1 Principle of the technique.

The PPE technique is based on the use of a pyroelectric transducer to detect the temperature rise due to periodic heating of a sample by induced light. A one-dimensional geometry as shown in Fig. 2.3 is assumed where *g*, *s*, *d* and *b* refer to the gas medium in front of the sample, the sample, the pyroelectric detector and the backing medium respectively. Since the observed signal output is affected by the

impedance of the detector and subsequent detection electronics, an equivalent circuit as shown in Fig. 2.4 is considered.

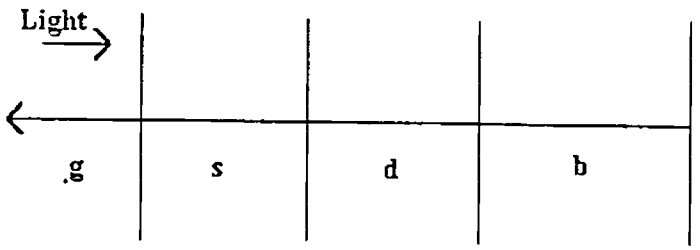

Fig. 2.3 One-dimensional geometry of PPE set up
g, *s*, *d* and *b* refer to the gas medium in front of the sample, the sample, the pyroelectric detector and the backing medium respectively

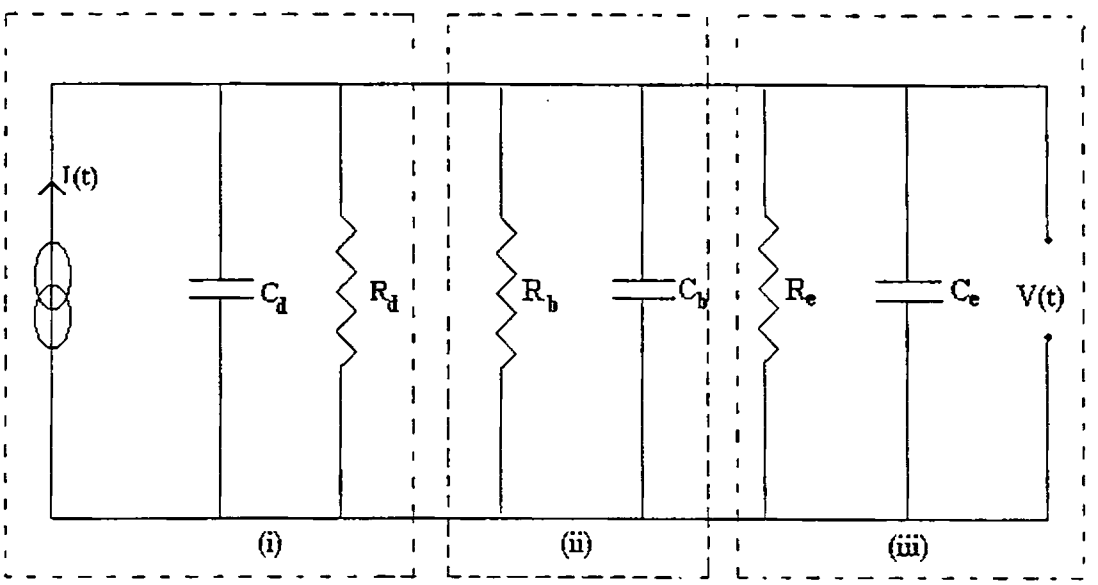

Fig. 2.4 Equivalent circuit for (i) the pyroelectric transducer (ii) the copper backing and (iii) the detection electronics

Here, the pyroelectric detector is described as an ideal current source with a parallel leakage resistance R_d, with a capacitance C_d supported on a backing having an equivalent parallel load resistance R_b and capacitance C_b, while the detection electronics is represented by an input capacitance C_e and a parallel load resistance

R_e. For an optically opaque and thermally thick sample and pyroelectric detector, the expression for temperature dependent PPE amplitude and phase are given by [49]

$$V(f,T) = \frac{I_0 \eta_s A R_s}{L_d\left[1+\left(\frac{f}{f_c}\right)^2\right]^{1/2}} \frac{P(T)}{\rho_d(T) c_{pd}(T)} \frac{exp\left[\left(\frac{\pi f}{\alpha_s}\right)^{1/2} L_s\right]}{\left[\frac{e_s(T)}{e_d(T)}+1\right]} \qquad (2.13)$$

and

$$\phi(f,T) = -tan^{-1}\left(\frac{f}{f_c}\right) - \left(\frac{\pi f}{\alpha_s(T)}\right)^{1/2} L_s \qquad (2.14)$$

where Io = intensity of incident radiation

η_s = non-radiative quantum efficiency

A = area of the pyroelectric transducer

R_d = resistance of the detector

$P(T)$ = pyroelectric coefficient of the detector

$\rho_d(T)$ = density of the detector

$C_{pd}(T)$ = heat capacity of the detector

f_c = critical frequency = $\frac{1}{2\pi RC}$, with

$\frac{1}{R} = \frac{1}{R_d} + \frac{1}{R_b} + \frac{1}{R_e}$ and $C = C_d + C_e + C_b$

f = modulation frequency

$\alpha_s(T)$ = thermal diffusivity of the sample

$e_s(T)$ = thermal effusivity of the sample

For a thermally thick sample ($\mu_s < L_s$) and a thermally thick pyroelectric detector ($\mu_d < L_d$) the expressions for the PPE phase and amplitude give formulae for the values of thermal diffusivity and thermal effusivity of the sample. This allows the determination of thermal conductivity and heat capacity of the sample, if the sample density is known. It is clear from Eqs. (2.13) and (2.14) that, thermal diffusivity $\alpha_s(T)$ of the sample can be calculated from the phase of the PPE signal, which when substituted into the expression for the PPE amplitude gives the thermal effusivity of the sample. Thermal conductivity and heat capacity of the sample can be calculated using the following relations.

$$K_s(T) = e_s(T)[\alpha_s(T)]^{1/2} \tag{2.15}$$

$$C_{p_s}(T) = \frac{e_s(T)}{\rho_s(T)[\alpha_s(T)]^{1/2}} \tag{2.16}$$

2.3.2 Measurement of thermal parameters

A schematic diagram of the PPE sample cell used for the measurements is shown in Fig. 2.5. A 120 mW He-Cd laser of $\lambda = 442$ nm is used as the optical heating source. A mechanical chopper (Model SR540) is used to modulate the light beam. A PVDF film of thickness 28 μm with pyroelectric coefficient = 0.25 x 10^{-8} V cm^{-1} K^{-1} at room temperature has been used as the pyroelectric detector. The room temperature values of the resistance and capacitance of the pyroelectric detector are 50 GΩ and 750 pF respectively [50]. The sample is attached to the pyroelectric detector by means of a thermally very thin layer of a compound, whose contribution to the signal is negligible. The pyroelectric detector attached to the sample is placed on a thermally thick backing medium made up of copper, which satisfies the boundary

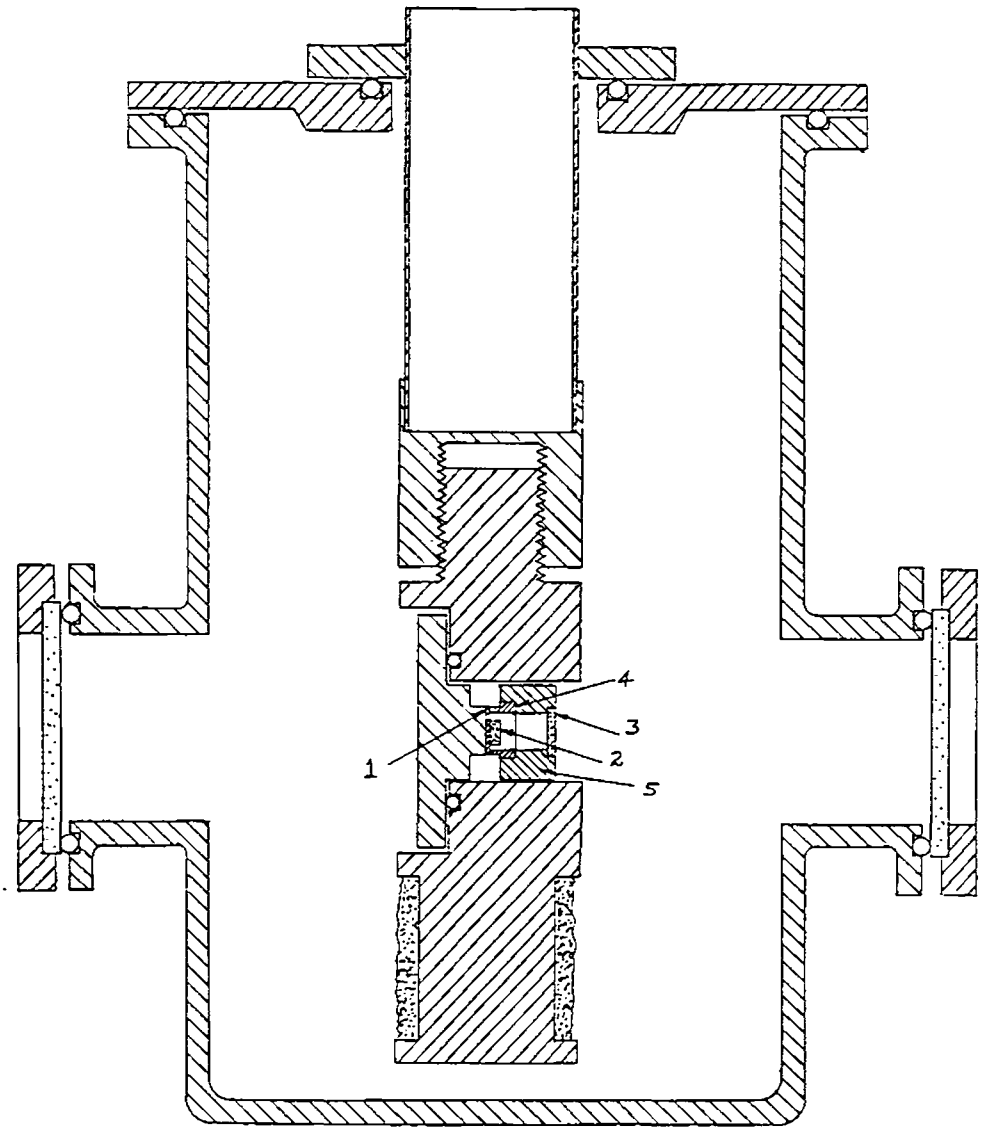

Fig. 2.5 Schematic diagram of the PPE cell

1. PVDF detector 2. sample 3. glass window 4. copper ring 5. teflon outer cover

condition $b_{bd} > 1$. The sample configuration for the PPE set up to measure thermal parameters is shown in Fig. 2.6. The frequency of modulation of light is kept above 30 Hz to ensure the thermal thickness of the sample, detector and backing medium. The signal output is measured using a dual phase lock-in amplifier (Model SR 830). A block diagram of the experimental set up is shown in Fig. 2.7.

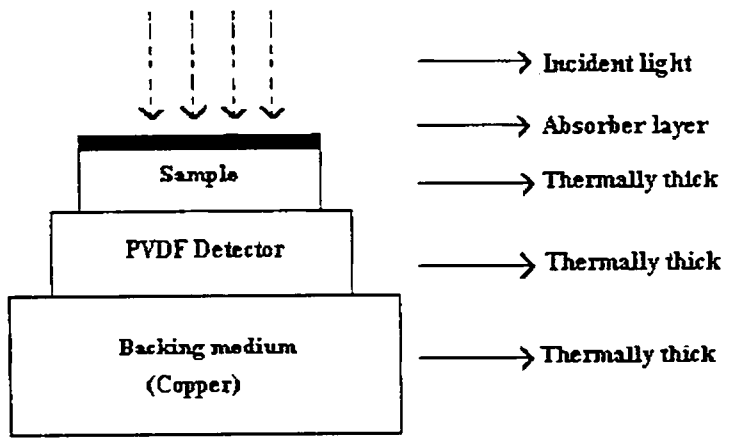

Fig. 2.6 The sample configuration for the PPE setup

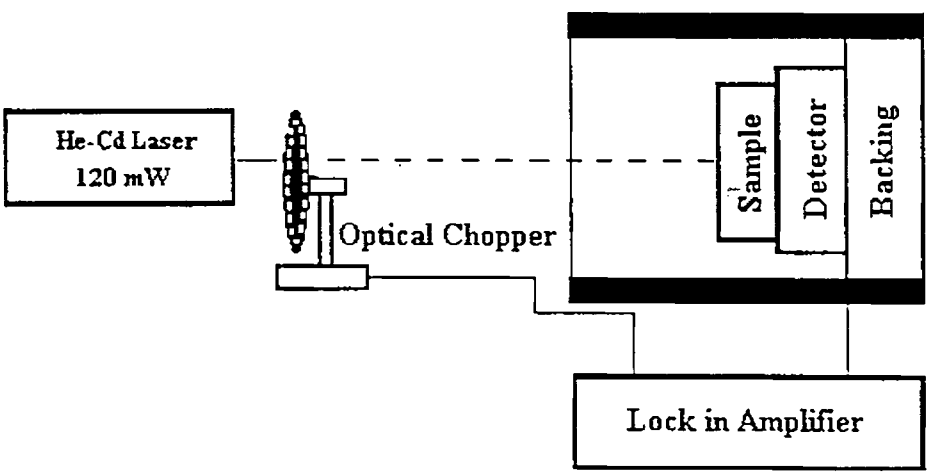

Fig. 2.7 Block diagram of the PPE set up

2. 4. Phototconductivity experiments

The basic requirements for a photoconductivity set up include a radiation source of sufficient intensity in the required spectral range, a conductivity cell in which sample is mounted and irradiated with the light beam and necessary instruments to measure the signal produced.

A schematic diagram of the photoconductivity cell used in our experiments is shown in Fig. 2.8. The cell consists of the following parts, (i) an outer chamber, (ii) a cylindrical tube which acts as liquid nitrogen reservoir for the purpose of making low temperature measurements and (iii) a sample holder. External electrical connections to the cell are provided through a port provided on the top plate of the chamber. This port is provided with four BNC connectors for connections from the sample, a D-type connector for taking the signal from the temperature sensor and another connector for heater supply.

2.4.1 Measurement of Photoconductivity

Photoconductivity measurements can be carried out either by d.c. (steady state) method or by a.c. (pulsed excitation) method. For the present investigations, we have used the d.c. method. In this method, the dark current (I_d) and the current under steady state illumination (I_{ill}) are measured. The photocurrent is given by [51]

$$I_{ph} = I_{ill} - I_d \qquad (2.17)$$

Photoconductivity can be measured by either the two-probe method or the four-probe method, depending on the resistivity and geometry of the sample. If the samples have high resistivity, contact resistance can be neglected and two-probe technique can be used, provided the sample has a regular shape. We have used the

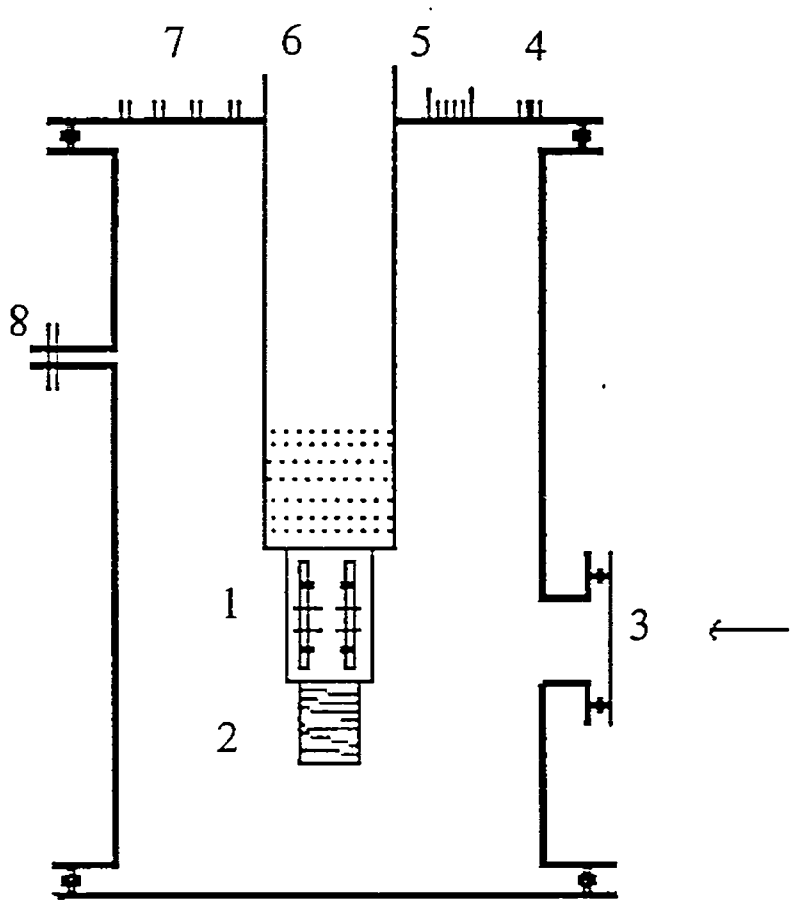

Fig. 2.8 A schematic diagram of the photoconductivity cell
(1) sample holder (2) heater (3) glass window (4) heater supply (5) connector for temperature sensor (6) liquid nitrogen reservoir (7) BNC connectors (8) connector to vacuum pump

two-probe method for our measurements and the block diagram of the experimental set up is shown in Fig. 2.9.

The samples are polished and shaped to exact square or rectangular shapes. The electrodes are connected either in coplanar or sandwich mode. In our measurements for bulk samples, the sandwich configuration has been used. The sample is sandwiched between two SnO_2 coated glass plates, which are conducting

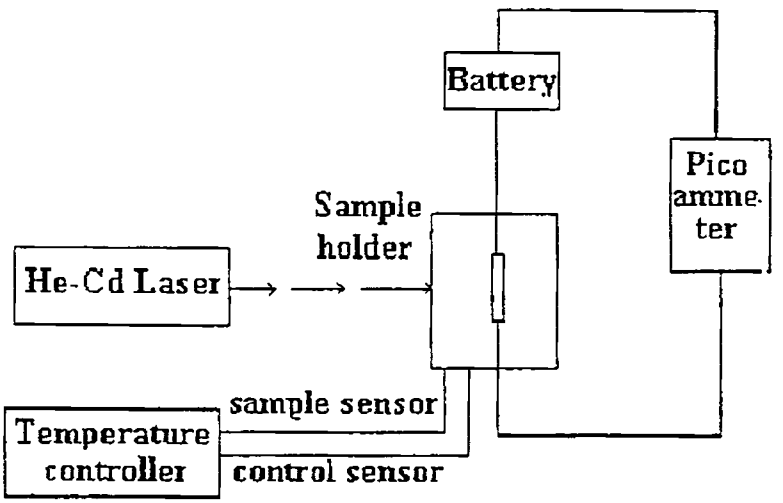

Fig. 2.9 Block diagram of the experimental set up for photoconductivity measurements

and transparent. In this arrangement, the sample can be illuminated through one of the electrodes. The contacts are found to be ohmic from a study of the V-I characteristics of the contacts. A Keithly auto arranging pico ammeter (Model 485) is used for measuring current.

2.5 Electrical switching measurements

Basically, electrical switching measurement setup is more or less the same as that of electrical conductivity. The block diagram of the experimental set up is shown in Fig. 2.10.

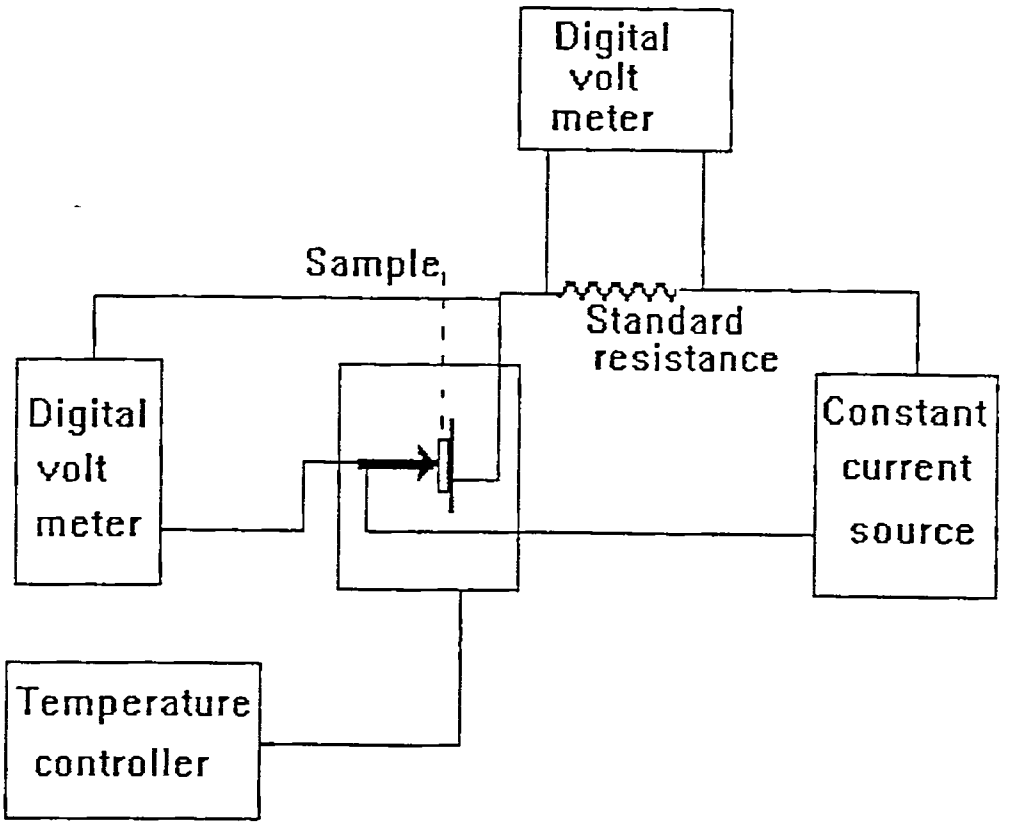

Fig. 2.10 Block diagram of the experimental set up for electrical switching measurements

In the case of switching studies, to get the *V-I* characteristics, a known current is sent through the sample from a constant current source. The voltage developed across the sample is measured by a digital voltmeter. The *V-I* characteristics are determined by varying the current values in steps. Though the current and voltage show a linear variation (ohmic behaviour) initially, for a particular value of current, the voltage across the sample attains a threshold value (V_{th}) and further increase in current results in a decrease of voltage and the sample deviates from the ohmic behaviour to a negative resistance region, which leads to a high conducting state.

2.5.1 Measurement of thermal parameters during electrical switching by PPE technique

A cross sectional view of the sample holder used to study thermal parameters during electrical switching is given in Fig. 2.11. The sample holder is made up of a copper rod having a diameter 5 cm.

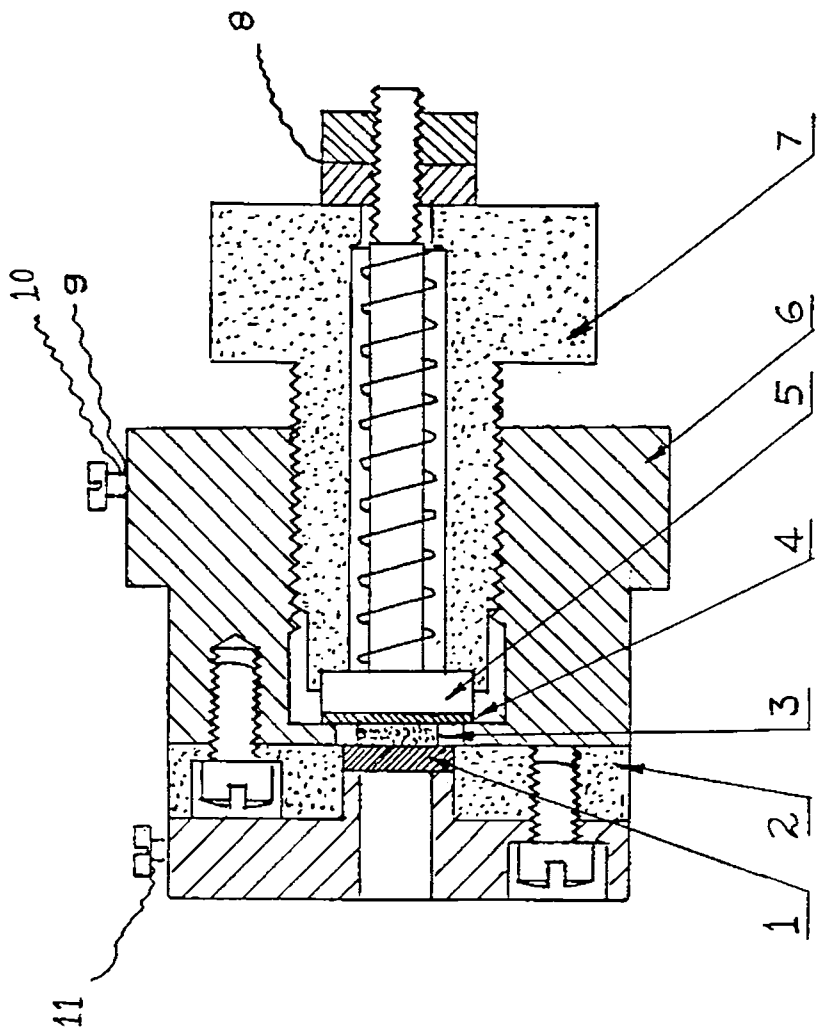

Fig. 2.11 Cross sectional view of photopyroelectric cell for measurment of thermal parameters during electrical switching

1. conducting glass 2. acrylic sheet 3. sample 4. PVDF film 5. copper backing 6. copper body 7. acrylic adjustable holder 8 & 9. connections to BNC 10 & 11. connections to current source

A PVDF film of diameter 10 mm and thickness 28 μm, both side coated with Ni-Cr, supported on a copper backing acts as the PPE detector. The backing is mounted on an adjustable holder made of perspex. Samples of thickness ≈ 0.2 mm are mounted on the PVDF film using a thin layer of heat sink compound whose contribution to the signal is negligible. Electrical connections are taken between points 10 and 11 in Fig. 2.11. The sample can be illuminated through the top electrode, which is made of conducting glass. The pyroelectric voltage is measured between points 8 and 9 in Fig 2.11. Other measurement procedures are as already discussed in the previous sections.

2.6 Radiation Source

Incandescent or arc lamps and lasers are two popular types of light sources currently used for photothermal as well as photoconductivity experiments. The lamp monochromator combination can provide continuous tunability over a wide wavelength range from the infrared to the vacuum ultra violet. High pressure Xenon arc lamps, high pressure Hg lamps, tungsten lamps etc. are the commonly used incandescent sources. A major drawback of these sources is the relatively low bandwidth throughput product. A monochromator output power of 0.1mW is typical for 1nm resolution using a high pressure Xe arc lamp. Consequently, the lamp-monochromator combination is used with strongly absorbing samples or where low resolution suffices.

Lasers are widely accepted light sources in photothermal experiments, especially for measuring weak absorption. This is mainly because of their high

spectral radiance resulting from the extremely narrow line widths and high collimation. Because of spectral purity, lasers can be effectively used for high resolution PA spectroscopy experiments. One main drawback of lasers is their limited tunability.

2.7 Modulation

Modulation of the incident light beam is essential for the generation of photothermal signals. Either the amplitude or the frequency of the incident beam can be modulated, amplitude modulation being the more commonly used method. Amplitude modulation can be achieved by one of the several methods such as mechanical, electrical, electro-optic etc. One of the inexpensive, efficient and common methods to accomplish amplitude modulation is to use a mechanical chopper. The depth of modulation in this case is $\approx$ 100%. While using a mechanical chopper, care should be taken to minimize the vibration noise as this may interfere with the signal generated and cannot be filtered off even by lock-in detection. In the case of electrical CW lasers, modulation can be achieved by varying the discharge tube current. Electro-optic modulation involves changing the plane of an incoming polarized light beam in a non-linear crystal (e.g. KDP, ADP etc.) by the application of a modulated electric field across the crystal. Frequency modulation can be employed to eliminate the photothermal signals generated due to wavelength independent absorption at the cell windows. In dye lasers, rapid frequency change can be obtained by using an electro-optic tuner in place of a birefrengent filter. Frequency modulation is well suited for narrow line width absorbers such as atomic and diatomic species.

2.8 UV-Vis-NIR Spectrophotometer

A UV-Vis-NIR spectrophotometer has been used to determine the optical band gap of samples under investigation. Hitachi model U-3410 double beam recording spectrophotometer has been employed for this purpose. It comprises of a monochromator section (including control section), display section, floppy disk section, graphics plotter and operating section. The system is equipped with various functions, which can be used in combination with a variety of optional accessories for all types of analytical applications and is especially suited for material characterization. This unit has a wavelength range 187 to 2600 nm with 0.07 nm resolution. The wavelength accuracy is 0.2 nm in the UV-Vis range and $\pm$ 1 nm in the NIR range. The monochromator adopts the model 340 prism / grating double monochromatic system. The lenses used in the conventional monochromator have all been replaced by mirrors to eliminate image deviation due to chromic aberration. The PbS detector converges the light beam with a torroidal mirror located below the photomultiplier. This permits placing the PbS symmetrically against the sample and reference beams whereby the two beams are completely balanced. A mechanical chopper is placed before the first monochromator to chop the light beam, which minimizes deviation in zero signal. The long life, easily replaceable iodine free tungsten lamp is used as the visible wavelength light source. The photometric output from the detector is fed through the preamplifier to an A/D converter and input into the computer, where it is discriminated into reference signal, sample signal and zero signal for storage by gate signals obtained in synchronization with rotation of the sector mirror for splitting the light beam. The reference signal is compared with a

predetermined standard value and used for controlling the voltage applied to the dynode of the photomultiplier.

2.9 Sample preparation

As already stated in the previous chapter, there exists a number of techniques to prepare amorphous materials. Since the amorphous phase is thermodynamically less stable than the corresponding crystalline form, its preparation can be regarded as the addition of excess free energy in some manner to the crystalline polymorph, which can be done by faster rate of cooling.

The most common method for preparing bulk amorphous material is the melt quenching technique. Amorphous materials produced in this manner are often been termed as glasses. The distinguishing feature of the melt quenching process of producing amorphous materials is that the amorphous solid is formed by continuous hardening (i.e., increase in viscosity) of the melt. On the other hand, crystallization of the melt occurs as a discontinuous solidification process. An essential prerequisite for the glass formation from the melt is that the cooling be sufficiently fast to preclude crystal nucleation and growth. The crystalline phase is thermodynamically more stable and crystal growth will always dominate over the formation of amorphous phase if allowed to take place. Cooling rate is often a critical factor in determining glass formation.

The most usual way of producing samples of easy glass formers is to seal the charge (1 to 10 g) in a fused silica or quartz ampoule under a good vacuum (~ 10^{-6} Torr) and keep the ampoule in a rocking or rotating furnace at sufficiently elevated temperatures so that the constituents become molten and can react. The rocking

motion ensures that a thorough mixing of the constituents takes place. The melt can be quenched either slowly by simply switching off the furnace, or more rapidly by plunging the ampoules into air or even more rapidly by bringing the ampoules immediately from the furnace into a liquid, preferably one with a high thermal conductivity and high latent heat of vapourization so that heat is conducted away from the sample as fast as possible without the formation of a thermally insulating vapour layer around the ampoule. In this manner, cooling rates of the order of 10^2 to 10^3 K/s are achievable. The parameters that are important in the melt quenching method are, (1) temperature of the furnace, (2) rate of cooling, (3) volume of the charge in the ampoule and (4) thickness of the wall of the ampoule. Materials produced in this manner are often in the form of a plug or a rod.

Chalcogenide glass samples for the present investigations have been prepared by the melt quenching technique. Appropriate quantities of the constituents are weighed and taken in quartz ampoules, which are then evacuated and sealed. The ampoules are then kept in a high temperature furnace and heated slowly to a temperature well above the melting points of the constituents. The ampoules are kept at that temperature for nearly 24 hours and then suddenly quenched to ice water. Then the ampoules are broken open to obtain the shiny glass samples. The amorphous nature of the samples is then confirmed by X-ray diffraction technique.

References

1. W. W. Wendlandt and H.G Hecht, *Reflectance Spectroscopy*, (Wiley, New York 1966)
2. P. A. Wilks Jr. and T. Hirschfeld, Appl. Spectrosc. Rev. **1**, (1986) 99
3. G. B. Wright (Ed), *Light Scattering in Solids*, (Springer-Verlag, Berlin and New York, 1969)
4. A. Rosencwaig, Opt. Commun. 7 (1973) 305
5. A. Rosencwaig, Anal. Chem. **47** (1975) 592A
6. A. Rosencwaig in *Advances in Electronics and Electron Physics*, Vol. 46, edited by L. Marton, (Academic Press, New York, 1978) pp. 207-311
7. A. Rosencwaig, *Photoacoustics and Photoacoustic Spectroscopy*, (Wiley, New York, 1980)
8. A. G. Bell, Amer. J. Sci. **20** (1880) 305
9. A. G. Bell, Phil. Mag. **11** (1881) 510
10. J. G. Parker, Appl. Opt. **12** (1973) 2974
11. A. Rosencwaig and A. Gersho, Science **190** (1975) 556
12. A. Rosencwaig and A. Gersho, J. Appl. Phys. **47** (1976) 64
13. W. J. Parker, R. J. Jenkins, C. P. Butler and G. L. Abdot, J. Appl. Phys. **32** (1961) 1679
14. B. Abeles, G. D. Cody and D. S. Beers, J. Appl. Phys. **31** (1960) 1585
15. M. J. Adams and G. F. Kirkbright, Analyst **102** (1977) 678
16. M. J. Adams and G. F. Kirkbright, Analyst **102** (1977) 281
17. K. Yamashita, H. Kasahara, K. Yamamoto and K. Abe, Jpn. J. Appl. Phys. **21**, suppl. 21-23 (1982) 107

18. U. Zammit, M. Marinelli, F. Scudieri and S. Martelluci, High Temp-High Pressure **18** (1986) 551

19. R. T. Swimm, Appl. Phys. Lett. **42** (1983) 955

20. A. Lachaine and P. Poulet, Appl. Phys. Lett. **45** (1984) 953

21. K. N. Madhusoodanan, Mini. R. Thomas and J. Philip, J. Appl. Phys. **62(4)** (1987) 1162

22. Sheenu Thomas and J. Philip, Rev. Sci. Instrum. **66** (1995) 3907

23. A. Mandelis, Chem. Phys. Lett. **108** (1984) 388

24. H. Coufal, Appl. Phys. Lett. **44** (1984) 59

25. H. Coufal and A. Mandelis, Ferroelectrics **118** (1991) 379

26. A. Mandelis, J. Vanniasinkam and S. Budhudu, Phys. Rev. B **48** (1993) 6808

27. M. Chirtoc and G. Mihailescu, Phys. Rev. B **40** (1989) 9606

28. J. Shen and A. Mandelis, Rev. Sci. Instrum. **66** (1995) 4999

29. A. Mandelis and K. F. Leung, J. Opt. Soc. Am. A **8** (1991) 186

30. A. Mandelis and M. M. Zver, J. Appl. Phys. **57** (1985) 4421

31. J. Shen, A. Mandelis and H. Tsai, Rev. Sci. Instrum. **69** (1998) 197

32. H. Coufal and Z. Fresenius, Anal. Chem. **324** (1986) 456

33. H. Coufal, IEEE Trans. Ultrason. Ferroelectric. Freq. Control **UFFC-33** (1986) 507

34. H. Coufal, Appl. Phys. Lett. **45** (1984) 516

35. H. Coufal, R. Grygier, D. Horne and J. Fromm, J. Vac. Sci. Technol. A **5** (1987) 2875

36. H. Coufal, J. Stöhr and K. Baberschke in *Photoacoustic and Photothermal Phenomena*, edited by P. Hess and J. Pelzl, (Springer, Heidelberg, 1988) p.25

37. T. Hinoue, S. Kawada, M. Murata and Y. Yokoyama, Chem. Lett. Jpn. (1988) 2061

38. *Photoacoustic and Thermal Wave Phenomena in Semiconductors*, edited by A. Mandelis, (Elsevier, New York, 1987)

39. R. K. Grygier, W. Knoll and H. Coufal, Can. J. Phys. **64** (1986) 1067

40. T. J. Chuang, H. Coufal and F. Träger, J. Vac. Sci. Technol. A **1** (1983) 236

41. D. Dădârlat, M. Chirtoc, R. M. Cândea and I. Bratu, Infrared Phys. **24** (1984) 469

42. M. Chirtoc, D. Dădârlat, I. Chirtoc and D. Bicanic, Spectrosc. Lett. **21** (1988) 413

43. M. Chirtoc, D. Dădârlat, I. Chirtoc and D. Bicanic in *Photoacoustic and Photothermal Phenomena*, edited by P. Hess and J. Pelzl, (Springer, Heidelberg, 1988)

44. M. Chirtoc and I. Chirtoc, Infrared Phys. **29** (1989) 847

45. G. B. Kasting, C. W. Garland and K. J. Lushington, J. Physique **41** (1980) 879

46. T. Thoen, H. Marynissen and W. van Dael, Phys. Rev. A **26** (1982) 2886

47. M. Marinelli, F. Murtas, M. G. Mecozzi, U. Zammit, R. Pizzoferrato, F. Scudieri, S. Martellucci and M. Marinelli, Appl. Phys. A **51** (1990) 387

48. U. Zammit, M. Marinelli, R. Pizzoferrato, F. Scudieri and S. Martellucci, J. Phys. E: Sci. Instrum. **21** (1988) 935

49. C. Preethy Menon and J. Philip, Meas. Sci. and Technol. **11** (2000) 1744

50. 1983 Kynar™ Piezo Film Technical Manuel (Penwalt Corp.) p.17

51. S. K. Tripathi and A. Kumar, J. Non-Cryst. Solids **104** (1988) 229

CHAPTER-3

Thermal conductivity and heat capacity of Pb-Ge-Se glasses exhibiting carrier type reversal

3.1 Introduction

Chalcogenide glasses containing sulphur, selenium or tellurium constitute a rich family of amorphous semiconductors. There has been an intense research activity on these glasses because of their wide ranging technological applications [1-5]. The effect of impurities on the electronic properties of chalcogenide glasses has been a subject of serious debate ever since their discovery [6].

Bulk chalcogenide glasses prepared by the melt quenching technique are, in general, *p*-type semiconductors owing to the fact that the number of electrons excited above the conduction band mobility edge is smaller than the number of holes excited below the valence band mobility edge [7]. Their conductivity cannot be made *n*-type by adding impurities as in the case of their crystalline counterparts. This behaviour is attributed to the local valence saturation of the dopant atom. These systems also contain positively and negatively charged defect states, known as valence alternation pairs (VAPs) [8, 9], which essentially pin the Fermi level near the middle of the band gap, making them rather insensitive to doping [10].

The creation of charged defects C_3^+ and C_1^- called VAPs, starting from a fully bonded network in which all atoms are in C_2^0 configuration can be described by,

$$2C_2^0 \rightarrow C_1^- + C_3^+ \tag{3.1}$$

The C_3^+ and C_1^- centres subsequently relax to a different configuration and the overall energy is lowered by the effective correlation energy U_{eff}. Whether U_{eff} is positive or negative affects dramatically the movement of the Fermi level when electrons are injected into the system either by the application of an external electric field or by the addition of dopant atoms. Adler and Yoffa [10] considered a single defect capable of being occupied by electrons, and used the grand partition function to calculate the Fermi level position as a function of the number of electrons per defect n ($0 < n < 2$). According to them,

$$E_F = E_{eff} - k_B T \ln\left\{\frac{2|n-1|}{1-|n-1|}\right\} \qquad 0 < n < 1 \tag{3.2a}$$

$$E_F = E_{eff} + U_{eff} + k_B T \ln\left\{\frac{2|n-1|}{1-|n-1|}\right\} \qquad 1 < n < 2, \text{ for } U_{eff} > 0 \tag{3.2b}$$

$$\text{and } E_F = E_{eff} - \frac{|U_{eff}|}{2} - \frac{k_B T}{2} \ln\left\{\frac{2}{n} - 1\right\}, \qquad \text{for } U_{eff} < 0 \tag{3.2c}$$

For positive U_{eff} materials there is a level at E_{eff} for singly occupied states and lying above it at a separation U_{eff} a level corresponding to doubly occupied centres. (Fig. 3.1a). As the electron concentration n increases from zero at $T = 0$ K, the Fermi level rises slowly in the lower singly occupied level. As soon as $n = 1$, The Fermi level jumps discontinuously across the gap of magnitude U_{eff} to the upper level, and subsequently rises gradually through this level until $n = 2$ and all states are doubly

occupied. However, for negative U_{eff} defects, the levels corresponding to double occupancy lie below those for single occupancy, and the density of lower levels is equal to the number of electrons introduced and thus this band is always full. (Fig. 3.1b). The injection of electrons into such a material therefore results in immediate double occupancy of levels without an intermediate n = 1 stage. Thus E_F remains pinned midway between the two levels at an energy E_F - U_{eff} / 2 for all values of n, except when n is very near 0 or 2, as given by Eq. (3.2c) and shown in Fig. 3.1b.

However, of late, it has been found that the addition of certain heavy elemental metallic impurities like Bi or Pb to certain chalcogenide glass systems can cause a change in the conduction type from p to n. This phenomenon of carrier type reversal (CTR) or $p \rightarrow n$ transition was first observed in Bi doped Ge-Se glasses [11, 12] and later in several other glass systems [13-16]. This has led to extensive research on these materials [17-24] and to a reconsideration of the existing theories of electronic structure of chalcogenide glasses [25].

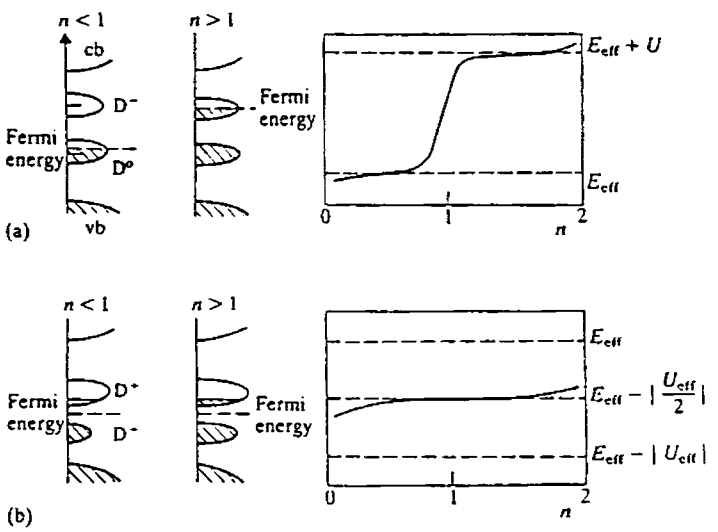

Fig. 3.1 Density of states and Fermi level as a function of electron occupation, n, for (a) $+U_{eff}$ defects; (b) $-U_{eff}$ defects [10].

In this chapter, we report the variations in thermal parameters such as thermal diffusivity (α), thermal effusivity (e), thermal conductivity (K) and heat capacity (c_p) as a function of composition in Pb-Ge-Se system of glasses. Also, the composition dependence of optical band gap of this system of glasses is reported. Pb-Ge-Se system forms homogeneous glass in the following two series.

(i) $Pb_{20}Ge_xSe_{80-x}$ (x = 17-24) and

(ii) $Pb_yGe_{42-y}Se_{58}$ (y = 0-20).

Both these series exhibit CTR at specific compositions [13]. In series I, CTR occurs at $x \approx 21$, while in series II, it occurs at $y \approx 8$ as evidenced by electrical transport measurements. Optical absorption studies were done using a UV-Vis-NIR spectrophotometer, while thermal parameters were measured using photopyro electric (PPE) and photoacoustic (PA) techniques. Details of the experiments, results obtained and a discussion of the results are given in the later sections.

3.2 Sample preparation

Glasses with general formulae $Pb_{20}Ge_xSe_{80-x}$ ($17 \leq x \leq 24$) and $Pb_yGe_{42-y}Se_{58}$ ($0 \leq y \leq 20$) have been prepared in the bulk form using the conventional melt quenching technique. Appropriate atomic proportions of high purity lead (4N), germanium (4N) and selenium (5N) are weighed and taken in cylindrical quartz ampoules, which are then evacuated and sealed. The ampoules are then placed in a furnace, in which the mixture is heated slowly to a temperature of 1000^0C. The ampoules are kept at 1000^0C for nearly 24 hours, with intermittent rotation, for homogeneous mixing of the constituents. Then the ampoules are quenched in ice water, resulting in a cooling rate of ~ 10^2 K/s. Ampoules are then broken open to obtain the glass

samples. The amorphous natures of the samples are confirmed by X-ray diffraction (XRD) technique.

3.3 Optical band gap measurements

Optical band gap of the samples under investigation are determined by recording their optical absorption spectra using a UV-Vis-NIR spectrophotometer. A Hitatchi Model U-3410 recording spectrophotometer has been employed for this purpose. The absorption spectra are recorded using UV-Vis-NIR spectrophotometer for all the samples of both the series. Typical spectra of two samples of either series are given in Figs. 3.2 and 3.3 respectively. Optical band gap can be determined graphically from the absorption spectrum. Variation of optical band gap with composition for $Pb_{20}Ge_xSe_{80-x}$ and $Pb_yGe_{42-y}Se_{58}$ systems are shown in Figs. 3.4 and 3.5 respectively.

3.4 Composition dependence of thermal parameters using PPE and PA techniques

Using the photopyroelectric (PPE) technique described in Chapter 2, thermal parameters of the samples can be determined simultaneously. Thin slices of samples with thickness of the order of 0.5 mm and area of the order of 3 x 3 mm^2 have been cut with a slow speed diamond wheel saw and then hand lapped and polished for the measurements. In the PPE technique, a thermally thick pyroelectric film is attached to one side of the sample, which is also thermally thick, and the combination is mounted on a thermally thick backing medium. The other side of the sample is

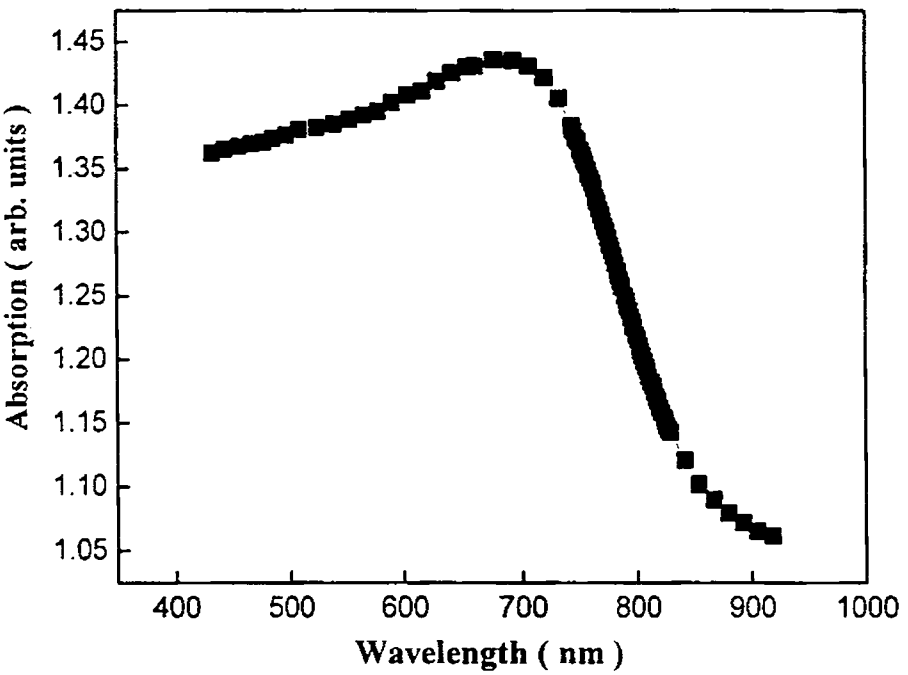

Fig. 3.2 Optical absorption spectrum of $Pb_{20}Ge_{22}Se_{58}$ glass.

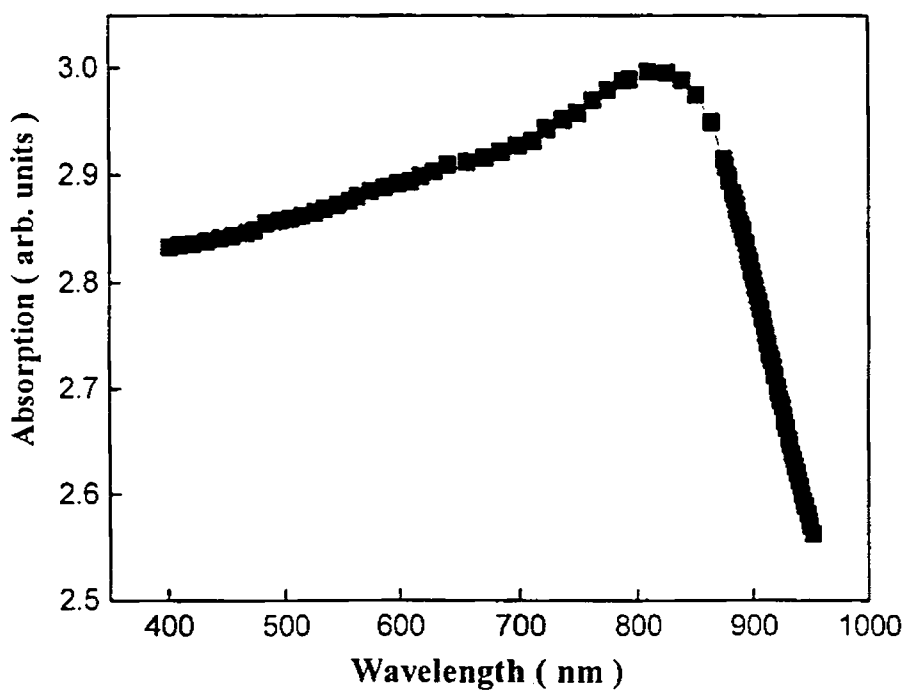

Fig. 3.3 Optical absorption spectrum of $Pb_{14}Ge_{28}Se_{58}$ glass.

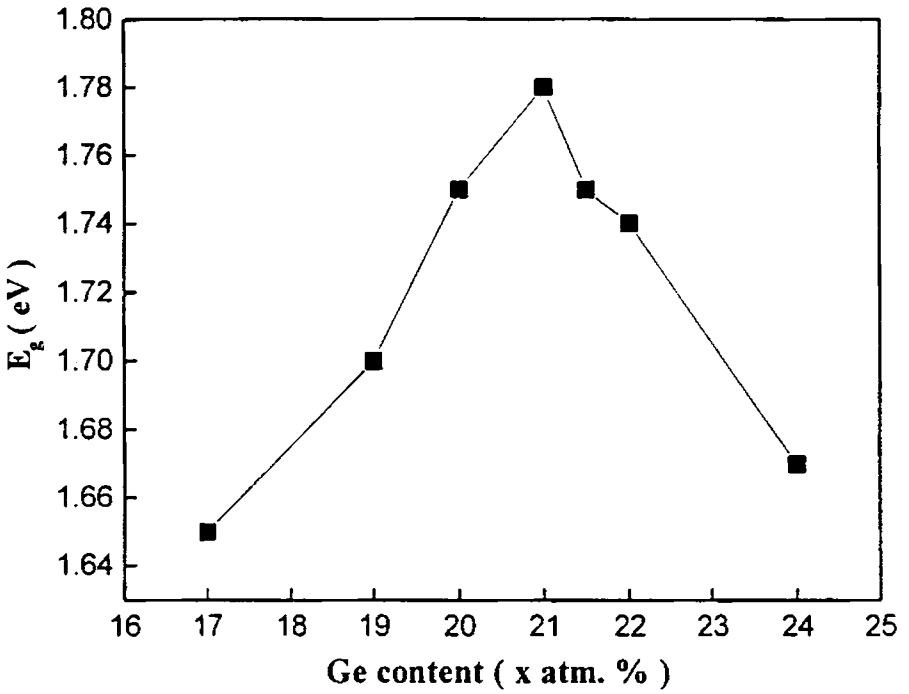

Fig. 3.4 Variation of optical band gap with composition for $Pb_{20}Ge_xSe_{80-x}$ glasses. Uncertainties in the values are less than 2%.

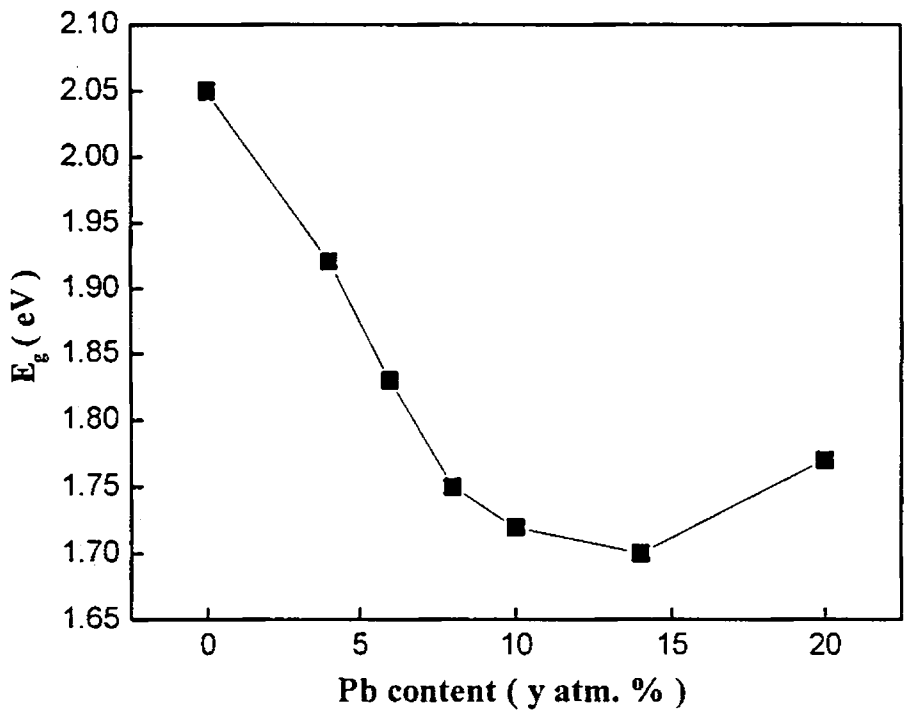

Fig. 3.5 Variation of optical band gap with composition for $Pb_yGe_{42-y}Se_{58}$ glasses. Uncertainties in the values are less than 2%.

illuminated by a beam of light, modulated in intensity, which gives rise to periodic temperature variations by optical absorption. The thermal waves so generated propagate through the sample and are detected by the pyroelectric detector. A mechanical chopper (Model SR540) has been used to modulate the light beam and the signal is measured using a dual phase lock-in amplifier (Model SR830). A 120 mW He-Cd laser of wavelength 442 nm has been used as the radiation source and a polyvinylidene difluoride (PVDF) film of thickness 28 μm, both sides coated with Ni-Cr film, as the pyroelectric detector.

A careful calibration of the experimental setup and procedure has been done prior to carry out the measurements. The thermal thickness of the PPE detector at the used modulation frequency has been ensured by plotting the PPE signal amplitude and phase with frequency with the detector itself acting as the sample. These are shown in Figs. 3.6 and 3.7 respectively. Similarly, the thermal thicknesses of the samples are also ensured and the corresponding plots are shown in Figs. 3.8 to3.11. A modulation frequency of 40 Hz has been used for the determination of thermal parameters of the samples, which ensures the thermal thickness of the sample, detector and the backing medium. Measurement of PPE signal phase and amplitude enables one to determine thermal diffusivity ($\alpha = K / \rho c_p$, ρ being the density of the sample) and thermal effusivity ($e = \sqrt{K \rho c_p}$) respectively of the sample under investigation. Once the density ρ of the sample is determined, thermal conductivity (K) and heat capacity (c_p) of the sample can be calculated. Measurement on each sample has been repeated many times. It is found that the variations of output signal (PPE amplitude and phase) between sample mountings are very small (less than 1%)

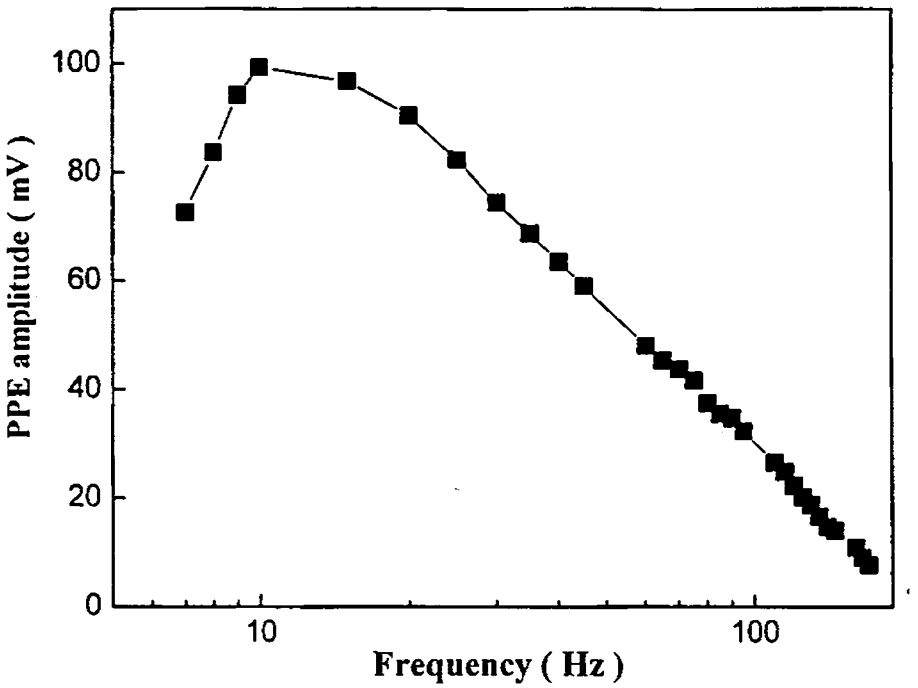

Fig. 3.6 Frequency dependence of PPE amplitude of PVDF film at room temperature.

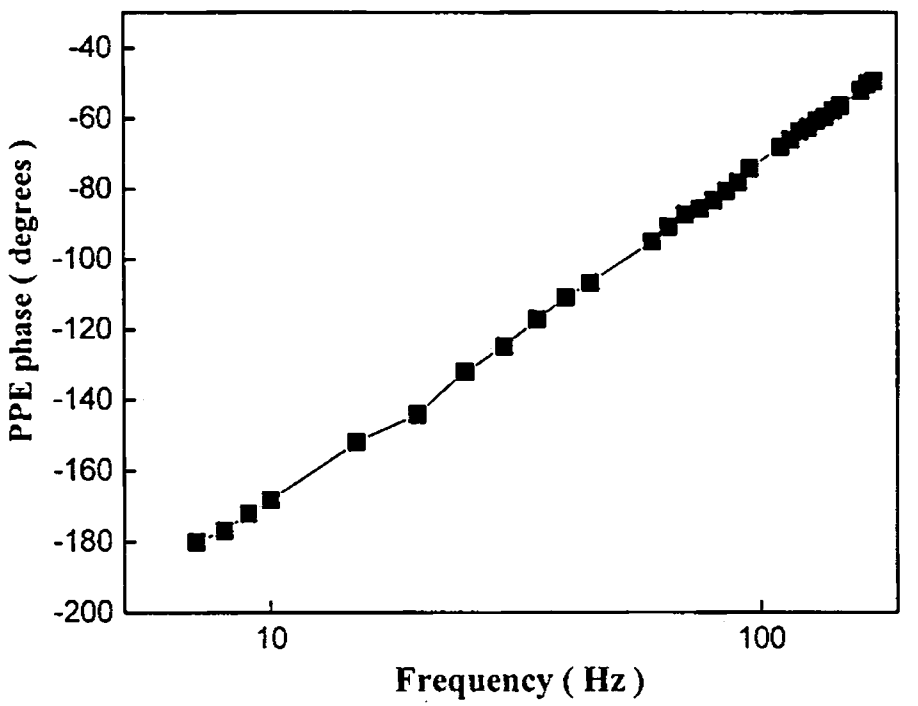

Fig. 3.7 Frequency dependence of PPE phase of PVDF film at room temperature.

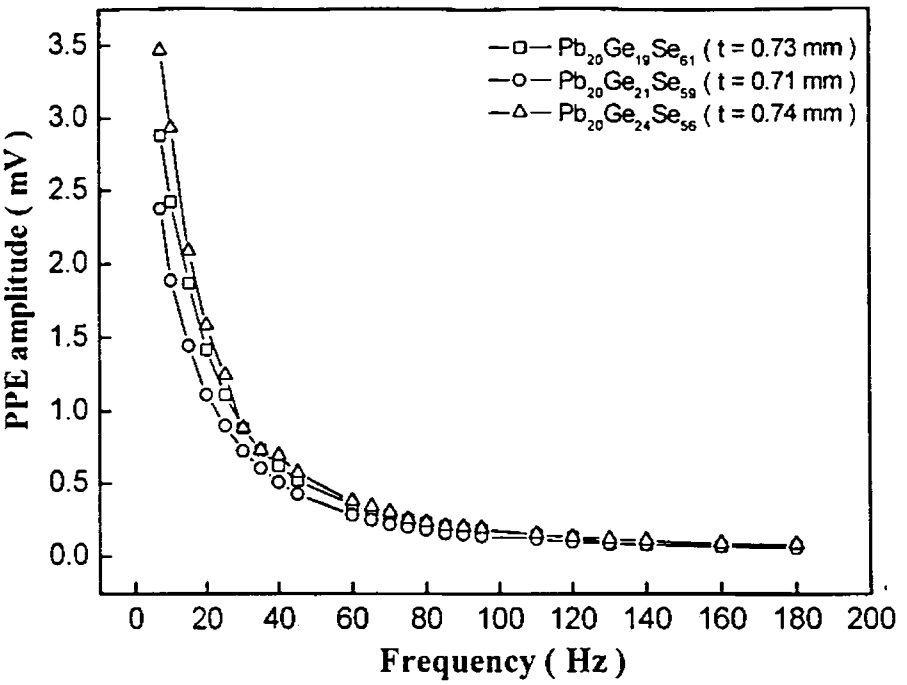

Fig. 3.8 Frequency dependence of PPE amplitude for different compositions of $Pb_{20}Ge_xSe_{80-x}$ glasses.

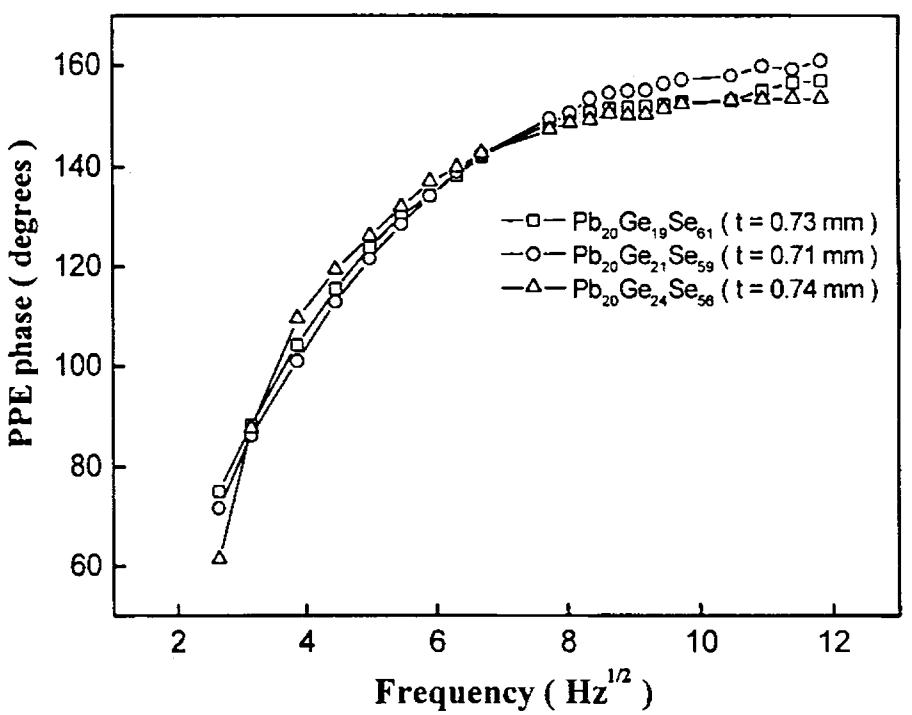

Fig. 3.9 Frequency dependence of PPE phase for different compositions of $Pb_{20}Ge_xSe_{80-x}$ glasses.

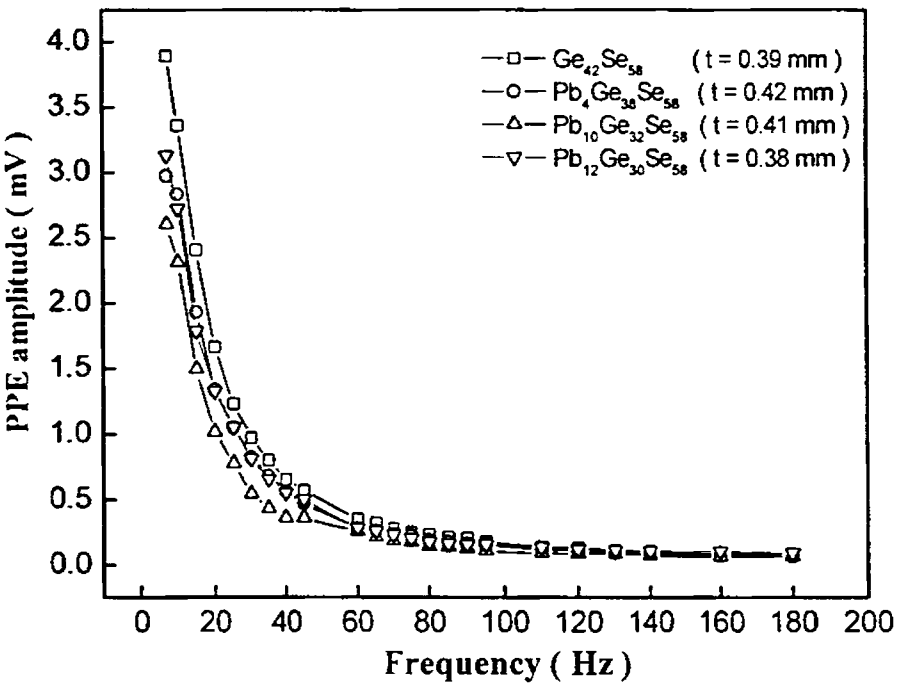

Fig. 3.10 Frequency dependence of PPE amplitude for different compositions of $Pb_yGe_{42-y}Se_{58}$ glasses.

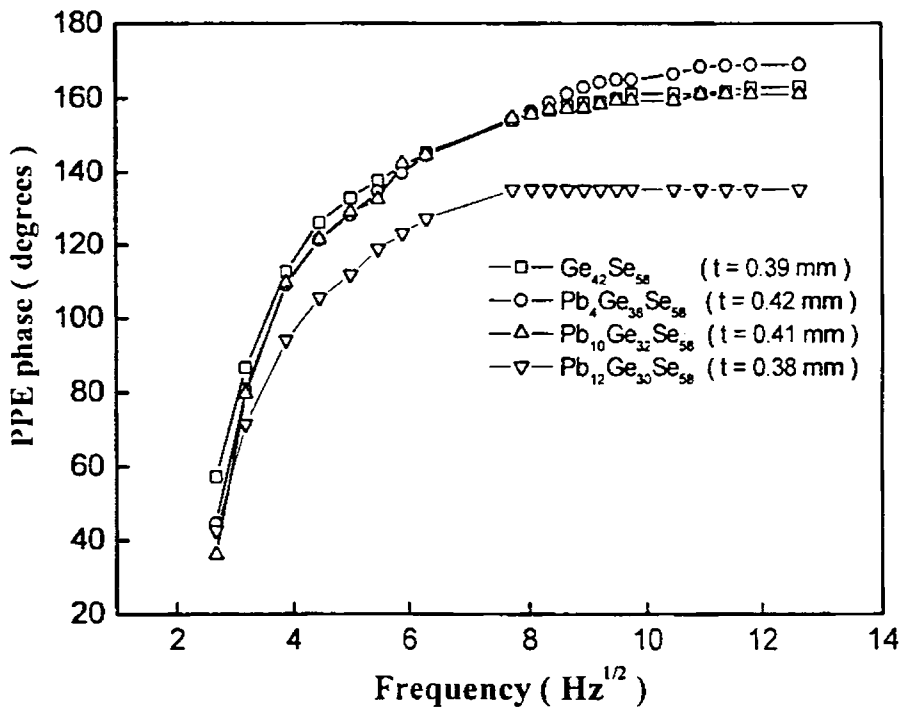

Fig. 3.11 Frequency dependence of PPE phase for different compositions of $Pb_yGe_{42-y}Se_{58}$ glasses.

ensuring that variations in thermal impedance between sample mountings are negligible. The estimated uncertainty in the measured values of K and c_p is less than 2%.

Composition dependence of thermal diffusivity of both the sets of glasses has been determined independently using the photoacoustic phase lag technique described in Chapter 2. The sample is mounted on a metallic ring using a thin layer of vacuum grease and placed in the sample chamber. Relative phase lag $\Delta\Psi = \Psi_F - \Psi_R$ of the generated PA signals between the front and rare surfaces of illuminations when the sample is irradiated by a single light beam is determined by rotating the PA cell freely by 180^0 about a vertical axis. In this case also, a He-Cd laser is used as the source of radiation and a mechanical chopper (Model SR540) is used to modulate the light beam. A dual phase lock-in amplifier (Model SR830) is used to measure the PA signal. Once $\Delta\psi$ is obtained, thermal diffusivity of the sample can be determined as described in Chapter 2.

3.5 Results

The variations of thermal diffusivity and thermal effusivity with Ge content (x) for series I glasses is shown in Fig. 3.12. Both the parameters show a clear change of slope at x = 21, the composition at which carrier type reversal occurs. Fig. 3.13 shows the corresponding curve for series II glasses. In this case, thermal diffusivity shows a minimum, while thermal effusivity shows a maximum at the critical composition (y = 8). Variation of thermal diffusivity as a function of composition for both the sets of glasses as obtained by the PA technique are shown in Figs. 3.14 and 3.15, which agree very well with those obtained by the PPE technique.

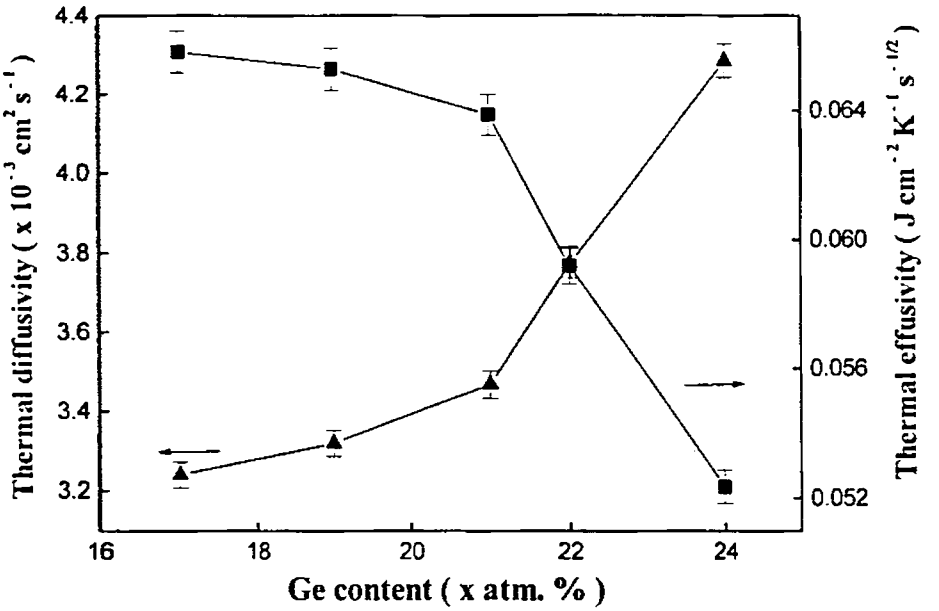

Fig. 3.12 Composition dependence of thermal diffusivity and thermal effusivity of $Pb_{20}Ge_xSe_{80-x}$ glasses.

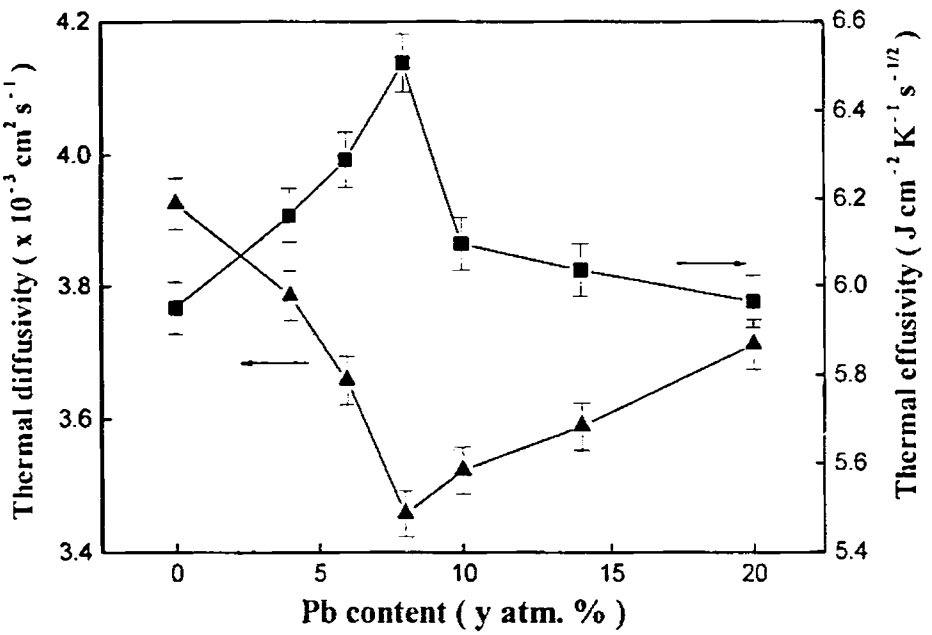

Fig. 3.13 Composition dependence of thermal diffusivity and thermal effusivity of $Pb_yGe_{42-y}Se_{58}$ glasses.

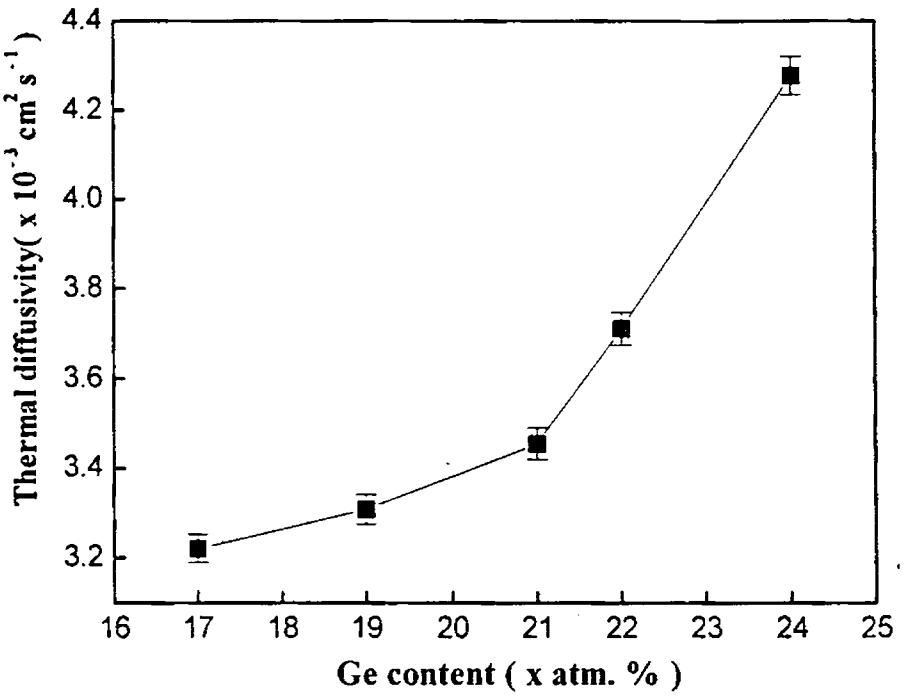

Fig. 3.14 Composition dependence of thermal diffusivity of $Pb_{20}Ge_xSe_{80-x}$ glasses (using PA phase lag technique).

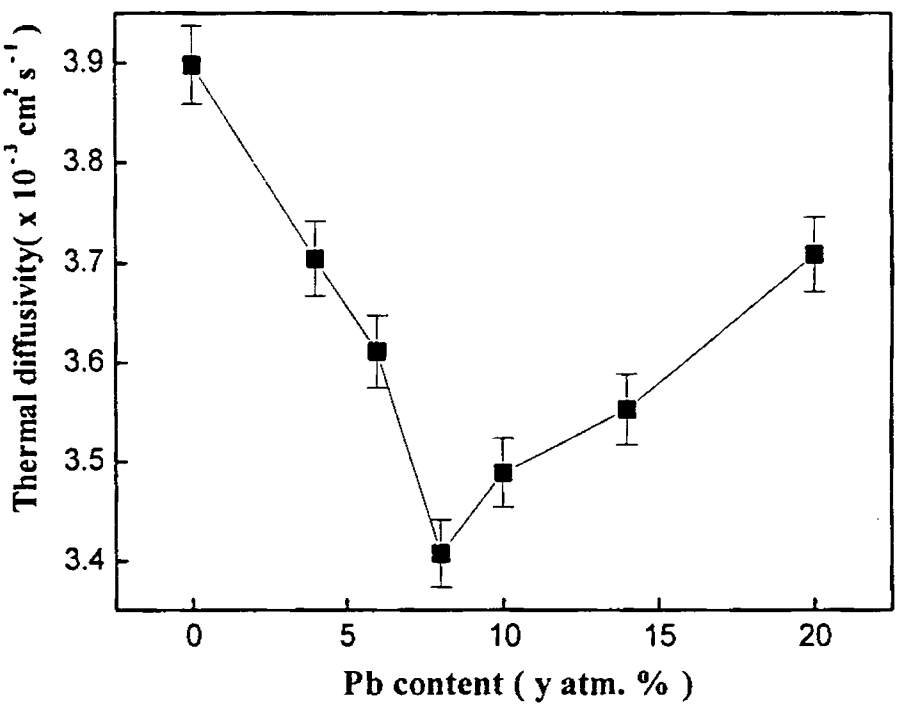

Fig. 3.15 Composition dependence of thermal diffusivity of $Pb_yGe_{42-y}Se_{58}$ glasses (using PA phase lag technique).

Densities of the samples are determined using Archimedean principle with liquid paraffin as the densiometric fluid. Figs. 3.16 and 3.17 show the variations of density as a function of composition for series I and series II glasses respectively.

The variations of thermal conductivity and heat capacity as a function of x for series I glasses is shown in Fig. 3.18. K as well as c_p decrease sharply beyond x = 21 indicating a clear anomaly at this composition. The anomalous changes of K and c_p can be also noted in the corresponding curves plotted against Pb content (y) for series II glasses, shown in Fig. 3.19. For this series, thermal conductivity drops significantly beyond $y = 9$ and heat capacity decreases faster with Pb content for $y > 9$.

3.6 Discussion of results

The observed decrease in thermal conductivity as the two sets of glasses undergo CTR may be explained as follows. Thermal conductivity in glassy semiconductors is dominated by the transport of heat by the vibration modes of the network. Primarily, molecular vibrations and defects in the structure limit the mean free paths of the propagating phonon modes. The electronic contribution to thermal resistance is rather small due to the low concentration of electrons in the medium. In chalcogenide glasses, electrical conduction is primarily p-type due to the presence of charged defect states. The thermal excitation of positively charged defect states creates long living holes, whereas the electrons excited from negatively charged defects recombine resulting in a larger concentration of holes. Consequently, chalcogenide glasses behave as p-type conductors.

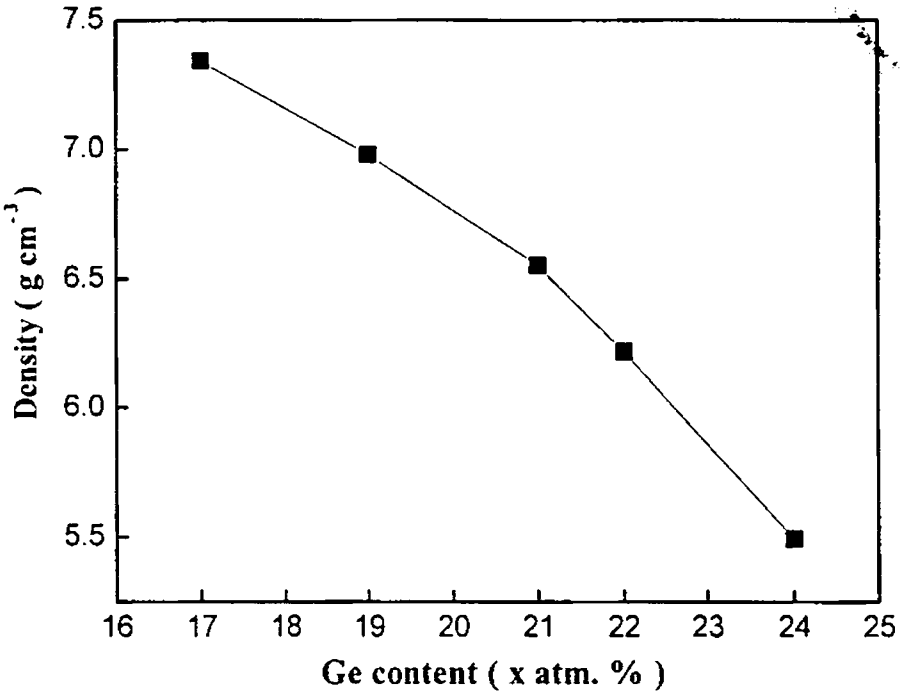

Fig. 3.16 Composition dependence of density of $Pb_{20}Ge_xSe_{80-x}$ glasses.

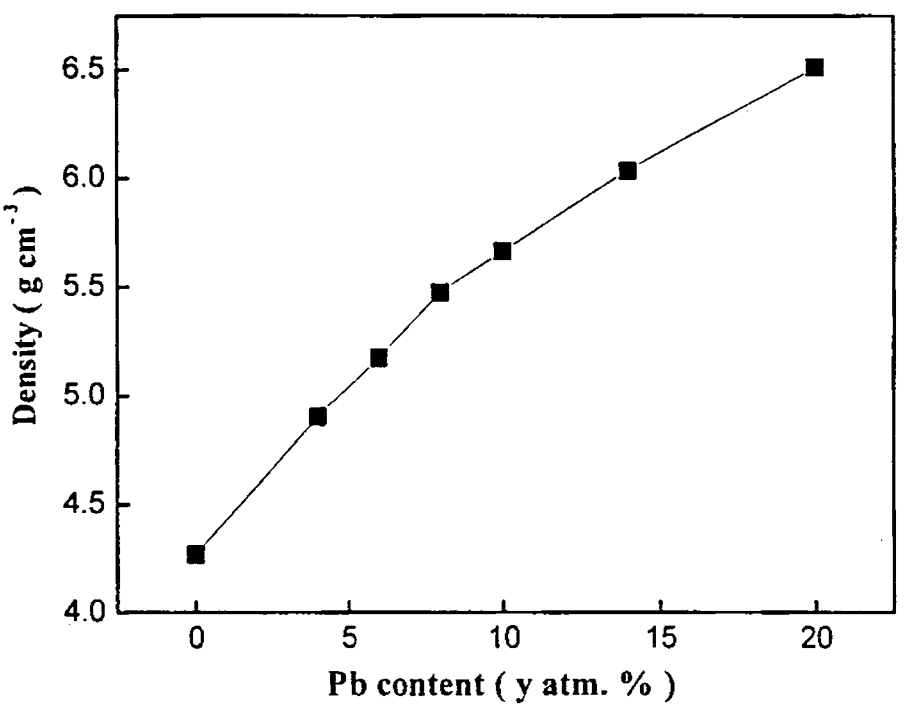

Fig. 3.17 Composition dependence of density of $Pb_yGe_{42-y}Se_{58}$ glasses.

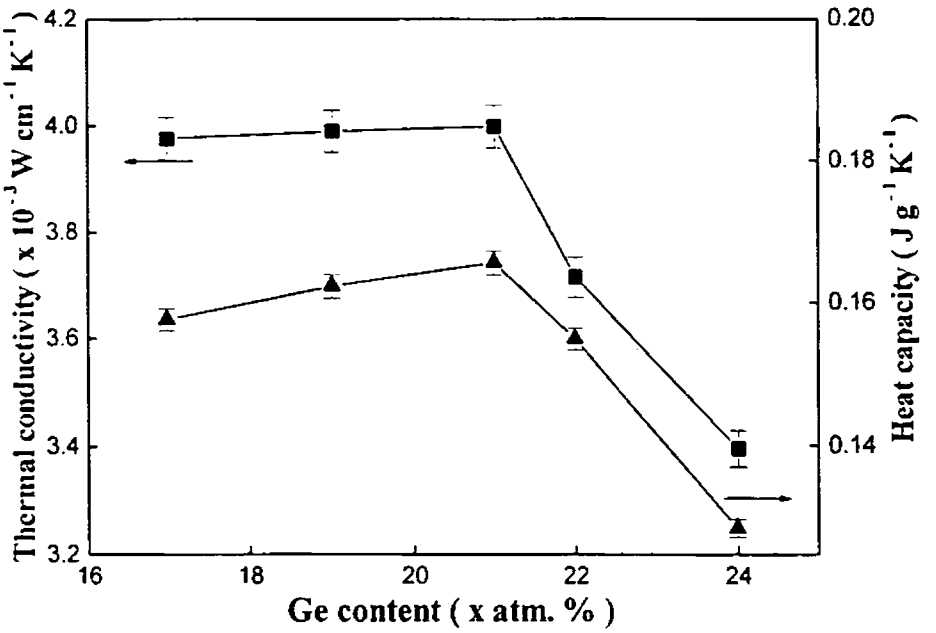

Fig. 3.18 Composition dependence of thermal conductivity and heat capacity of $Pb_{20}Ge_xSe_{80-x}$ glasses.

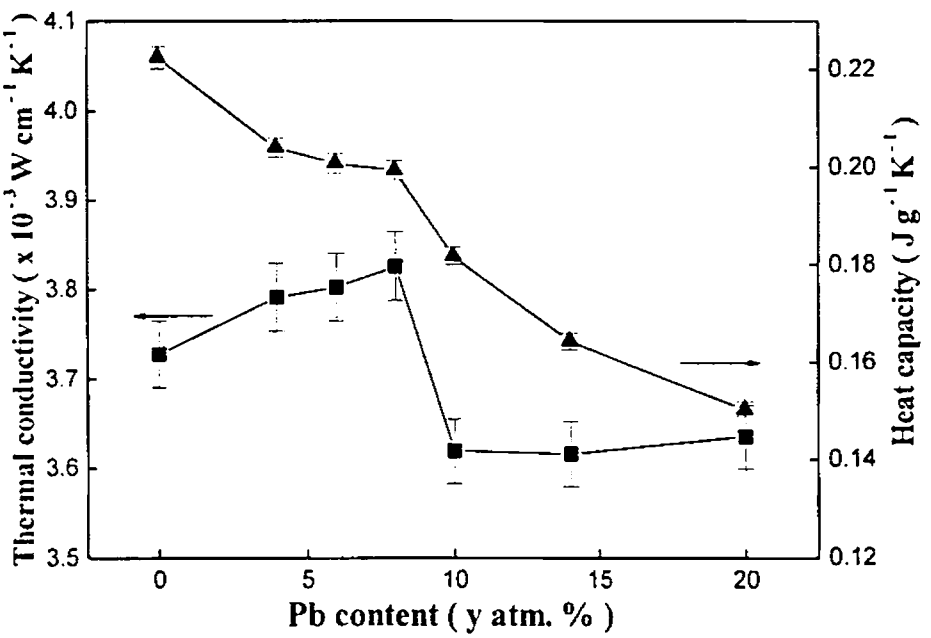

Fig. 3.19 Composition dependence of thermal conductivity and heat capacity of $Pb_yGe_{42-y}Se_{58}$ glasses.

The total density of valence alternation centres (N) is given by

$$N = [C_1^-] + [C_3^+] \tag{3.3}$$

In the absence of a metallic additive, the positively and negatively charged native defects are equal in number ($[C_1^-] = [C_3^+]$) and $N = 2N_0$, where N_0 denotes the concentrations of individual native-charged defects.

The concentration of native VAPs equilibrating at the quenching or glass transition temperature (T_g), is also given by

$$N_0^2 = [C_3^+][C_1^-] = N_A^2 \exp\left(-E_{VAP}/kT_g\right) \tag{3.4}$$

where N_A is the density of the chalcogen and E_{VAP} is the energy required to create a valence alternation defect pair from a normally bonded chalcogen.

The electron concentration in the absence of additives (n_0) is given by [26]

$$n^2 [C_3^+]/[C_1^-] = N_c^2 \exp(-2\varepsilon_n/kT) = n_0^2 \tag{3.5}$$

where N_c is the effective density of conduction band states. The activation energy for the electron, $\varepsilon_n \approx E_g/2$, where E_g is the mobility gap.

It is assumed that additives such as Pb equilibrate at T_g and yield positive centres of concentration $[A^-]$, where A denotes the additive. In order to calculate the thermal activation energy for various concentration of $[A^+]$, the total density of valence alternation centres (N_0) that equilibrate with $[A^-]$ during glass transition, and remaining constant in the range of interest, $T < T_g$, has to be determined.

Assuming that n_0 is small compared to N_0, the defect concentrations after the addition of metal atoms into the chalcogenide glass, can be estimated from [26]

$$[C_1^-]^* = \tfrac{1}{2}[A^-] + (N_0^2 + \tfrac{1}{4}[A^-]^2)^{1/2} \tag{3.6}$$

$$[C_3^+]^* = -\tfrac{1}{2}[A^-] + (N_0^2 + \tfrac{1}{4}[A^-]^2)^{1/2} \tag{3.7}$$

Here, $[A^-]$ is treated as an independent variable for determining $[C_1^-]^*$ and $[C_3^+]^*$ at T_g. The total concentration of VAPs after the addition of metal atom (N_{mod}) is given by

$$N_{mod} = [C_1^-]^* + [C_3^+]^* = 2\,(N_0^2 + \tfrac{1}{4}[A^-]^2)^{1/2} \qquad (3.8)$$

From Eq. (3.8), it is clear that the concentration of charged additives has to approach or exceed N_0 in order to have any appreciable effect. The electron concentration after the incorporation of the additive can be estimated from

$$n^2\,(2\,N_0^2/[A^-] + n) = 2[A^-]\,n_0^2 \qquad (3.9)$$

When $n >> 2\,N_0^2/[A^-]$, i.e., for high additive concentrations, Eq. (3.9) simplifies to the form

$$n = (2\,[A^+])^{1/3}\;n_0^{2/3} \qquad (3.10)$$

For lower impurity concentrations, $n << 2\,N_0^2/[A^-]$, Eq. (3.9) reduces to

$$n = [A^+]\,n_0/N_0 \qquad (3.11)$$

This expression describes the enhancement in electron concentration by the incorporation of charged impurities.

In the case of $Pb_yGe4_{2-y}Se_{58}$ system of glasses, the addition of Pb into Ge-Se glass converts some of Se_3^+ centres into Se_1^- centres while Ge_3^- centres remain unchanged. Consequently, the number of Se_3^+ centres that can undergo thermal excitation as per the Kolobov *et al.* model [27] decreases. Hence there is a decrease in the number of free holes formed by the conversion of Se_3^+ centres into Se_1^- centres. Moreover, with the decrease in the number of Se_3^+ centres, the number of traps that can capture electrons excited into the conduction band decreases. This

results in an overall increase in the electron concentration in the medium. In addition, there is a simultaneous increase in the number of Se_1^- charged defect states, which enhances the number of shallow acceptors that capture holes from the valence band. These two effects together shift the Fermilevel towards the conduction band resulting in *p* to *n* transition at a particular Pb concentration. Consequent increase in electron concentration reduces the phonon mean free path resulting in a decrease in thermal conductivity for $y > 9$ in these glasses (Fig. 3.19). The small extremum in heat capacity at the transition composition is also a result of this increase in electron concentration. Since the effect is small, the enhancement in heat capacity for compositions with Pb content larger than $y = 9$ is not really visible.

In $Pb_{20}Ge_xSe_{80-x}$ glasses, the number of Ge_3^- charged defect states increase as Ge concentration increases. Consequently, the number of Se_3^+ centres that can undergo thermal excitation decreases. Since the electronegativities of Pb and Ge are similar, the formation of charged defects and increase in electron concentration leading to CTR occur as in the case of $Pb_yGe_{42-y}Se_{58}$ glasses.

CTR in these glasses have been explained [23] in terms of the formation of sp^3d^2 energy band of Pb^{2+} ions just above and separated from the sp lone pair levels of Se. The *p* to *n* transition in series I glasses occur by the upward movement of the lone pair levels, closing in the sp^3d^2 lone pair band gap, while in series II it occurs as the sp^3d^2 band spreads bringing about a decrease in the gap to a similar level as in series I. In both cases, there is an increase in the electron concentration as well as charged defect states, which bring about a decrease in thermal conductivity during CTR. The electronic contribution to heat capacity increases due to larger

concentration of electrons in the medium consequent to *p* to *n* transition, which is reflected in the experimental results.

3.7 Conclusions

Composition dependence of thermal parameters in Pb-Ge-Se system of glasses that exhibit the phenomenon of CTR has been investigated using PPE and PA techniques. Anomalous variations are found in the thermal parameters at compositions where CTR has been reported to occur. The results are explained in terms of enhancement in electron concentration during the *p* to *n*-type change over in these materials.

References

1. D. Lathrop and H. Eckert, J. Phys. Chem. **93** (1989) 7895
2. K. J. Rao and R. Mohan, J. Phys. Chem. **84** (1980) 1917
3. S. Asokan, M. V. N. Prasad, G. Parthasarathy and E. S. R. Gopal, Phys. Rev. Lett. **7** (1989) 808
4. K. J. Rao and S. Balasubramanyan, J. Phys. Chem. **98** (1994) 9216
5. A .V. Kolobov and S. R. Elliot, Adv. Phys. **40** (1991) 625
6. R. A. Street and N. F. Mott, Phys. Rev. Lett. **35** (1975) 1293
7. N. F. Mott and E. A. Davis, *Electronic Processes in Non-Crystalline Materials* (Clarendon, Oxford, 1979)
8. M. Kastner, D. Adler and H. Fritzsche, Phys. Rev. Lett. **37** (1976) 1504
9. M. Kastner, J. Non-Cryst. Solids **31** (1978) 223
10. D. Adler and E. J. Yoffa, Phys. Rev. Lett. **36** (1976) 1197
11. N. Tohge, Y. Yamamoto, T. Minami and M. Tanaka, Appl. Phys. Lett. **34** (1979) 640
12. N. Tohge, T. Minami and M. Tanaka, J. Non-Cryst. Solids **38-39** (1980) 283
13. N. Tohge, H. Matsuo and T. Minami, J. Non-Cryst. Solids **95-96** (1987) 809
14. R. M. Mehra, Sandeep Kohli, Amit Pandir, V. K. Sachdev and P. C. Mathur, J. Appl. Phys. **81** (1997) 7842
15. S. Murugavel and S. Asokan, Phys. Rev. B **58** (1998) 4449
16. K. L. Bhatia, G. Parthasarathy, A. Sharma and E. S. R. Gopal, Phys. Rev. B **38** (1988) 6342
17. S. Kumar, S. C. Kashyap and K. L. Chopra, J. Appl. Phys. **72** (1992) 2066
18. P. Kounavis and E. Mytilineou, J. Non-Cryst. Solids **201** (1996) 119

19. L. Tichy, H. Ticha, A. Pacesova and J. Petzlt, J. Non-Cryst. Solids **128** (1991) 191

20. V. K. Bhatnagar, K. L. Bhatia, V. Yadav and N. Kishore, Phys. Rev. B **39** (1989) 11203

21. K. L. Bhatia, D. P. Gosain, G. Parthasarathy and E. S. R. Gopal, Phys. Rev. B **34** (1986) 8786

22. J. C. Phillips, Phys. Rev. B **36** (1987) 4265

23. B. Vaidhyanathan, S. Murugavel, S. Asokan and K. J. Rao, J. Phys. Chem. B **101** (1997) 9717

24. K. L. Bhatia, S. K. Malik, N. Kishore and S. P. Singh, Philos. Mag. B **66** (1992) 587

25. S. R. Elliot in *Disordered Semiconductors,* edited by M. A. Kastner, G. A. Thomas and S. R. Ovshinsky. (Plenum, New York, 1987) 219

26. H. Fritzsche and M. Kastner, Philos. Mag. B **37** (1978) 285

27. A. V. Kolobov, M. Kondo, H. Oyangi, R. Durny, A. Matsuda and K. Tanaka, Phys. Rev. B **56** (1997) 485

CHAPTER-4

Thermal conductivity and heat capacity of Bi-Ge-Se and Pb-In-Se glasses exhibiting CTR

4.1 Introduction

Chalcogenide glasses are remarkably resistant to electrical doping by the incorporation of dopant atoms. The Fermi level is considered to be pinned effectively by the presence of charged defect centres [1, 2] and holes are the predominant charge carriers. The discovery that the addition of Bi to Ge-Se glass system changes the conduction type from *p* to *n* [3, 4] has therefore attracted a great deal of scientific attention. Later, it has been found that the phenomenon of carrier type reversal (CTR) occurs in some other glass systems also, when doped with Bi or Pb [5-8]. A number of papers have been published on various physical properties of chalcogenide glass systems exhibiting carrier type reversal [9-14].

Several mechanisms have been proposed to account for the doping behaviour of Bi. Most propose that the effect of Bi is to upset the equilibrium between oppositely charged native defect centres (C_3^+ and C_1^-), being incorporated in a charged state, thereby allowing the Fermi level to become unpinned. Electrical resistivity, thermoelectric power and optical absorption coefficient measurements on $Ge_{20}Bi_xSe_{80-x}$ system of glasses by Tohge *et al.* [15] shows a gradual decrease in resistivity with increasing Bi content up to 9 at.% and a decrease by about four

orders of magnitude between x = 9 and 10%, but remained almost constant for x > 10 at.%. Composition dependence of Seeback coefficient shows a change of sign around 8 at. % of Bi.

In the $Pb_xIn_{25-x}Se_{75}$ system, carrier type reversal occurs at $x \approx 5$ at. % [7]. Composition dependence of activation energy shows a clear change of slope around the critical composition, while Seebeck coefficient changes its sign from positive to negative. In this case, Pb enters the network in Pb^{2+} ionized state; alter the concentrations of C_3^+ and C_1^- centres that result in the unpinning of the Fermi level.

In this chapter we report the results of our work on the composition dependence of thermal parameters viz., thermal diffusivity, thermal effusivity, thermal conductivity and heat capacity of $Ge_{20}Bi_xSe_{80-x}$ ($2 \leq x \leq 12$) and $Pb_xIn_{25-x}Se_{75}$ ($2 \leq x \leq 15$) systems measured using the photopyroelectric (PPE) and photoacoustic (PA) techniques. Thermal parameters show anomalous variations at the critical compositons at which CTR occurs. Experimental details, results obtained and a discussion of the results are given in the following sections.

4.2 Experimental details

Bulk semiconducting glasses with the general formulae $Ge_{20}Bi_xSe_{80-x}$ ($2 \leq x \leq 12$) and $Pb_xIn_{25-x}Se_{75}$ ($2 \leq x \leq 15$) have been prepared by the conventional melt quenching technique described in detail in Chapter 2. Appropriate quantities of high purity constituents are taken in quartz ampoules, which are then evacuated and sealed and kept in a high temperature furnace at a temperature $\approx$ 1000°C for nearly 24 hours. Ampoules are then quenched in ice water, at a cooling rate ~ 200 Ks^{-1}, to obtain the glass samples.

Thermal parameters of the samples are determined using the PPE and PA techniques described already in Chapters 2 and 3. Samples of thickness ~ 0.5mm and area ~ 3x3 mm^2, prepared by cutting with a slow speed diamond wheel saw and polished by hand lapping are used for the measurements. Optical band gap of $Pb_xIn_{25-x}Se_{75}$ glasses are determined using a UV-Vis-NIR spectrophotometer following the absorption technique.

4.3 Results and discussion

The optical absorption spectrum of one sample of the Pb-In-Se system under study is shown in Fig. 4.1. Optical band gap is determined graphically from the absorption spectrum. The composition dependence of optical band gap for this glass system is shown in Fig. 4.2. It is seen that the optical band gap decreases with increasing Pb content.

Thermal parameters of the samples are determined using the PPE technique. The thermal thickness of the samples are ensured by plotting the PPE amplitude and phase with modulation frequency. These plots are shown in Figs. 4.3 to 4.6. Thermal diffusivity (α) of the samples is determined from the PPE signal phase and thermal effusivity (e) from the PPE signal amplitude.

Composition dependences of α and e for the two sets of glasses are shown in Figs. 4.7 and 4.8. Using the PA technique α has been independently determined and these are shown in Figs. 4.9 and 4.10, which agrees well with the values obtained by PPE technique.

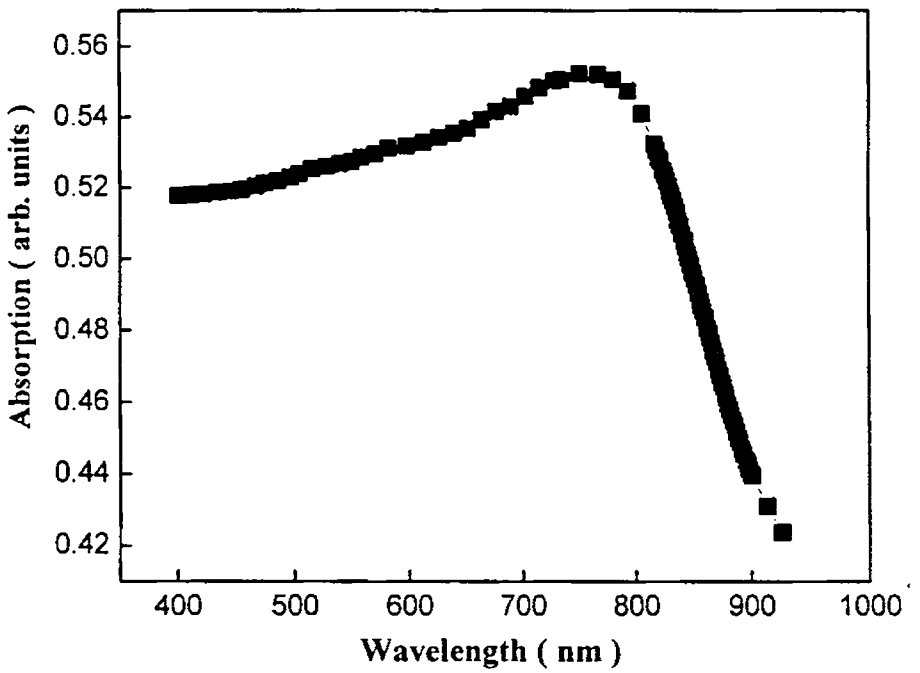

Fig. 4.1 Optical absorption spectrum of $Pb_2In_{23}Se_{75}$ glass

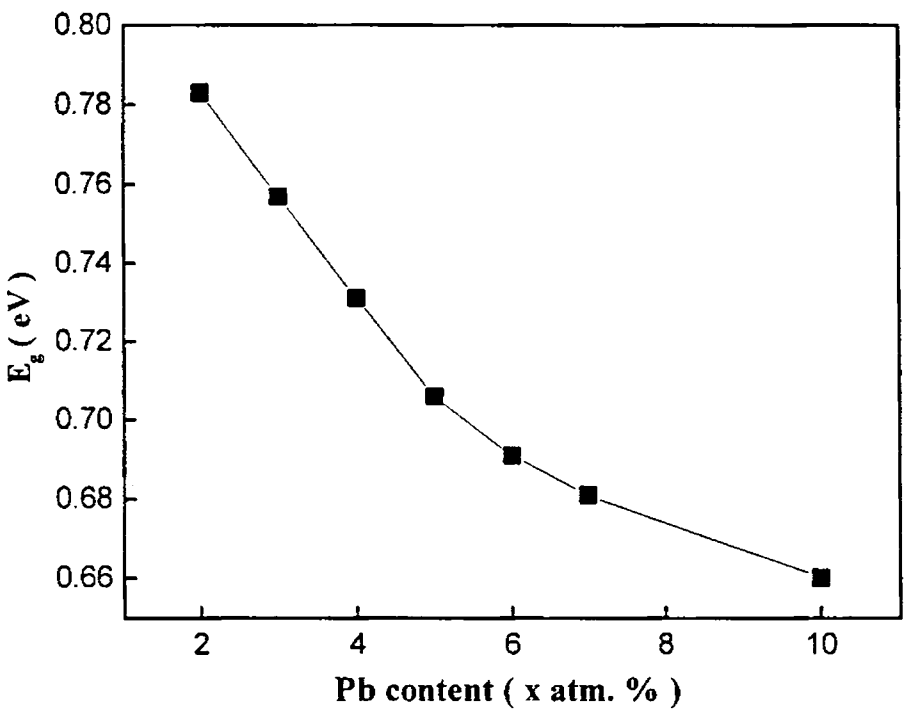

Fig. 4.2 Composition dependence of optical band gap (E_g) of $Pb_xIn_{25-x}Se_{75}$ glasses. Uncertainties in the values are less than 2%

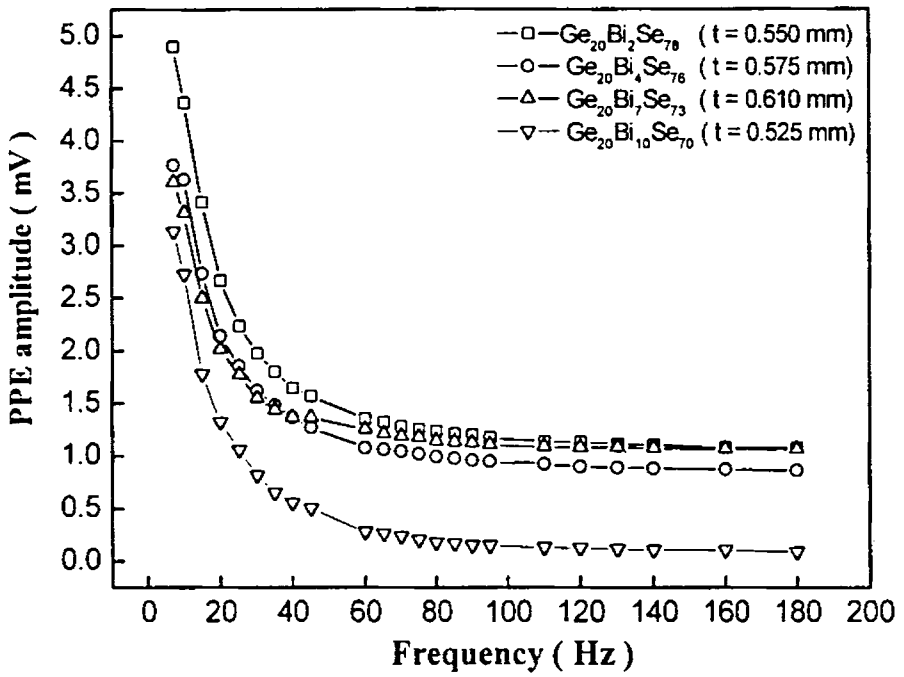

Fig. 4.3 Frequency dependence of PPE amplitude of $Ge_{20}Bi_xSe_{80-x}$ glasses

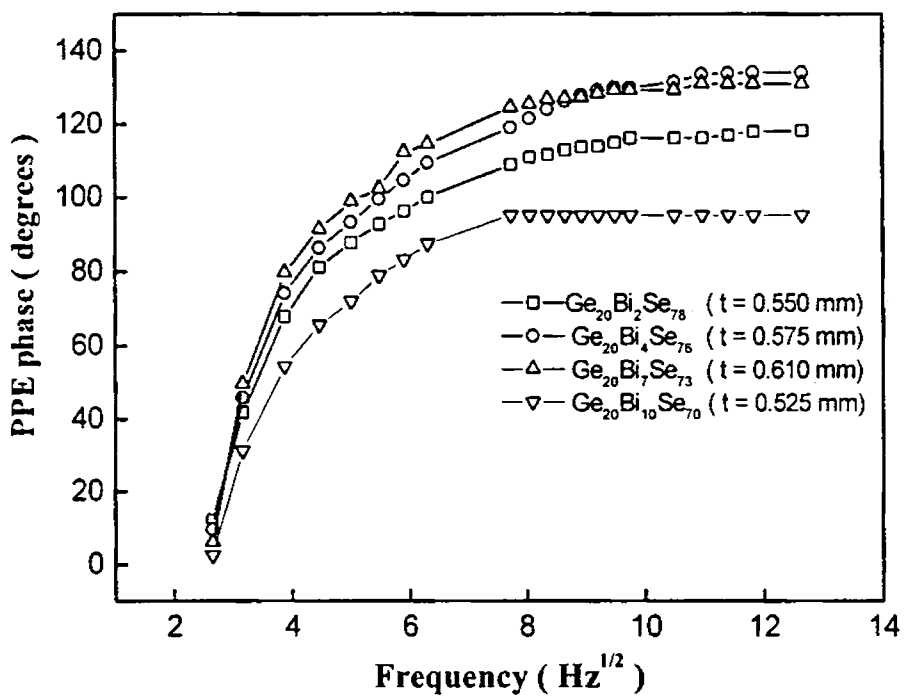

Fig. 4.4 Frequency dependence of PPE phase of $Ge_{20}Bi_xSe_{80-x}$ glasses

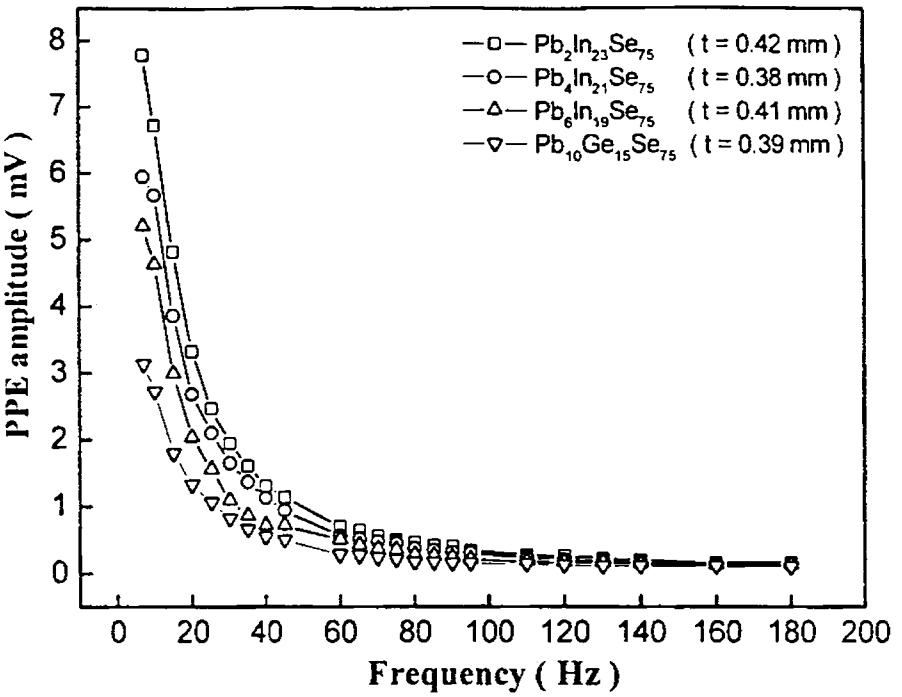

Fig. 4.5 Frequency dependence of PPE amplitude of $Pb_xIn_{25-x}Se_{75}$ glasses

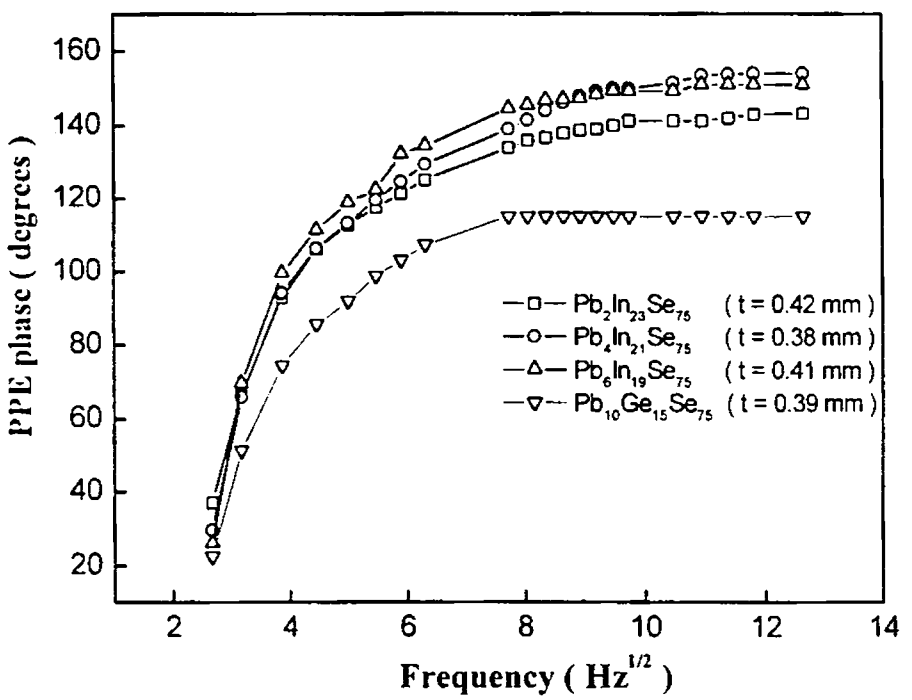

Fig. 4.6 Frequency dependence of PPE phase of $Pb_xIn_{25-x}Se_{75}$ glasses

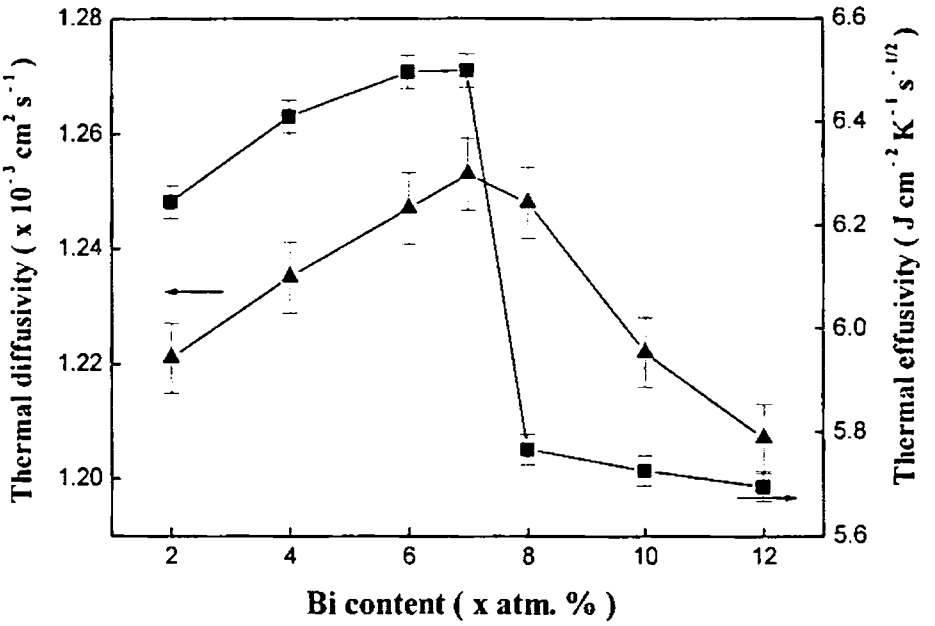

Fig. 4.7 Composition dependence of thermal diffusivity and thermal effusivity of $Ge_{20}Bi_xSe_{80-x}$ glasses employing PPE technique

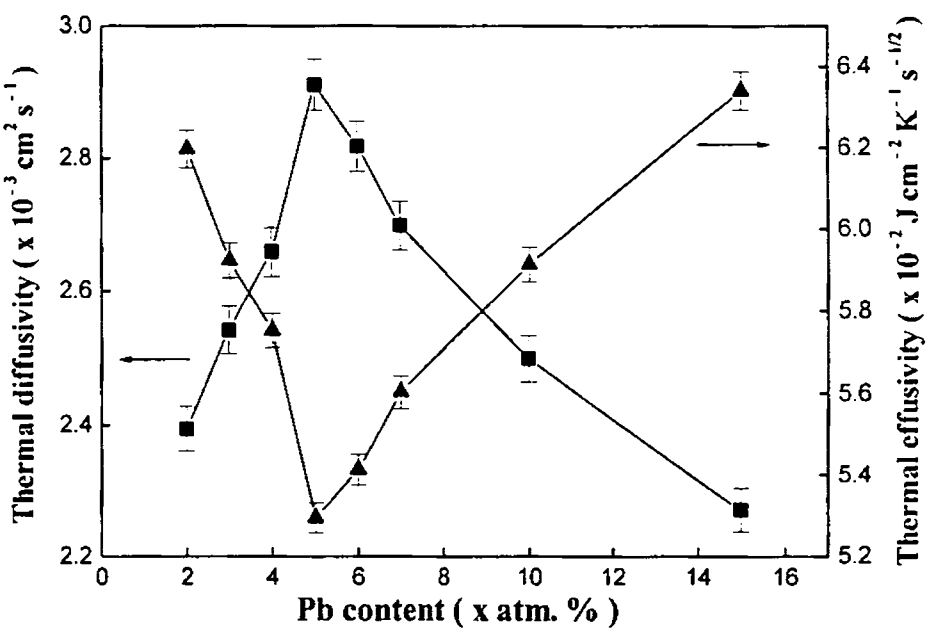

Fig. 4.8 Composition dependence of thermal diffusivity and thermal effusivity of $Pb_xIn_{25-x}Se_{75}$ glasses employing PPE technique

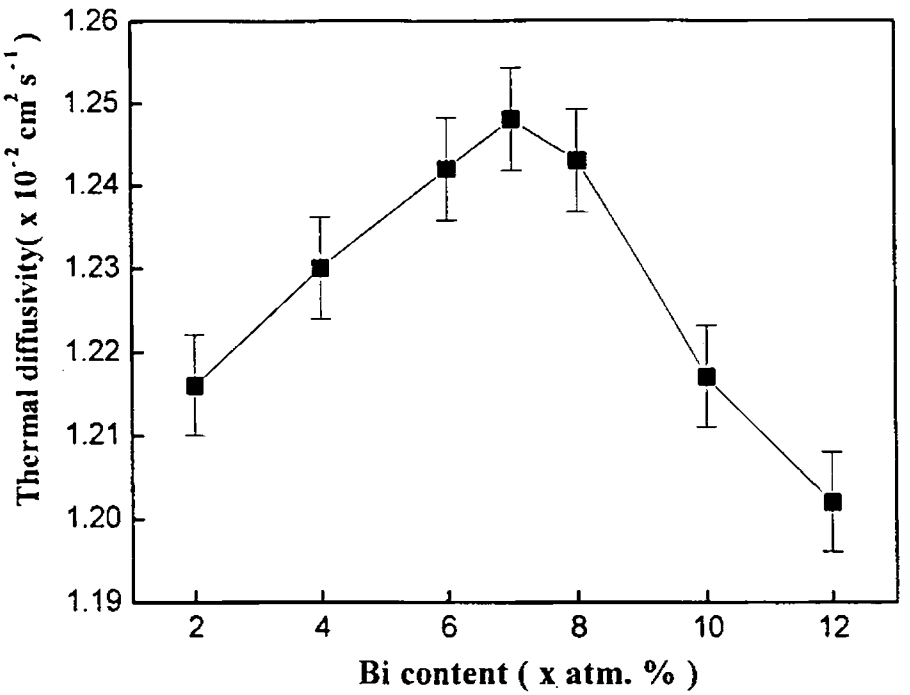

Fig. 4.9 Composition dependence of thermal diffusivity of $Ge_{20}Bi_xSe_{80-x}$ glasses employing PA phase lag technique

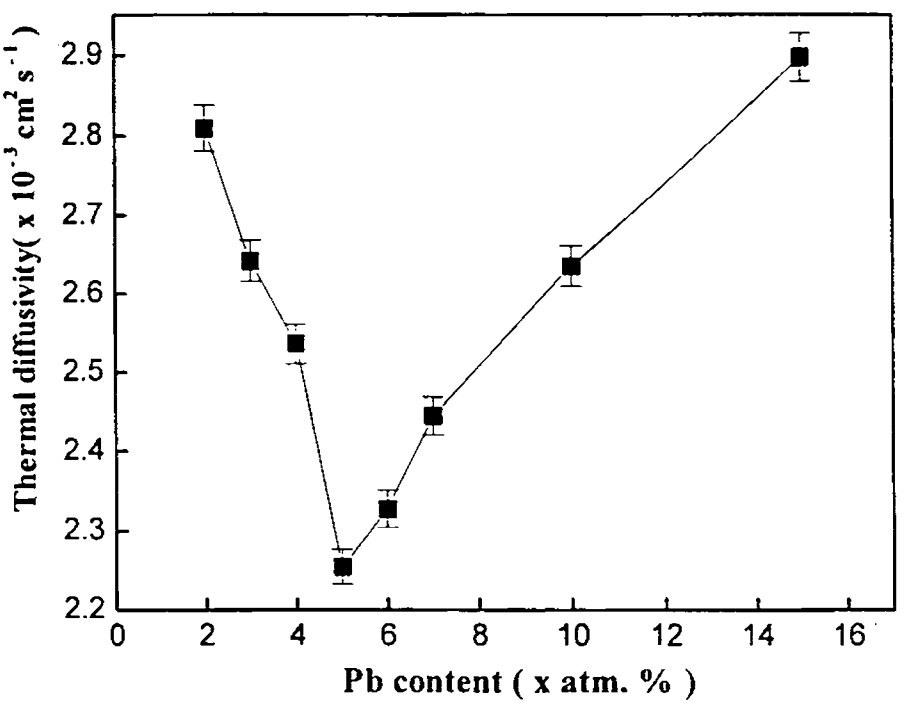

Fig. 4.10 Composition dependence of thermal diffusivity of $Pb_xIn_{25-x}Se_{75}$ glasses employing PA phase lag technique

Sample mass densities have been determined using Archemedis principle, with liquid paraffin used as the densiometric fluid. Figs. 4.11 and 4.12 show the composition dependence of densities of $Ge_{20}Bi_xSe_{80-x}$ and $Pb_xIn_{25-x}Se_{75}$ systems of glasses respectively. It is seen that density increases with Bi content for the first set and increases with Pb content for the second set.

Thermal conductivity and heat capacity of the samples have been determined using the relations $K = e(\alpha)^{1/2}$ and $c_p = e/\rho(\alpha)^{1/2}$. Figs. 4.13 and 4.14 show the composition dependence of K and c_p for Ge-Bi-Se and Pb-In-Se systems of glasses respectively. It can be seen that anomalous variations occur at the compositions corresponding to CTR in the composition dependence of thermal parameters.

From Fig. 4.7 it is seen that α increases gradually with Bi content up to 7 at.% of Bi, beyond which it decreases, which agrees with an earlier report [16]. Thermal effusivity also shows a maximum at 7 at. % of Bi which corresponds to the $p \rightarrow n$ transition composition. However, density increases monotomically with Bi content, as can be seen from Fig. 4.11. Thermal conductivity shows a maximum at x = 7, beyond which there is a sharp decrease. Heat capacity shows a sharp decrease around the critical composition (Fig. 4.13).

Various structural models have been put forward to account for CTR observed in Ge-Bi-Se glasses. These could be viewed as two groups, normally the electronic [17] and the structural inhomogeneity [18] groups. The electronic model considers the existence of Bi in various defect configurations, which perturbs the concentration of VAPs and results in the unpinning of the Fermi level. On the other hand, the structural inhomogeneity model assumes these glasses as phase separated into n-type tetradymite Bi_2Se_3 clusters with diameter less than 40Å [10] in the rest of

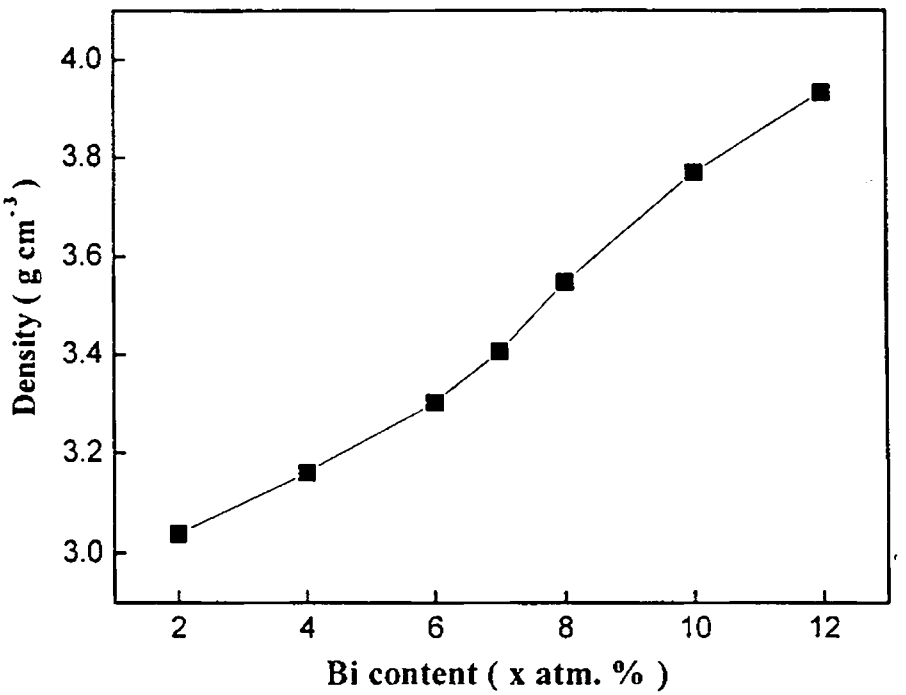

Fig. 4.11 Composition dependence of density of $Ge_{20}Bi_xSe_{80-x}$ glasses

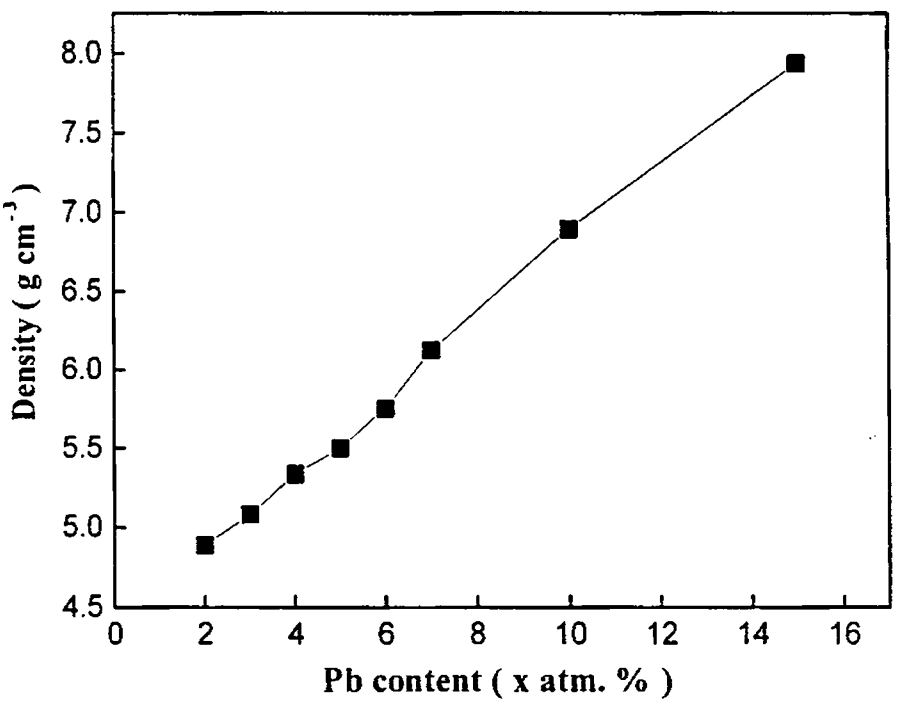

Fig. 4.12 Composition dependence of density of $Pb_xIn_{25-x}Se_{75}$ glasses

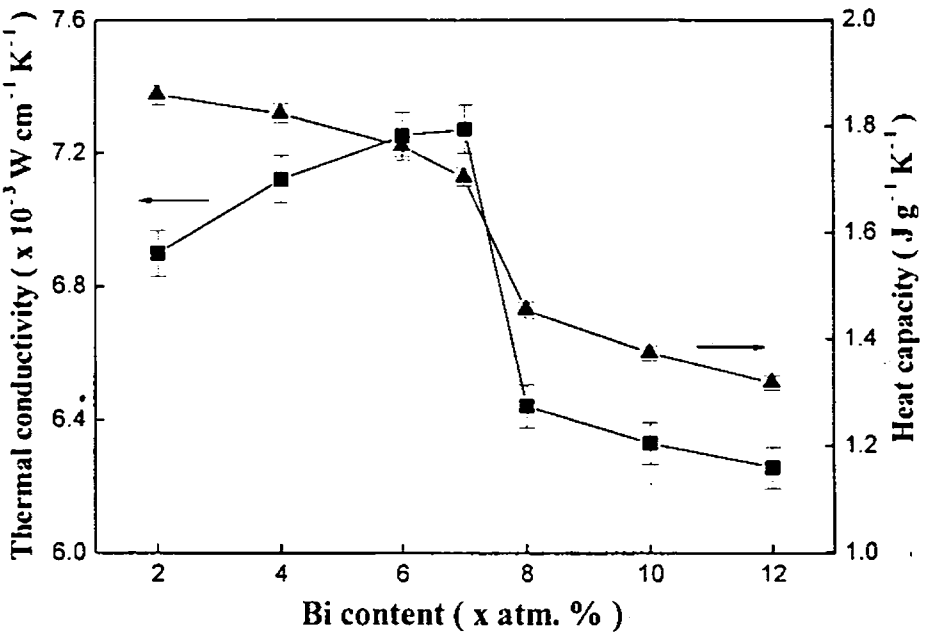

Fig. 4.13 Composition dependence of thermal conductivity and heat capacity of $Ge_{20}Bi_xSe_{80-x}$ glasses employing PPE technique

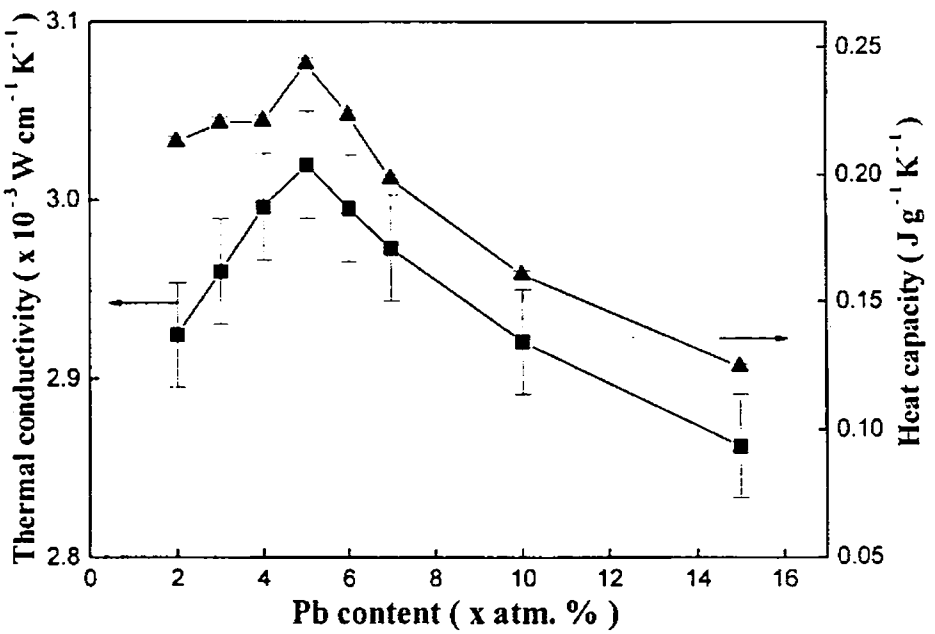

Fig. 4.14 Composition dependence of thermal conductivity and heat capacity of $Pb_xIn_{25-x}Se_{75}$ glasses employing PPE technique

the matrix at the microscopic level. Therfore at the conductivity percolation [18], or mechanical threshold [10], these glasses show a conductivity change. Measurements on the double stage crystallization in these glasses support the phase separations at the microscopic level [19].

According to the constraints theory by Phillips and Thorpe [10, 20], for the IV_x-V_{100-x} binary glasses, mechanical threshold occurs around x_c = 20 at. %. However, for Ge_xSe_{100-x} glasses, mechanical threshold occurs at a slightly higher value of x (x = 23 at. %) [21]. This is attributed to the fact that not all the bond bending constraints are effective in hindering intercluster motion. $Ge_{20}Bi_xSe_{80-x}$ glasses can be represented as $Bi_{2z}Se_{3z}$ + $Ge_{20}Se_{80-5z}$. At lower Bi percentage, the localized unconstructed Se^- defects are present at the Bi_2Se_3 tetramite surfaces. Theses clusters are uniformly dispersed in the rest of $GeSe_2$ and Se flexible chains. which make the material *p*-type. As the value of x increases, the mechanical stiffness of the combined medium increases. At x = 6 at. %, $Bi_6Ge_{20}Se_{74}$ = Bi_6Se_9 + $Ge_{20}Se_{65}$ and $Ge_{20}Se_{65}$ = Ge_ySe_{100-y} with y = 24, which agrees with the elastic stiffness threshold composition y_c = 23 of the glasses found in other experiments [21]. For $x \geq$ 6 at. % the mechanical misfit between these clusters is high, which leads to the plastic deformation of tetradymite clusters and as a result, the Se^- density increases. The high density of these Se^- defects evolves in a percolative manner at mechanical threshold and produces the *n*-type conduction in these glasses.

According to the charged dangling bond model, when bismuth is added to the Ge-Se network, the equilibrium between positively and negatively charged dangling bonds which pin the Fermi level near the middle of the gap gets affected

[3]. As a result, the Fermi level gets unpinned and moves towards the conduction band.

Elliot and Steel [22] have suggested that the $p \rightarrow n$ transition in these glasses is accompanied by a significant change in the local structural order surrounding the Bi impurity atoms. At low Bi concentrations, Bi-Se bond remains covalent in character and at higher Bi concentrations it becomes partially ionic with slight increase in bond lengths. According to them, the process of dissolution of Bi impurity in the Se rich regions at lower concentrations produce Se^- centres making the Bi impurities positively charged. Further addition of Bi in larger concentrations do not produce appreciable additional defects as it enters in a modified network. Consequently, the absorption edges are not appreciably affected. According to Bhatia *et al.* [23], at lower Bi concentrations there is little change in activation energy E_{av}, where as at higher concentrations, a considerable decrease in E_{av} is observed, which can be explained on the basis of the shift of the Fermi level towards the conduction band.

The dependence of thermal diffusivity and thermal conductivity on Bi concentration show maxima at the critical compositions that lies close to the mechanical threshold predicted by the constraints model. The increase in α and K may be attributed to the mechanical stiffening of Ge-Se network with Bi_2Se_3 clusters dispersed in it. The elastic misfit between the Bi_2Se_3 cluster and $GeSe_2$ network is relieved by distortions of the Se atom chains for $x < 7$. When $x \geq 7$, the grown up Bi_2Se_3 clusters find themselves embedded in a matrix of increased mechanical rigidity. Heat capacity shows a sharp decrease around the transition composition, which is in agreement with an earlier report [19].

For $Pb_xIn_{25-x}Se_{75}$ system, carrier type reversal occurs around x = 5 at. % [7]. From Fig. 4.2, it can be seen that the optical band gap decreases with increasing Pb content. Thermal diffusivity (α) shows a minimum and thermal effusivity (e) a maximum at x = 5. Thermal conductivity (K) and heat capacity increase upto the critical composition compositon corresponding to CTR and thereafter decrease.

According to Mehra *et al.* [7], the Fermi level is pinned and placed towards the valence band at an energy of 0.73 eV for $In_{25}Se_{75}$. However, when Pb enters the network, the band picture changes drastically. It is assumed that Pb enters the network in Pb^{2+} ionized state as in other Pb containing chalcogenide glasses. Consequently Se_1^- centres are formed, and the equilibrium between Se_1^- and Se_3^+ centres gets disturbed. As a result, the Fermi level gets unpinned and moves towards the conduction band resulting in n-type conductivity.

Since Pb is more electro positive than Se or In, the lone-pair electrons adjacent to Pb atoms will have higher energies than those remote from Pb atoms. This results in a broadening and tailing of the valence band. This leads to the observed decrease in E_g with increasing Pb concentration.

The thermal parameters viz., α, e, K and c_p of $Pb_xIn_{25-x}Se_{75}$ glasses show anomalous variations at x = 5. While α shows a minimum, e shows a maximum. K and c_p decrease beyond x = 5. As already stated in Chapter 3, thermal conductivity in these glasses is dominated by the transport of heat by the vibration modes of the network. As the electron concentration is increased during $p \rightarrow n$ transition, the phonon mean free path gets reduced. This results in the decrease in thermal conductivity beyond the critical composition

4.4 Conclusions

Thermal parameters of Ge-Bi-Se and Pb-In-Se systems of glasses exhibiting carrier type reversal are studied as functions of compositions. It is found that the carrier type reversal gets reflected in the thermal parameters measured using the PPE technique. A decrease is observed in thermal conductivity beyond the *p-n* transition composition. This is explained on the basis of enhancement in carrier concentration in the samples.

References

1. R. A. Street and N. F. Mott, Phys. Rev. Lett. **35** (1975) 1293
2. M. Kastner, D. Adler and H. Fritzsche, Phys. Rev. Lett. **37** (1976) 1504
3. N. Tohge, Y. Yamamoto, T. Minami and M. Tanaka, Appl. Phys. Lett. **34** (1979) 640
4. N. Tohge, T. Minami and M. Tanaka, J. Non-Cryst. Solids **38-39** (1980) 283
5. N. Tohge, H. Matsuo and T. Minami, J. Non-Cryst. Solids **95-96** (1987) 809
6. K. L. Bhatia, G. Parthasarathy, A. Sharma and E. S. R. Gopal, Phys. Rev. B **38** (1988) 6342
7. R. M. Mehra, Sandeep Kohli, Amit Pundir, V. K. Sachdev and P. C. Mathur, J. Appl. Phys. **81** (1997) 7842
8. S. Murugavel and S. Asokan, Phys. Rev. B **58** (1998) 4449
9. V. K. Bhatnagar, K. L. Bhatia, V. Yadav and N. Kishore, Phys. Rev. B **39** (1989) 11203
10. J. C. Phillips, Phys. Rev. B **36** (1987) 4265
11. K. L. Bhatia, S. K. Malik, N..Kishore and S. P. Singh, Philos. Mag. B **66** (1992) 587
12. L. Tichy, H. Ticha, A. Pacesova and J. Pelzlt, J. Non-Cryst. Solids **128** (1991) 191
13. S. Kumar, S. C. Kashyap and K. L. Chopra, J. Appl. Phys. **72** (1992) 2066
14. B. Vaidhyanathan, S. Murugavel, S. Asokan and K. J. Rao, J. Phys. Chem. B **101** (1997) 9717
15. N. Tohge, T. Minami, Y. Yoshitaka and M. Tanaka, J. Appl. Phys. **51** (1980) 1048

16. Sheenu Thomas and J. Philip, Solid State Commun. **107** (1998) 423

17. S. R. Elliot and A. T. Steel, J. Phys. C: Solid State Phys. **20** (1987) 4335

18. L. Tichy, H. Ticha, A. Triska and P. Nagels, Solid State Commun. **53** (1985) 399

19. M. K. Rabinal, K. S. Sangunni, E. S. R. Gopal and S. V. Subramanyam, Solid State Commun. **88** (1993) 251

20. J. C. Phillips and N. F. Thorpe, Solid State Commun. **53** (1985) 699

21. W. Bresser, P. Boolchand and Suranyi, Phys. Rev. Lett. **56** (1986) 2493

22. S. R. Elliot and A. T. Steel, Phys. Rev. Lett. **57** (1986) 1316

23. K. L. Bhatia, G. Parthasarathy and E. S. R. Gopal, J. Non-Cryst. Solids **69** (1985) 189

CHAPTER-5

Photoconductivity in chalcogenide glass systems exhibiting CTR

5.1 Introduction

The effect of impurities on the electronic properties of chalcogenide glasses has been a subject of great interest ever since their discovery [1]. In recent years, a great deal of efforts has been expended to understand the role of Bi or Pb in controlling the mechanism of electrical conduction in bulk chalcogenide glasses. It is known that bulk semiconducting glasses behave like intrinsic *p*-type semiconductors and are insensitive to impurity doping. Fermi level is considered to be pinned due to the equilibrium between positively and negatively charged dangling bonds [2, 3]. However, it is found that when Bi or Pb is added to certain chalcogenide glass systems, a carrier type reversal (CTR) from *p* to *n* occurs at certain doping levels [4-9]. Several researchers have reported results on electrical conductivity, activation energy, thermoelectric power, thermal analysis, structure and vibration states of Pb as well as Bi doped glasses across the compositions at which carrier type reversals are reported to occur [10-17].

In this chapter, we report the results of our photoconductivity measurements in $Pb_{20}Ge_xSe_{80-x}$ ($17 \leq x \leq 24$), $Pb_yGe_{42-y}Se_{58}$ ($0 \leq y \leq 20$) and $Pb_xIn_{25-x}Se_{75}$ ($0 \leq x \leq 15$) systems of glasses, all of them exhibiting CTR at definite compositions. As already stated in Chapter 1, *p* to *n* transitions are reported to occur in these systems

at specific compositions. Photoconductivity as well as photodetectivity, which is the ratio of photoconductivity to the corresponding dark conductivity, have been measured as a function of composition, and it is seen that the carrier type reversal gets clearly reflected in these properties. Temperature dependence of these parameters have also been studied and reported. The results are analyzed in terms of the existing photoconductivity models. The experimental methods, results obtained and a discussion of the results are outlined in the following sections.

5.2 Sample preparation and experimental details

Bulk glasses in the required composition range have been prepared by the conventional melt quenching technique. Appropriate quantities of high purity constituent elements are weighed and taken in quartz ampoules, which are then evacuated and sealed. Ampoules are then kept in a high temperature furnace at 1000^0C for 24 hours with intermittent rotation of the ampoules for uniform mixing of the constituents. Ampoules are then quenched in ice water at a cooling rate ~ 200 Ks^{-1}. The amorphous natures of the samples have been confirmed by XRD technique.

Photoconductivity measurements are carried out as described in Chapter 2. Samples with thickness of the order of 0.5 mm and surface area of the order of 3 x 3 mm^2 have been used for the present measurements. The sample is sandwiched between two SnO_2 coated conducting, transparent glass plates acting as electrodes. The sample holder is kept in an enclosed chamber, which can be evacuated and heated. The temperature of the sample is measured and controlled within ± 0.1 K using a temperature controller (Lakeshore Cryotronics, Model DRC 82C). A

120mW He-Cd laser (λ = 442 nm) is used as the source of light to initiate photoconduction. The current is measured using a picoammeter in a two probe setup. Steady state (d. c.) photoconductivity is obtained as the difference between the total conductivity under illumination and the corresponding dark conductivity.

The electrical activation energy of all the samples has been determined by measuring their dark conductivity (σ) as a function of temperature (T) and plotting log σ versus $1/T$.

5.3 Results

The composition dependence of photoconductivity and photodetectivity for $Pb_{20}Ge_xSe_{80-x}$ system of glasses are shown in Fig. 5.1. At x = 21, which corresponds to the $p \rightarrow n$ transition composition, photoconductivity shows a minimum, while photodetectivity shows a sharp dip. Fig. 5.2 shows the composition dependence of photoconductivity and photodetectivity for the $Pb_yGe_{42-y}Se_{58}$ system. In this case, at the critical composition y = 8, both photoconductivity and photodetectivity show sharp increases. The composition dependence of photoconductivity and photodetectivity of $Pb_xIn_{25-x}Se_{75}$ system shown in Fig. 5.3, also exhibits a similar behaviour at x = 5, which is the critical composition at which CTR occurs.

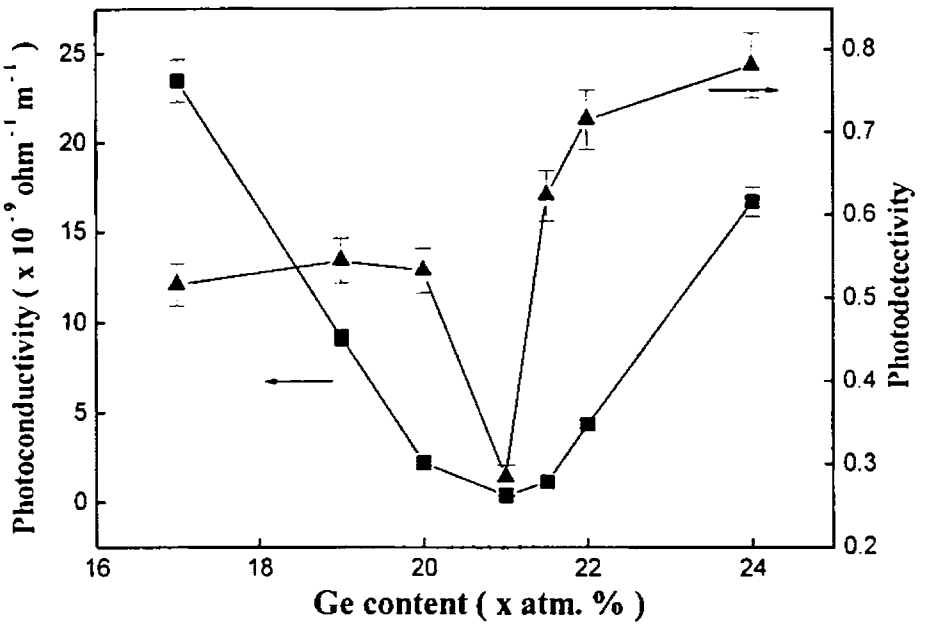

Fig. 5.1 Composition dependence of photoconductivity and photodetectivity of $Pb_{20}Ge_xSe_{80-x}$ glasses

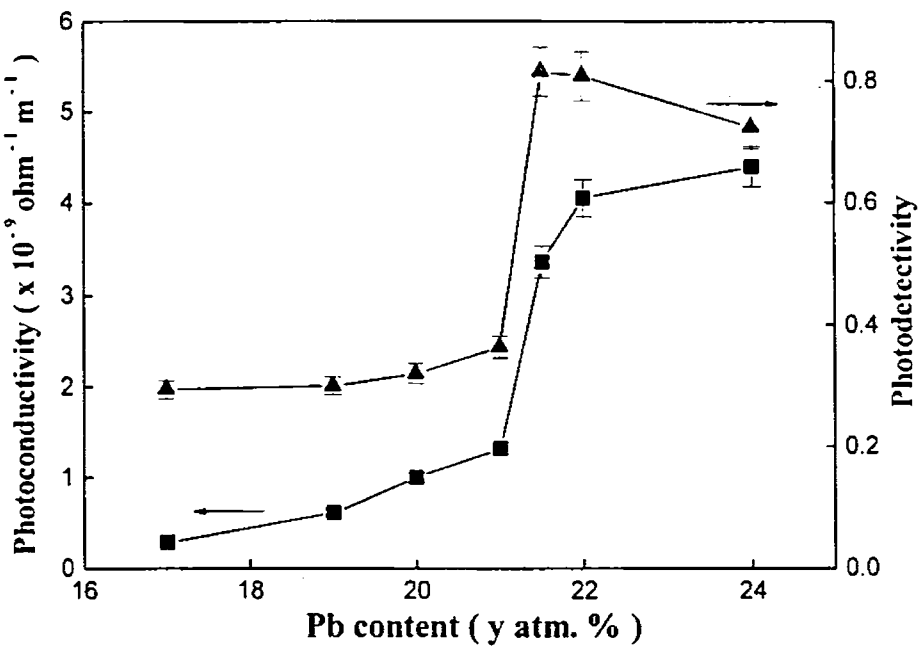

Fig. 5.2 Composition dependence of photoconductivity and photodetectivity of $Pb_yGe_{42-y}Se_{58}$ glasses

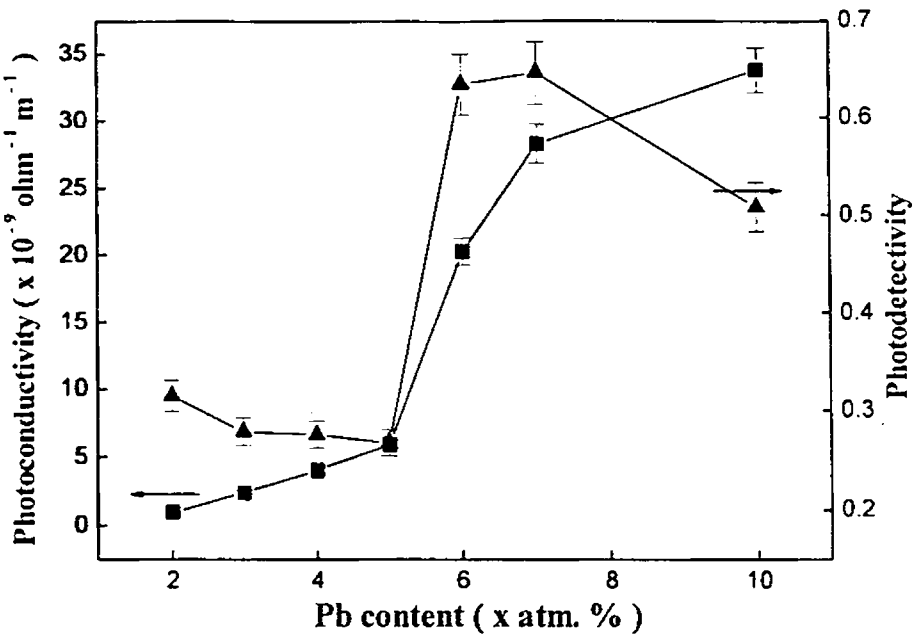

Fig. 5.3 Composition dependence of photoconductivity and photodetectivity of $Pb_xIn_{25-x}Se_{75}$ glasses

Temperature dependence of photoconductivity and photodetectivity has also been carried out on selected compositions on either side of the critical composition for all the three glass systems. The results are shown in Figs. 5.4, 5.5 and 5.6. It may be noted that for all the compositions in the three series, photoconductivity increases with temperature, while photodetectivity decreases with temperatures. Figs. 5.7, 5.8 and 5.9 show the composition dependence of activation energy for electrical conduction for the three systems. Uncertainties in the measured values are less than 2%. Anomalous variations occur at the transition compositions for all the three glass systems.

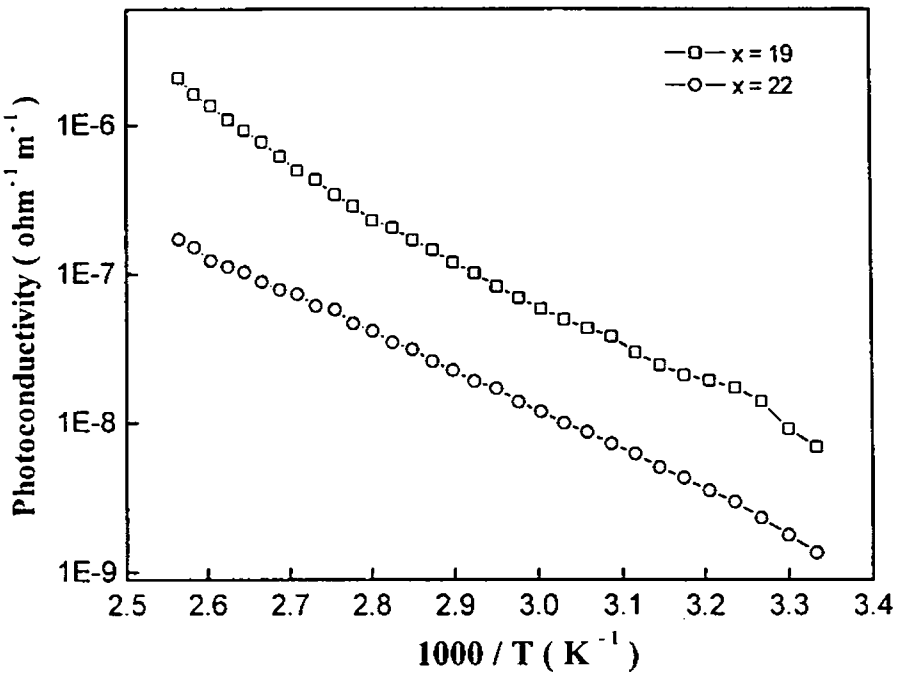

Fig. 5.4a Temperature dependence of photoconductivity of $Pb_{20}Ge_xSe_{80-x}$ glasses

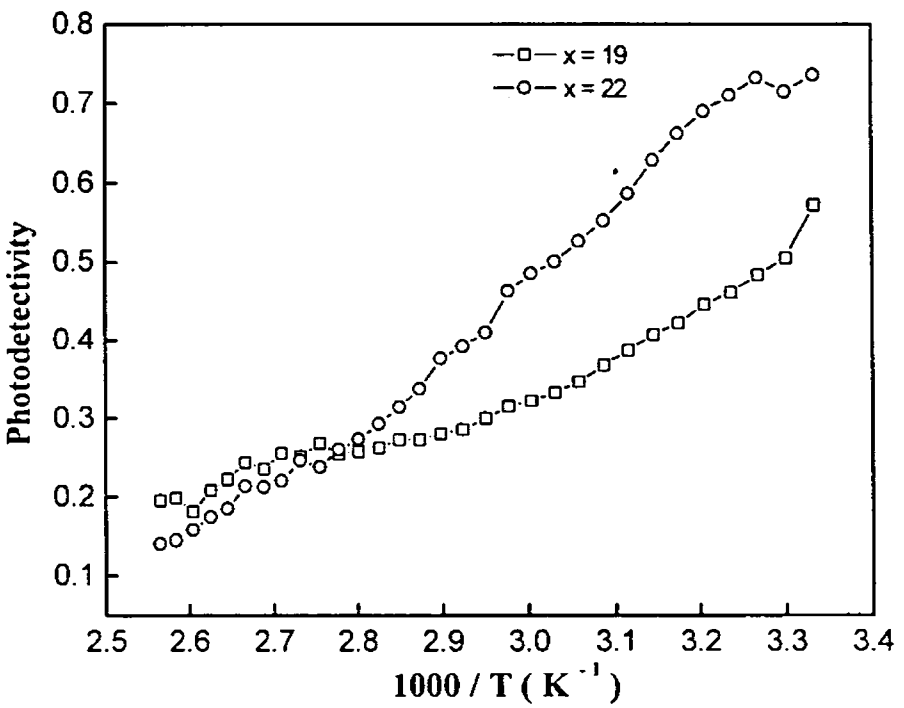

Fig. 5.4b Temperature dependence of photodetectivity of $Pb_{20}Ge_xSe_{80-x}$ glasses

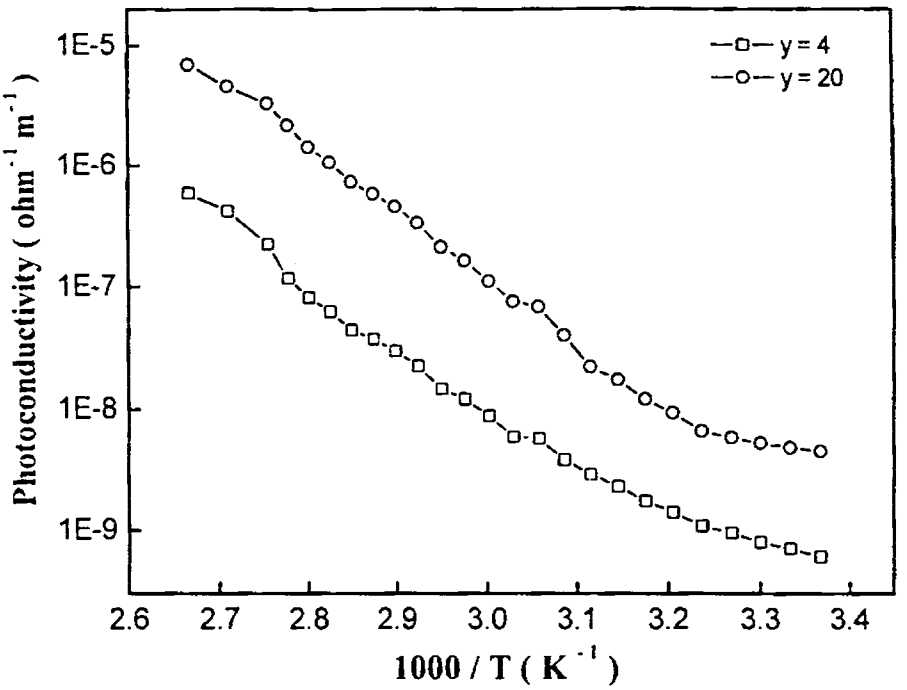

Fig. 5.5a Temperature dependence of photoconductivity of $Pb_yGe_{42-y}Se_{58}$ glasses

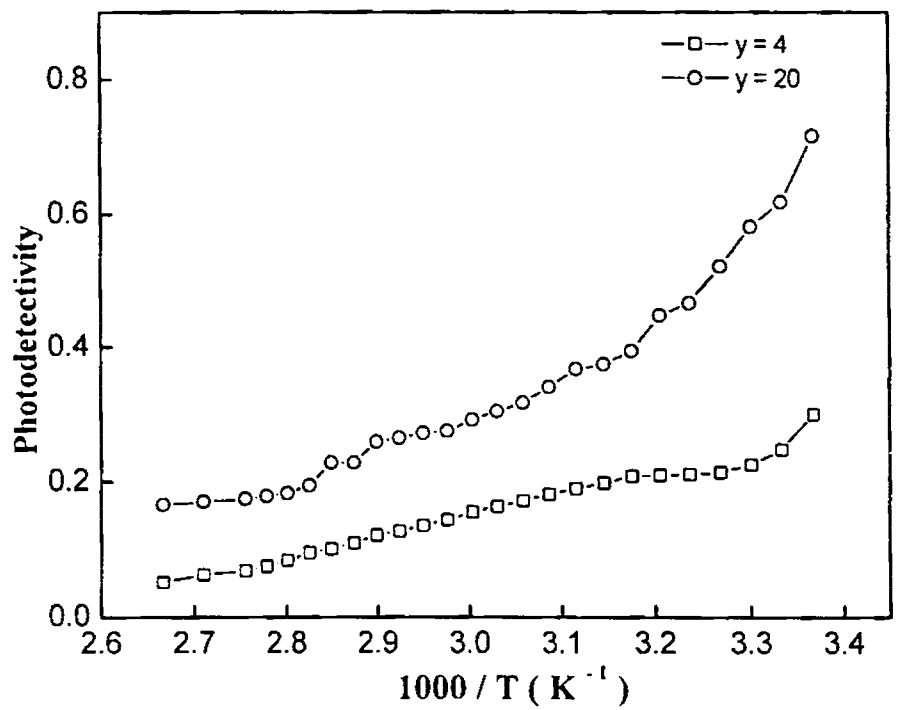

Fig. 5.5b Temperature dependence of photodetectivity of $Pb_yGe_{42-y}Se_{58}$ glasses

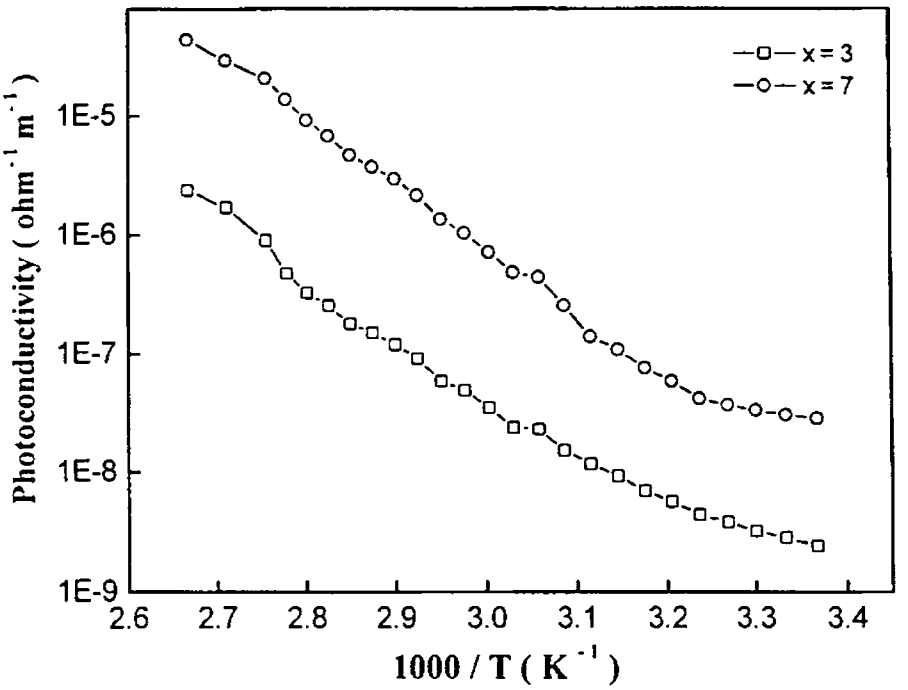

Fig. 5.6a Temperature dependence of photoconductivity of $Pb_xIn_{25-x}Se_{75}$ glasses

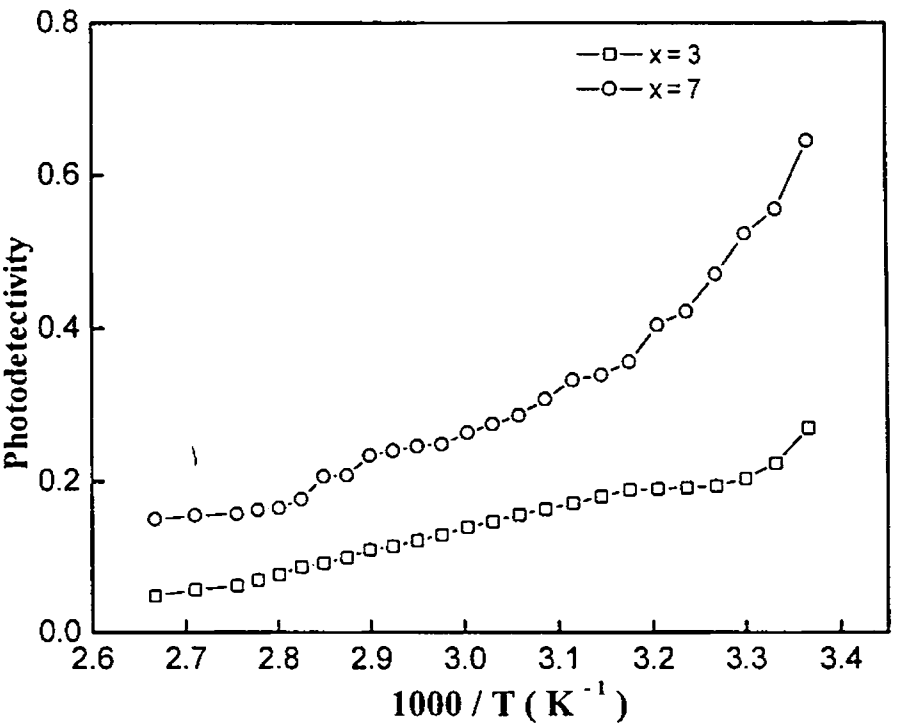

Fig. 5.6b Temperature dependence of photodetectivity of $Pb_xIn_{25-x}Se_{75}$ glasses

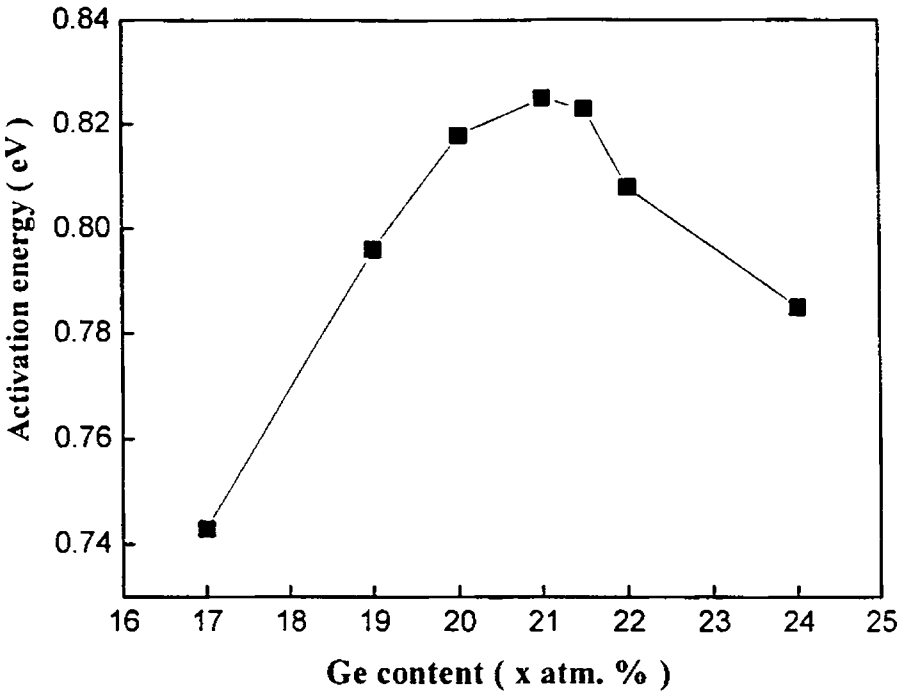

Fig. 5.7 Composition dependence of activation energy of $Pb_{20}Ge_xSe_{80-x}$ glasses

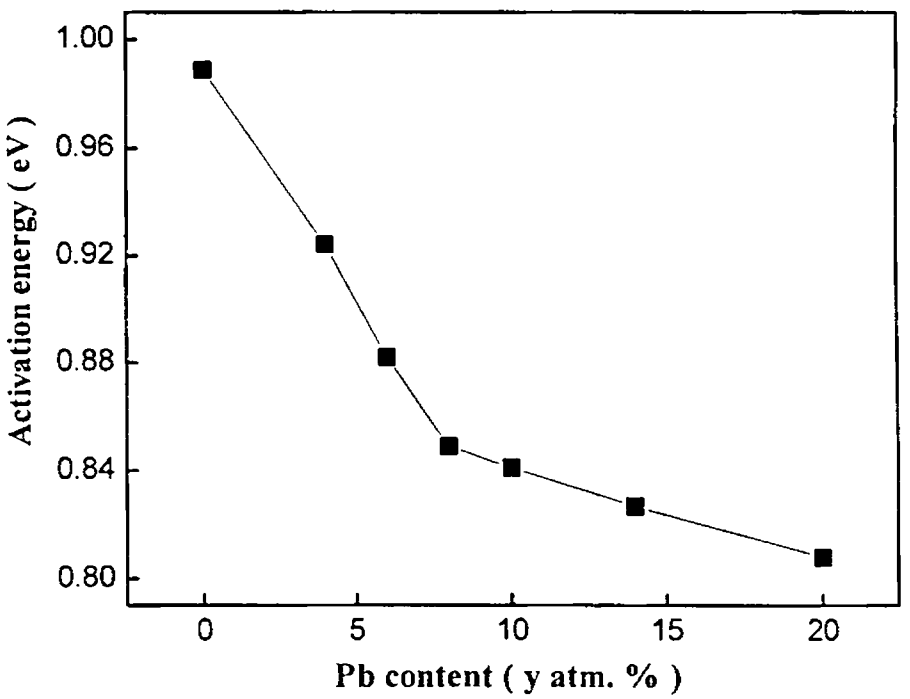

Fig. 5.8 Composition dependence of activation energy of $Pb_yGe_{42-y}Se_{58}$ glasses

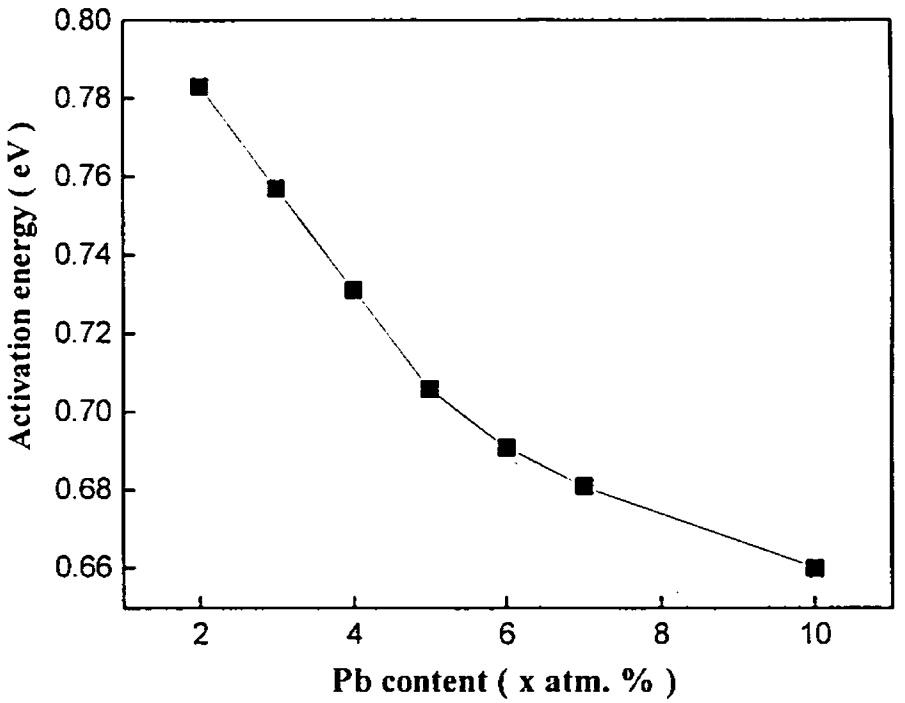

Fig. 5.9 Composition dependence of activation energy of $Pb_xIn_{25-x}Se_{75}$ glasses

5.4 Discussion of Results

The results show that the $p \rightarrow n$ transitions exhibited by the Pb-Ge-Se and Pb-In-Se systems are clearly reflected in photoconductivity measurements. For $Pb_{20}Ge_xSe_{80-x}$ system, photoconductivity decreases upto the transition composition and then increases, exhibiting a threshold minimum, while photodetectivity shows a sharp dip. For $Pb_yGe_{42-y}Se_{58}$ and $Pb_xIn_{25-x}Se_{75}$ systems, both photoconductivity and photodectivity show sharp increases at the critical composition.

Presence of charged defect pairs of the type C_3^+ and C_1^- are characteristic of chalcogenide glasses [18]. Their formation can be represented by a reaction of the form,

$$2C_2^0 \rightarrow C_1^- + C_3^+ \qquad (5.1)$$

where C represents a chalcogen. The superscript is the formal charge on the chalcogen and the subscript denotes the number of covalent bonds by which the chalcogen atom is connected to other atoms. Charge transport in chalcogenide glasses occurs through the participation of charged defects. The motion of C_3^+ centres in chalcogenide glasses is more facile than that of C_1^- centres so that chalcogenide glasses are generally *p*-type conductors.

When Pb is introduced into the Ge-Se network, C_1^- centres are created and their concentration is equal to that of Pb itself. Vaidhyanathan *et al.* [16] have calculated the values for the ratios of different types of defects in $Pb_yGe_{42-y}Se_{58}$ glasses. It is seen that as the Pb atom concentration increases from 5 to 20, the value of $[C_1^-]/[C_2^0]$ increases by a factor of 10, while the value of $[C_3^+]/[C_2^0]$ decreases by a factor of 10. This means that the ratio, $[C_1^-]/[C_3^+]$ vary by nearly two orders of magnitude. For low values of y, C_3^+ centres are major charge carriers and the glasses are *p*-type. As y increases, C_1^- centres become the dominant charge carriers and the system switches to an *n*-type semiconductor. At the same time, the activation energy decreases with y, which means that the concentration of C_3^+ increases with y, and so the transition is gradual in this case. For $Pb_{20}Ge_xSe_{80-x}$ system, activation energy increases with increasing x. Therefore, the concentration of C_3^+ decreases and C_1^- increases, so that $p \rightarrow n$ transition in this system is rather sharp.

Vaidhyanathan *et al.* have proposed a band structure model to account for the transition exhibited by the Pb-Ge-Se system [16]. The proposed band energy diagram is shown in Fig. 5.10. Here it is assumed that Ge is always tetrahedrally coordinated and Pb is octahedrally coordinated. In this structure, the top of the lone

pair band is constituted of C_1^- states. Electron transport between C_1^- states takes place through an empty sp^3d^2 state. When the Pb concentration is increased, sp^3d^2 band as well as the C_1^- states increases rapidly, and hence the electronic contribution to conductivity also increases. Thus, the $p \rightarrow n$ transition in $Pb_yGe_{42-y}Se_{58}$ system occurs due to the spreading of the sp^3d^2 band, which causes a decrease in the sp^3d^2 lone pair band gap. In $Pb_{20}Ge_xSe_{80-x}$ system, for small values of x, sp^3d^2 band is well above the lone pair band. As the value of x increases, the lone pair band spreads upwards in energy because of the perturbation of lone pair levels caused by the presence of larger number of tetrahedrally bonded centres. As a result, the sp^3d^2 band and the lone pair band become closer, and the electronic contribution to the conductivity increases. Thus the CTR in $Pb_{20}Ge_xSe_{80-x}$ system occurs due to the upward movement of the lone pair levels, closing in the sp^3d^2 lone pair band gap.

For $Pb_yGe_{42-y}Se_{58}$ system, the composition dependence of photoconductivity shows that photoconductivity increases with y, with a sharp increase at $y \approx 8$. For this series activation energy decreases with y, with a clear slope change at the critical composition. Also, in this case, a spreading of the sp^3d^2 band occurs resulting in CTR. For the $Pb_{20}Ge_xSe_{80-x}$ system, photoconductivity shows a minimum at $x = 21$. For this series, activation energy shows a maximum at that composition and CTR occurs due to an upward shift of the lone pair levels.

In the case of $Pb_xIn_{25-x}Se_{75}$ system, it is seen that both photoconductivity and photodetectivity show sharp increases at $x = 5$, the critical composition. In this case also, it is assumed that Pb atoms are present in the Pb^{2+} ionized state. The formation of negatively charged Se centres, which occurs as a result of the addition of Pb,

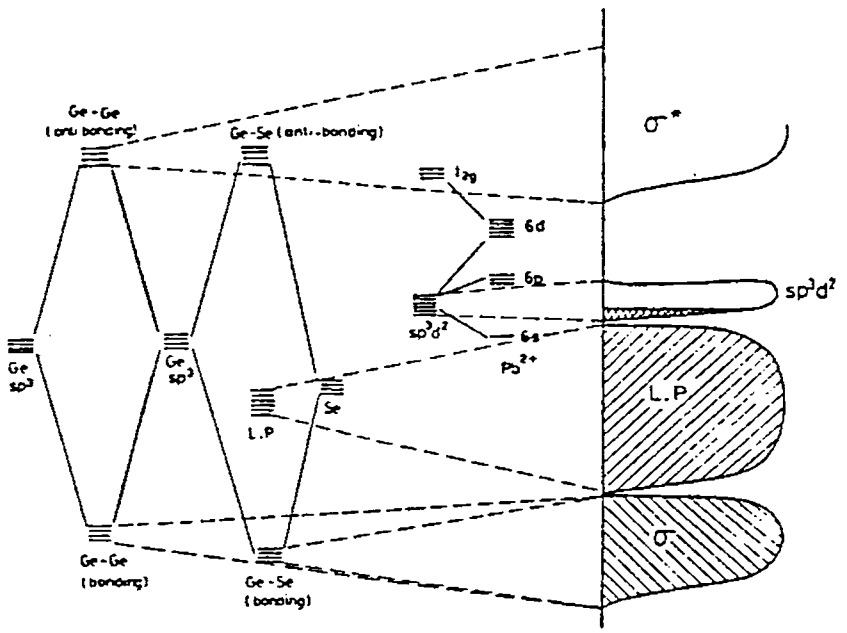

Fig. 5.10 Molecular orbital scheme used for the formation of energy levels and the schematic energy band diagram constructed for $Pb_yGe_{42-y}Se_{58}$ glasses [16]

disturbs the equilibrium between Se_1^- and Se_3^+ centres. Since Pb is more electropositive than selenium or indium, the lone pair electrons adjacent to Pb atoms will have higher energies than those remote from Pb atoms, causing a broadening and tailing of the lone pair valence band.

Photoconductivity, which is the excess conductivity due to incident radiation, can be expressed as [19],

$$\Delta\sigma = e\left(\Delta n\mu_n + \Delta p\mu_p\right) \qquad (5.2)$$

where Δn and Δp are the changes in the electron and hole densities due to irradiation and μ_n and μ_p are their respective mobilities in the medium. The photoconducting behaviour of these samples is close to that of a Type II photoconductor as per the ABFH model [20]. According to this model, the photoconductivity behaviour of

chalcogenide glasses have been classified into Type I and Type II. For Type I photoconductors, photoconductivity has a maximum at a specific temperature T_m. For $T < T_m$, photoconductivity magnitude is generally larger than the dark conductivity, while for $T > T_m$, it is smaller than dark conductivity. For Type II photoconductors, the photoconductivity maximum is absent. Photoconductivity increases monotonically with increasing temperature and in general, photoconductivity is much smaller than dark conductivity. On the basis of the energy level diagram suggested by the ABFH model, transitions from localized to localized states are dominant in a Type II photoconductor, over the whole measurable range. The temperature dependence of photoconductivity of Pb-Ge-Se and Pb-In-Se systems show that photoconductivity increases monotonically with temperature in the temperature range in which measurements are carried out. Moreover, the magnitude of photoconductivity is less than that of dark conductivity. This means that the photoconductivity behaviour of these samples is close to that of a Type II photoconductor.

5.5 Conclusions

Photoconductivity measurements in $Pb_{20}Ge_xSe_{80-x}$, $Pb_yGe_{42-y}Se_{58}$ and $Pb_xIn_{25-x}Se_{75}$ systems of glasses have been carried out. All the three systems exhibit $p \rightarrow n$ transition, and these transitions are clearly reflected in the present measurements. Temperature dependence of photoconductivity and photodetectivity has been reported and the results are analyzed in terms of the existing models. The results show that all the samples under study show photoconductivity properties close to Type II photoconductors as per the ABFH model.

References

1. D. Lathrop and H. Eckert, J. Phys. Chem. **93** (1989) 7895
2. N. F. Mott, E. A. Davis and R. A. Street, Philos. Mag. B **32** (1975) 96
3. M. Kastner, D. Adler and H. Fritzsche, Phys. Rev. Lett. **37** (1976) 1504
4. N. Tohge, Y. Yamamoto, T. Minami and M. Tanaka, Appl. Phys. Lett. **34** (1979) 640
5. N. Tohge, T. Minami and M. Tanaka J. Non-Cryst. Solids **38-39** (1980) 283
6. N. Tohge, H. Matsuo and T. Minami, J. Non-Cryst. Solids **95-96** (1987) 809
7. K. L. Bhatia, G. Parthasarathy, A. Sharma and E. S. R.Gopal, Phys. Rev. B **38** (1988) 6342
8. R. M. Mehra, Sandeep Kohli, Amit Pundir, V. K. Sachdev and P. C. Mathur, J. Appl. Phys. **81** (1997) 7842
9. S. Murugavel and S. Asokan, Phys. Rev. B **58** (1998) 4449
10. S. Kumar, S. C. Kashyap and K. L. Chopra, J. Appl. Phys. **72** (1992) 2066
11. P. Kounavis and E. Mytilineou, J. Non-Cryst. Solids **201** (1996) 119
12. L. Tichy, H. Ticha, A. Pacesova and J. Pelzlt, J. Non-Cryst. Solids **128** (1991) 191
13. V. K. Bhatnagar, K. L. Bhatia, V. Yadav and N. Kishore, Phys. Rev. B **39** (1989) 11203
14. K. L. Bhatia, D. P. Gosain, G. Parathasarathy and E. S. R. Gopal, Phys. Rev B **34** (1986) 8786
15. J. C. Phillips, Phys. Rev. B **36** (1987) 4265
16. B. Vaidhyanathan, S. Murugavel, S. Asokan and K. J. Rao, J. Phys. Chem. B **101** (1997) 9717

17. K. L. Bhatia, S. K. Malik, N. Kishore and S. P. Singh, Philos. Mag. B **66** (1992) 587

18. R. A. Street and N. F. Mott, Phys. Rev. Lett. **35** (1975) 1293

19. R. H. Bube, *Photoconductivity of Solids*, (Krieger, New York, 1978)

20. C. Arnouldussen, R. H. Bube, E. A. Fagen and S. Holmberg, J. Appl. Phys. **43** (1972) 1798

CHAPTER 6

Thermal conductivity and heat capacity in In-Te glasses during electrical switching

6.1 Introduction

The phenomenon of electrical switching in amorphous chalcogenide semiconductors has attracted a great deal of scientific attention ever since its discovery in 1968 [1]. Electrical switching is the rapid and reversible transition between a highly resistive OFF state and a conductive ON state, driven by an external electric field and characterized by a threshold voltage. Primarily, there are two types of switchings observed in chalcogenide glasses, namely, threshold [2] and memory [2, 3] as already stated in Chapter 1. In threshold type switching, the ON state persists only while a current flows down to a certain holding voltage, whereas in memory type switching, the ON state is permanent until a suitable reset current pulse is applied.

To understand the phenomenon of electrical switching in chalcogenide glasses, a great deal of effort has been expended [4-9]. Network connectivity, rigidity and nature of bonding have important roles to play in the process of electrical switching. The structure of chalcogenide glasses exhibiting memory switching usually consists of long Te chains in which atomic rearrangements occur easily [10]. They possess high electrical conductance, which can result in large power dissipation. The application of a high electric field leads to the crystallization

of the glass, and as a result, the sample remains in the low resistance ON state even after the removal of the field. In threshold switching materials, structural cross-linking of chains is generally higher and the structural reorganization is more difficult. They have relatively high thermal stability and a large energy barrier for crystallization.

A number of Te based binary and ternary glass systems like Al-Te, As-Te, Ge-Te, In-Te, As-Se-Te, Ge-As-Te, Al-As-Te etc [11-18] exhibit the phenomenon of memory switching. A highly conducting crystalline filament is expected within the material as a cause of the memory switching [5, 19, 20]. In this chapter, we report the results of our investigations on the variation of thermal parameters of the In-Te system of glasses during electrical switching.

6.2 Sample preparation and experimental details

Five compositions of In_xTe_{100-x} system of glasses with x = 20, 25, 30, 35 and 40 have been prepared by the conventional melt quenching technique using high purity constituent elements. The amorphous natures of the samples have been confirmed using the X-ray diffraction technique.

To determine the variation of thermal parameters during electrical switching the photopyroelectric (PPE) technique has been employed. Details of the sample holder and experimental set up are already described in detail in Chapter 2 of the thesis.

The thermal diffusivity and effusivity of each sample are determined by measuring the photopyroelectric signal phase and amplitude as already described. The electrical switching characteristics have been determined and the required electric field / current levels have been maintained to keep the sample in the ON

state or OFF state during PPE measurements. It is found that it is difficult to keep the sample in the switching state for measurements. PPE amplitude and phase undergo considerable fluctuations during switching. So stable measurements could be done only before switching and after switching. The results are outlined in the following section, followed by a discussion of the results.

6.3 Results and discussion

Electrical switching in In_xTe_{100-x} (x = 20-40) bulk samples have already been studied and reported [17]. Fig. 6.1 shows the V-I characteristics of $In_{40}Te_{60}$ glass. The region OA that corresponds to the OFF state has three sub regions. In region 1, current increases linearly with voltage, while in region 2, current has an exponential dependence on the square root of the voltage following the relation

$$I = I_0 exp\left(\frac{V}{V_0}\right)^{1/2} \tag{6.1}$$

In region 3, current increases exponentially with voltage following the relation

$$I = I_0 exp\left(\frac{V}{V_0}\right) \tag{6.2}$$

Here region 1 corresponds to the ohmic behaviour of the material. In region 2 current increases with square root of the applied voltage. This is because of the changes in quasi equilibrium within the material due to the applied electric field [21]. This region follows Poole-Frenkal law [22]. When the applied field is increased further, the generation of carriers due to change in equilibrium reaches saturation exponentially which corresponds to region 3.

If the applied field is increased further, a transition from OFF state to ON state occurs at a high conduction region where $I \propto V^n$ ($n > 2$) and is followed by a

negative resistance region. The region AS in Fig. 6.1 corresponds to electrical switching in the material with a negative differential resistance. The field induced carrier generation provides the required operation of a positive feed back mechanism during the occurrence of this instability condition. In the region SM, the material has practically zero differential resistance.

The *V-I* characteristics of three different compositions of In-Te glass system are shown in Fig. 6.2. It is found that the threshold field increases with In content. As the In content increases, the number of Te-Te bonds decreases. The stoichiometric composition $In_{40}Te_{60}$ contains only In-Te heteropolar bonds. Since the bond energy of the heteropolar bonds is higher than that of homopolar bonds, this composition is the most stable one [23-25]. So field induced carrier generation occurs at lower fields in other compositions compared to the stoichiometric $In_{40}Te_{60}$.

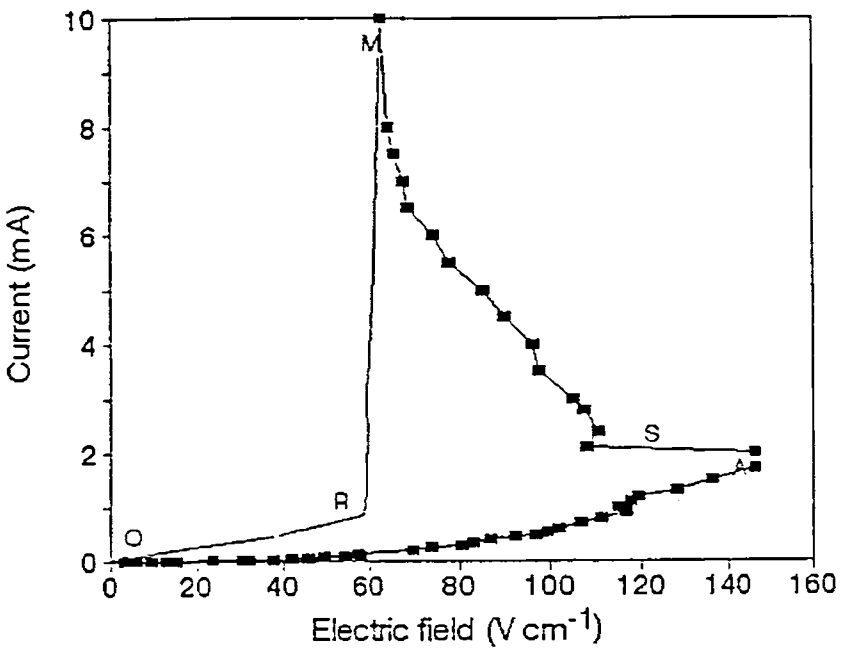

Fig. 6.1 Switching behaviour of $In_{40}Te_{60}$ glass [17]

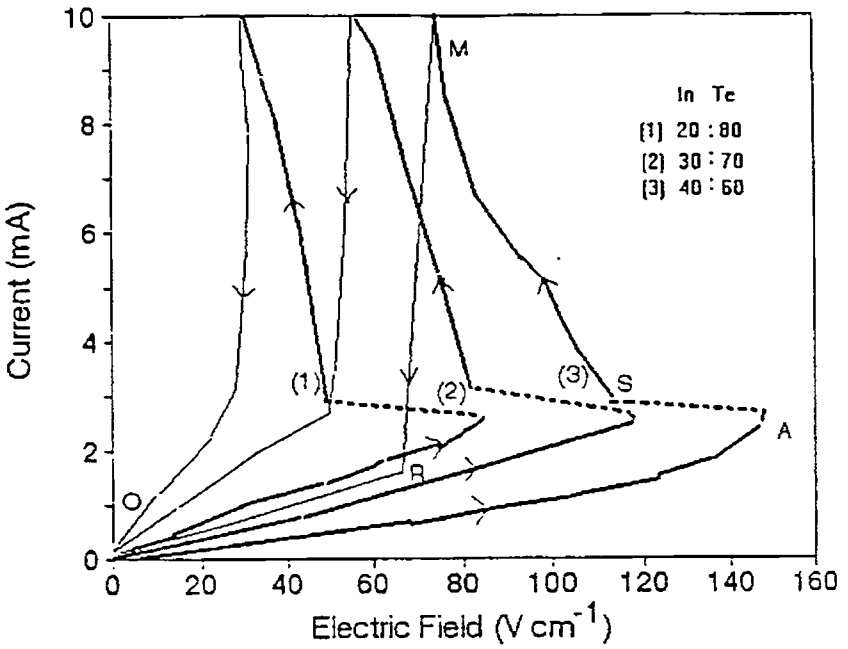

Fig. 6.2 Switching behaviour of three different compositions of In_xTe_{100-x} system of glasses [17]

Figures 6.3–6.12 show the variations of thermal parameters of these samples during electrical switching. It is found that thermal diffusivity (α), thermal effusivity (e) and thermal conductivity (K) show increases after switching. However, heat capacity (c_p) does not show any appreciable variation. It is believed that memory switching occurs in those chalcogenide glasses in which cross-linking atoms are too few. Such glasses have lesser thermal stability [20] and consequently, crystallize easily when heated. It is suggested that memory switching phenomenon is caused by the phase transition of the material from glassy to crystalline state due to Joule heating [19]. In the crystalline state, the conduction is higher as the disorder is significantly lesser. The formation of a crystalline conducting channel in a memory glass during switching has been confirmed by electron microscope and optical reflectivity investigations [19].

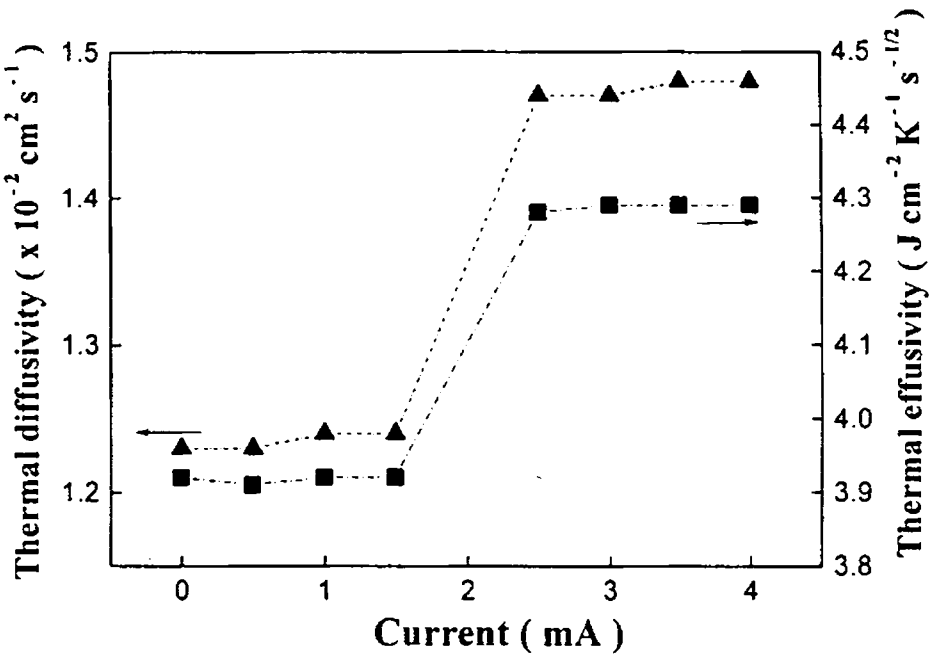

Fig. 6.3 Variation of thermal diffusivity and thermal effusivity for $In_{20}Te_{80}$ glasses. Threshold voltage is 85 V cm^{-1}.

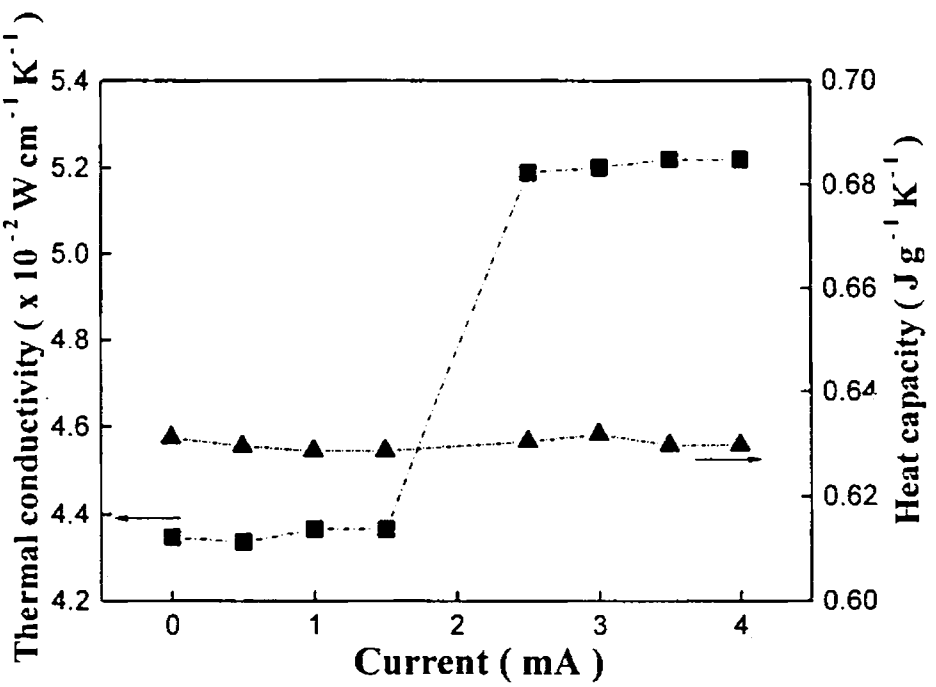

Fig. 6.4 Variation of thermal conductivity and heat capacity for $In_{20}Te_{80}$ glasses. Threshold voltage is 85 V cm^{-1}.

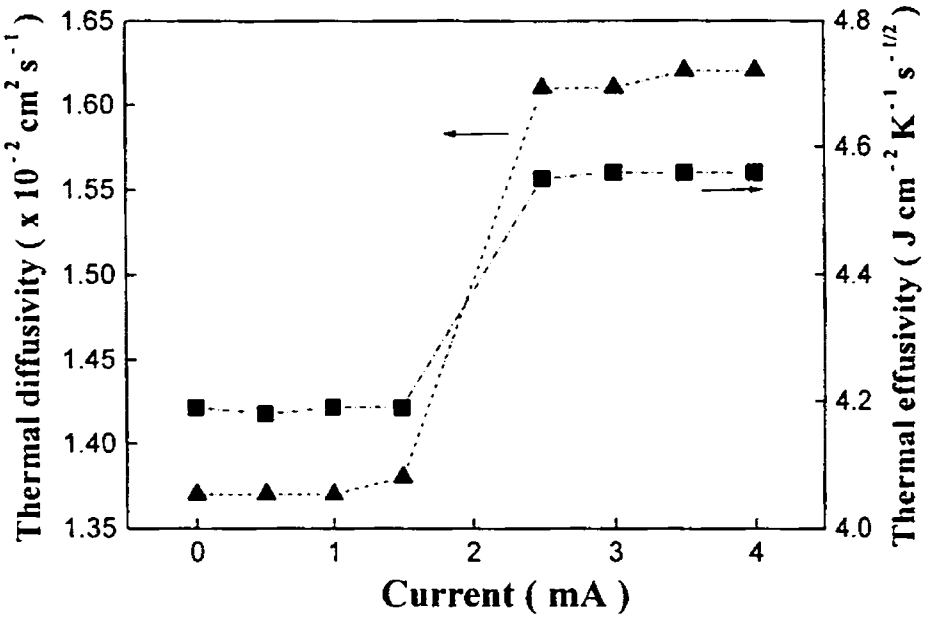

Fig. 6.5 Variation of thermal diffusivity and thermal effusivity for $In_{25}Te_{75}$ glasses. Threshold voltage is 97 V cm^{-1}.

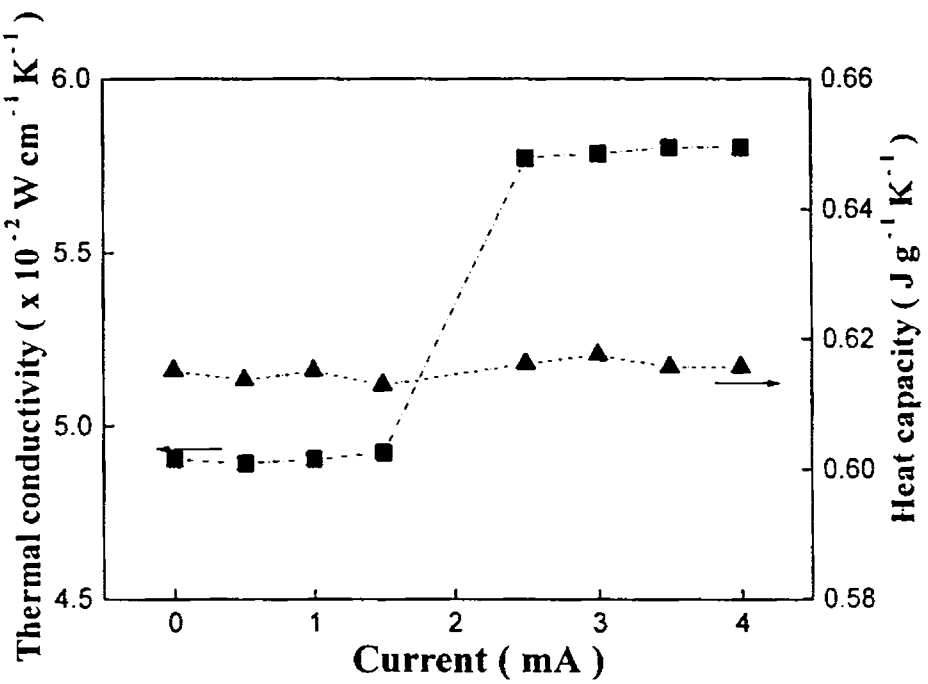

Fig. 6.6 Variation of thermal diffusivity and thermal effusivity for $In_{25}Te_{75}$ glasses. Threshold voltage is 97 V cm^{-1}.

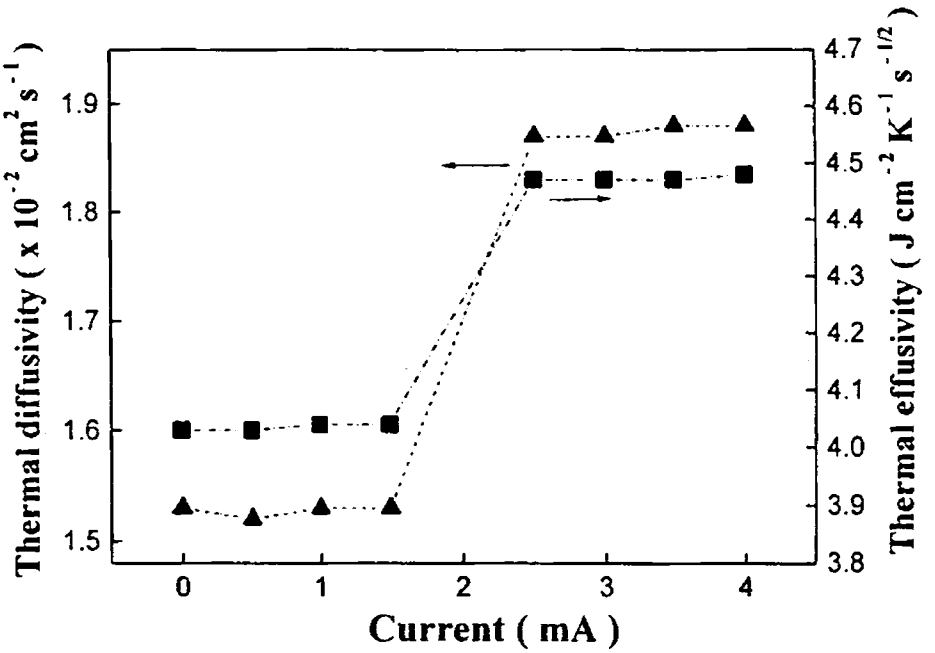

Fig. 6.7 Variation of thermal diffusivity and thermal effusivity for $In_{30}Te_{70}$ glasses. Threshold voltage is 120 V cm^{-1}.

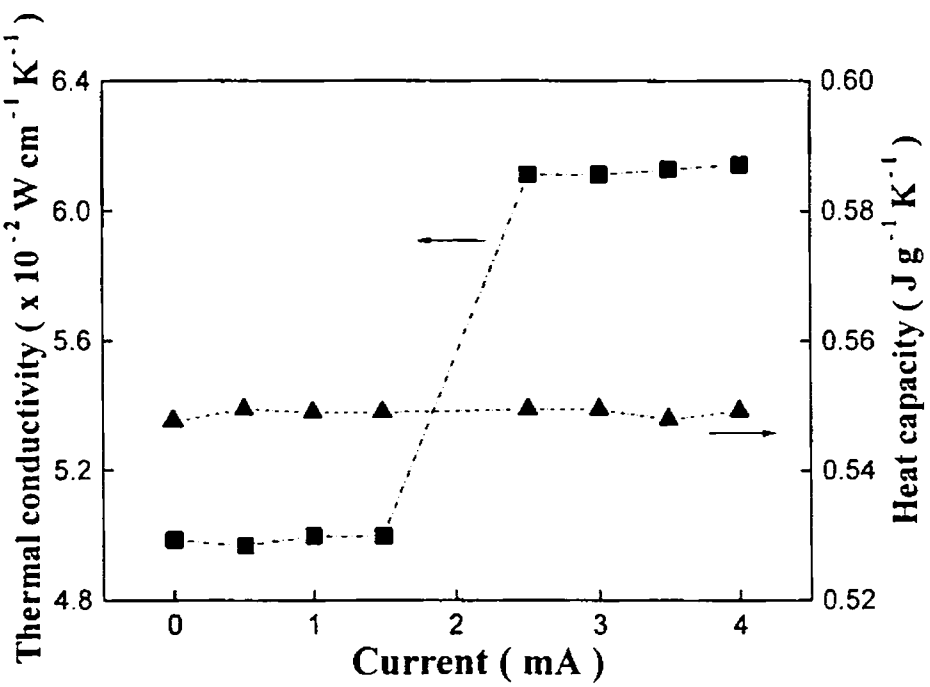

Fig. 6.8 Variation of thermal conductivity and heat capacity for $In_{30}Te_{750}$ glasses. Threshold voltage is 120 V cm^{-1}.

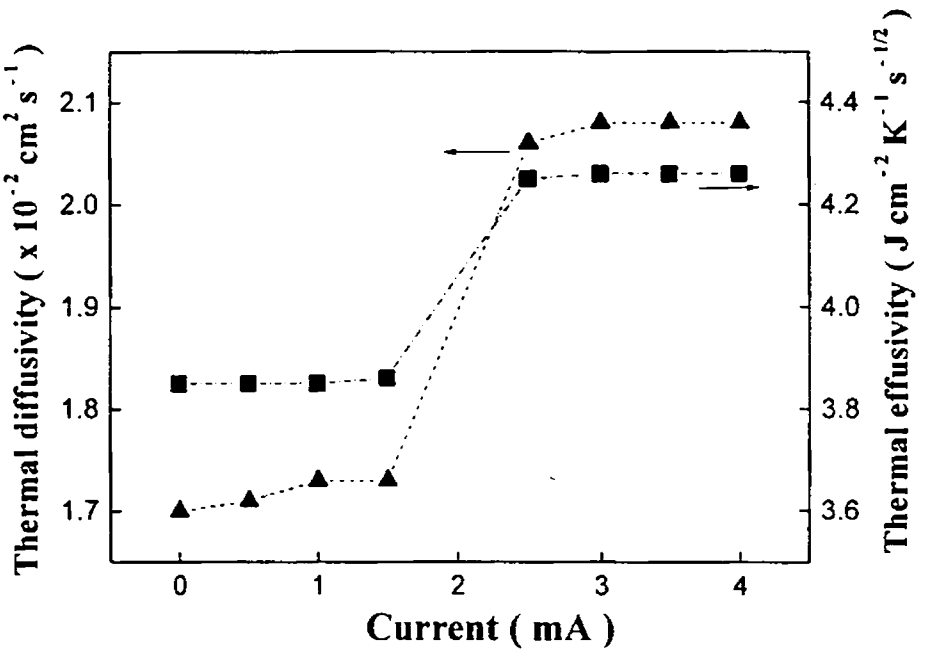

Fig. 6.9 Variation of thermal diffusivity and thermal effusivity for $In_{35}Te_{65}$ glasses. Threshold voltage is 130 V cm^{-1}.

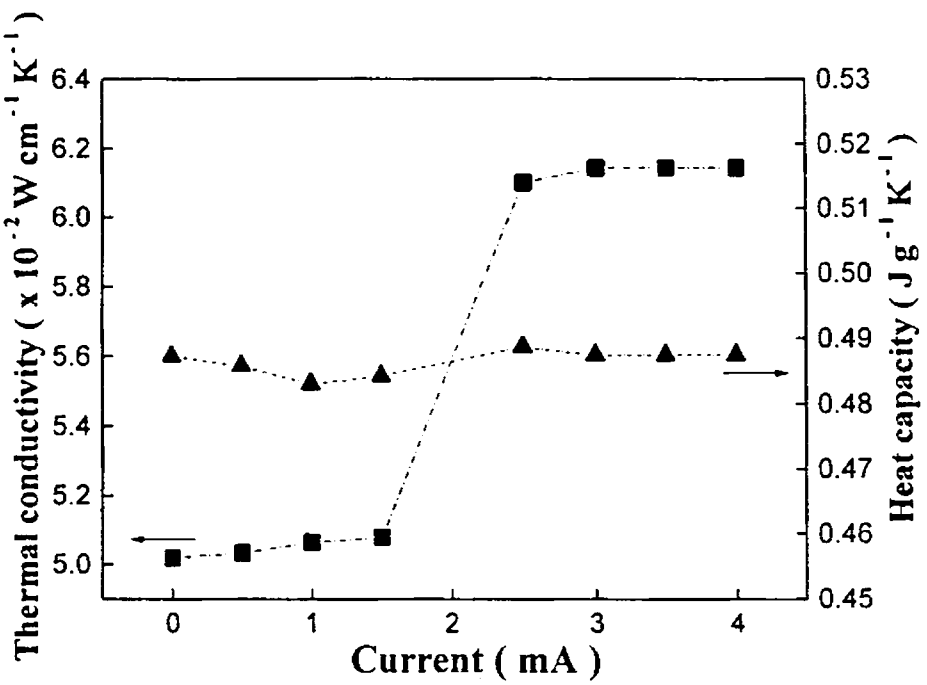

Fig. 6.10 Variation of thermal diffusivity and thermal effusivity for $In_{35}Te_{65}$ glasses. Threshold voltage is 130 V cm^{-1}.

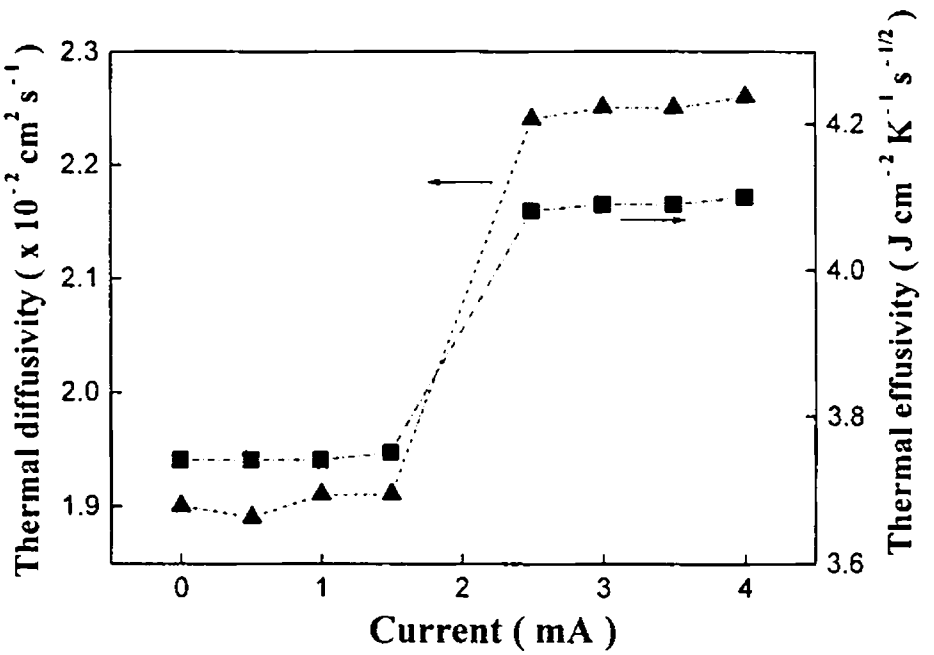

Fig. 6.11 Variation of thermal diffusivity and thermal effusivity for $In_{40}Te_{60}$ glasses. Threshold voltage is 145 V cm^{-1}.

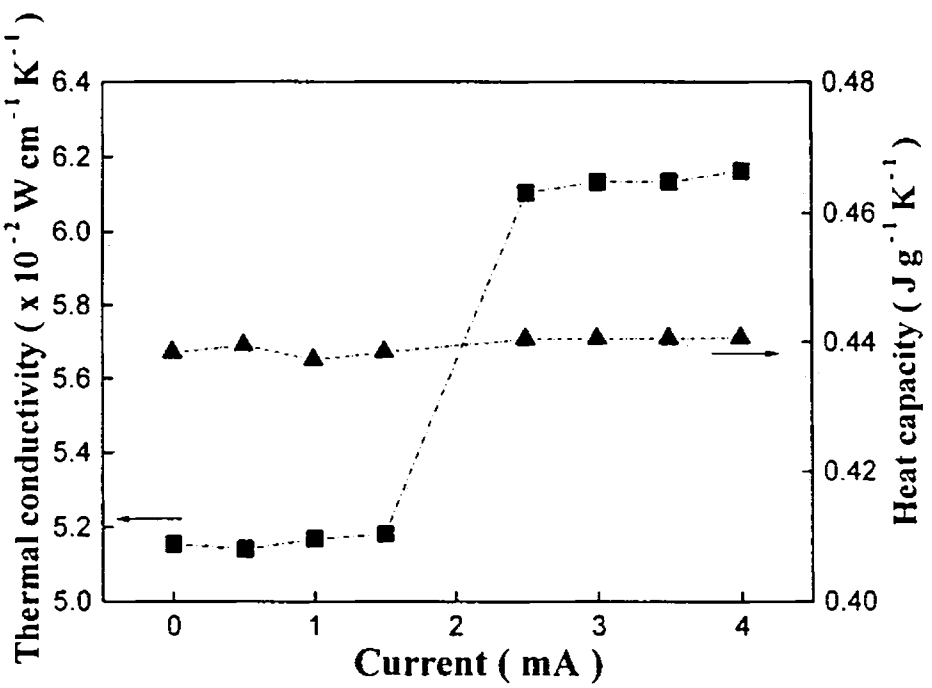

Fig. 6.12 Variation of thermal diffusivity and thermal effusivity for $In_{40}Te_{60}$ glasses. Threshold voltage is 145 V cm^{-1}.

The increase in thermal conductivity can be interpreted as due to the formation of these crystalline conducting channels. Along these channels one can expect a larger concentration of charge carriers leading to a higher electronic contribution to thermal conductivity. Or, one can state that the phonon mean free path in the channel regions increase leading to a corresponding enhancement in thermal conductivity. One cannot expect this effect to get reflected in heat capacity values. A more detailed quantitative description of the observed effects requires more experimental data.

6.4 Conclusions

Thermal parameters of In_xTe_{100-x} ($20 \leq x \leq 40$) system of glasses, which exhibit the phenomenon of electrical switching, have been determined using photopyroelectric technique. Variations of α, e and K during switching have also been studied. It is found that these parameters show increase during switching whereas the heat capacity does not show any significant variation during switching.

References

1. S. R. Ovshinsky, Phys. Rev. Lett. **21** (1968) 1450
2. D. Adler, *Amorphous Semiconductors* (CRC, Butterworths, London, 1971)
3. R. Landauer and J. W. F. Woo, *Comments on Solid State Phys.* **4** (1972) 139
4. S. R. Ovshinsky and H. Fritzsche, Met. Trans. **2** (1971) 641
5. A. E. Owen and J. M. Robertson, *IEEE Trans. on Electron Devices* **20** (1973) 105
6. D. Adler and S. C. Moss, J. Vac. Sci. Technol. **9** (1972) 1182
7. D. Adler, H. K. Henisch and N. F. Mott, Rev. Mod. Phys. **50** (1978) 209
8. K. Nakashima and K. C. Rao, J. Non-Cryst. Solids **33** (1979) 189
9. A. G. Stevenson, J. Non-Cryst. Solids **21** (1976) 319
10. S. R. Ovshinsky and K. Sapru, *Proc. of the Seventh Int. Conf. on Amorphous and Liquid Semiconductors*, edited by W. E. Spear (Institute of Physics, Bristol, 1977) 447
11. E. Babenskas *et al.*, J. Non-Cryst. Solids **90** (1987) 601
12. S. Balyavichyus, A. Deksins, A. Poshkus and N. Shiktorov, Fiz. Tekh. Poluprovodn.**18** (1984) 1513; [Sov. Phys. Semocond. **18** (1984) 947]
13. S. S. K. Titus, R. Chatterjee, S. Asokan, and A. Kumar, Phys. Rev. B. **48** (1993) 14650
14. S. Prakash, S. Asokan and D. B. Ghare, Semicond. Sci. Technol. **9** (1994) 1484
15. R. Chatterjee, S. Asokan and S. S. K. Titus, J. Phys. D. **27** (1994) 2624
16. K. Tanaka *et al*, J. Non-Cryst. Solids **12** (1973) 100
17. G. Mathew and J. Philip, Indian J. of Pure and Appl. Phys. **36** (1998) 463

18. S. Murugavel and S. Asokan, Phys. Rev. B. **58** (1998) 3023

19. H. Fritzsche, *Amorphous and Liquid Semiconductors*, edited by J. Tauc (Plenum, London, 1974) 313

20. D. Adler, Sci. Amer. **236** (1976) 36

21. N.F. Mott and E.A. Davis, *Electronic Processes in Non-crystalline Materials*, (Clarendon, Oxford, 1979)

22. R. L. Hargraves, P. R. Mason and J. C. Anderson, J. Phys. D: Appl. Phys. **7** (1974) 85

23. R. T. Sanderson, *Chemical Bonds and Bond Energy*, Vol. **21** (Academic Press, NewYork, 1971)

24. J. C. Philips, J. Non-Cryst Solids **43** (1981) 37

25. A. Feltz, M. Phole, H. Steil and G.Hesms, J. Non-Cryst. Solids **69** (1984) 271

CHAPTER 7

Thermal properties across thresholds in Ge-As-Se glasses

7.1 Introduction

Systematic studies on the variation of various mechanical, optical, chemical, thermal and elastic properties [1-7] of chalcogenide glasses with average coordination number have gained considerable interest among solid state physicists, in view of their many potential applications in solid state devices. According to Phillips' constraints theory [8], the optimum condition for glass formation is,

$$N_c = N_d \tag{7.1}$$

where N_c and N_d are the constraints and the degrees of freedom per atom respectively. The constraints are in the sense of Lagrangian mechanics [9] and are due to the directional covalent bonds. As already stated in Chapter 1 of the thesis, the total number of constraints on an atom is,

$$N_c = \frac{Z}{2} + (2Z-3) \tag{7.2}$$

for covalent glasses. For 3-dimensional network, $N_d = 3$ and we get,

$$3 = \left(\frac{Z}{2}\right) + (2Z - 3) \tag{7.3}$$

or $Z = 2.4$. This is a surprising result because it is not material specific and there are no adjustable parameters involved in the calculation [8].

Later, Tanaka extended Phillips' ideas to 2-dimensional glass structures [10, 11]. Assuming a hypothetical material having a plane lattice laid in 3-D space, the constraints balancing equations for the layer material gets modified as,

$$3 = \left(\frac{Z}{2}\right) + (Z - 1) \tag{7.4}$$

This expression gives a value Z = 2.67, i.e., the average coordination number of glasses having a stable layer structure is 2.67.

Transition from an under constrained to an over constrained network has been interpreted by Thorpe [12, 13] in terms of percolation of rigidity in an inhomogeneous medium containing both rigid and floppy regions. Anomalous features in many physical properties have been reported around Z = 2.4 and Z = 2.67 as well as the chemical threshold in several systems.

The ternary glass system Ge-As-Se has got one of the largest glass forming regions among chalcogenide glasses. Therefore, it is particularly well suited to test the validity of the above concepts. Germanium, arsenic and selenium are elements of groups IV, V, and VI respectively of the same period. This brings about the covalent character of the interaction between their atoms and results in a broad glass-forming region. In the three component Ge-As-Se system, selenium will react with germanium and produce structural units of $GeSe_{4/2}$. When germanium is introduced into arsenic selenides, gradual composition changes takes place in the system forming $GeSe_{4/2}$ and $AsSe_{3/2}$ structural units. Also, formation of complex structural units like $As_2Ge_{4/2}Se_{4/2}$ occurs. Approximate thermo chemical calculations indicate that in the three component Ge-As-Se system, there can be several sections with

different contents of structural units, and consequently, with different physical and chemical properties. There can be sections in which the structure is determined mainly by bonds of the selenium type [14].

The composition dependence of many physical properties of Ge-As-Se system of glasses show anomalous variations at Z = 2.4 and Z = 2.67. Elastic constants of Ge-As-Se glasses show a threshold behaviour at Z = 2.4 [15], but the data do not match with a previous report [16]. A study of the Z dependence of ΔC_p measured at T_g shows a minimum at 2.4. But the persistent infrared spectral hole burning studies of the effect of network topology on low temperature relaxation in Ge-As-Se system of glasses do not show any indication of a rigidity transition or any other unusual features at Z = 2.4 [17]. On the other hand, the composition dependence of optical band gap and thermal diffusivity show threshold maxima at Z = 2.67 [18].

In this chapter, we report the variation of thermal parameters, viz., thermal diffusivity, thermal effusivity, thermal conductivity and heat capacity as a function of the average coordination number Z for $Ge_xAs_{25}Se_{75-x}$ system of glasses. The photopyroelectric technique described in Chapter 2 has been used for the determination of the above thermal parameters. The compositions have been chosen to produce an average atomic coordination Z ranging from 2.30 to 2.80. Average coordination number Z of a ternary glass of the form $A_xB_yC_{100-x-y}$ is given by

$$Z = [x N_A + y N_B + (100-x-y) N_C]/100 \qquad (7.5)$$

where, N_A, N_B and N_C are the coordination numbers of the elements A, B and C respectively and x and y are the atomic weight percentages of the elements A and B respectively in the network glass.

7.2 Sample preparation and experimental details

Glass samples with the general formula, $Ge_xAs_{25}Se_{75-x}$ ($2.5 \leq x \leq 27.5$) have been prepared by the melt quenching technique. Appropriate quantities of high purity constituents are taken in quartz ampoules, which are evacuated and sealed. The ampoules are kept in an electrical furnace and slowly heated to 1000^0 C. They are kept at 1000^0 C for nearly 24 hours with intermittent rotation of the ampoules for homogeneous mixing of the constituents. Then the ampoules are quenched in ice water to obtain the glassy samples. The amorphous natures of the samples are confirmed by X-ray diffraction technique.

Thermal parameters of the samples have been determined using the photopyroelectric (PPE) technique described in earlier chapters. Samples of thickness ≈ 0.5 mm have been used for the measurements. A He-Cd laser (λ = 442 nm) has been used as the source of radiation and a PVDF film of thickness 28 μm, both sides coated with Ni-Cr as the detector. Light modulation is achieved using a mechanical chopper (Model SR540). PPE signal is measured using a dual phase lock-in amplifier (Model SR830).

7.3 Results and discussion

Thermal thicknesses of the samples are confirmed by plotting the PPE signal amplitude and phase as a function of modulation frequency. These plots are shown in Figs. 7.1 and 7.2.

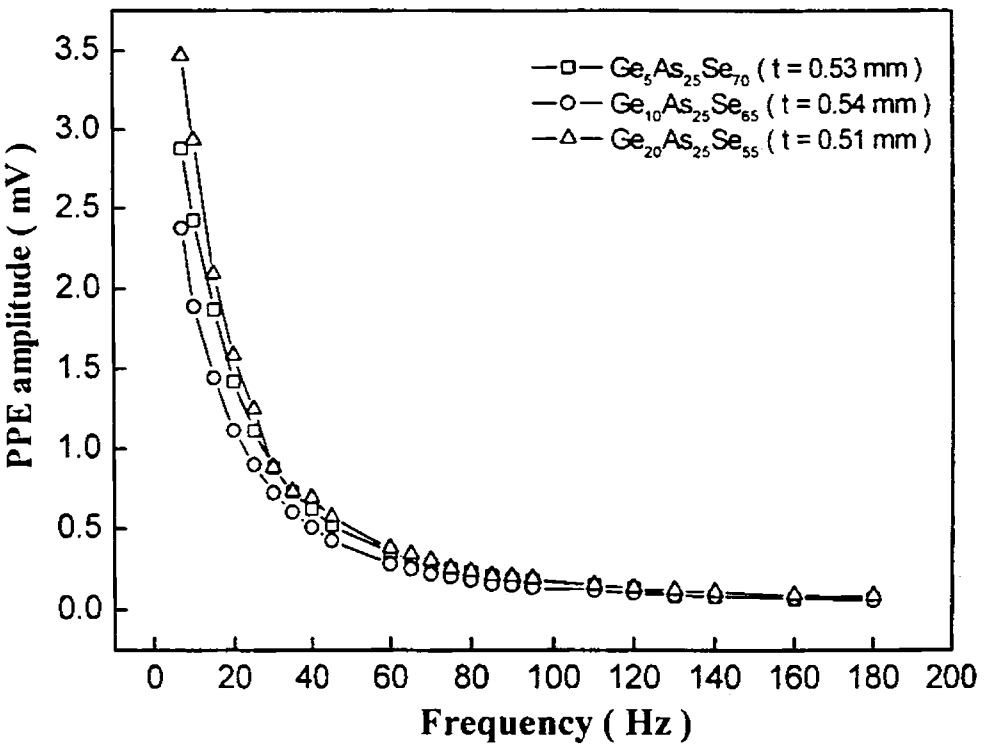

Fig. 7.1 Frequency dependence of PPE amplitude for different compositions of $Ge_xAs_{25}Se_{75-x}$ glasses

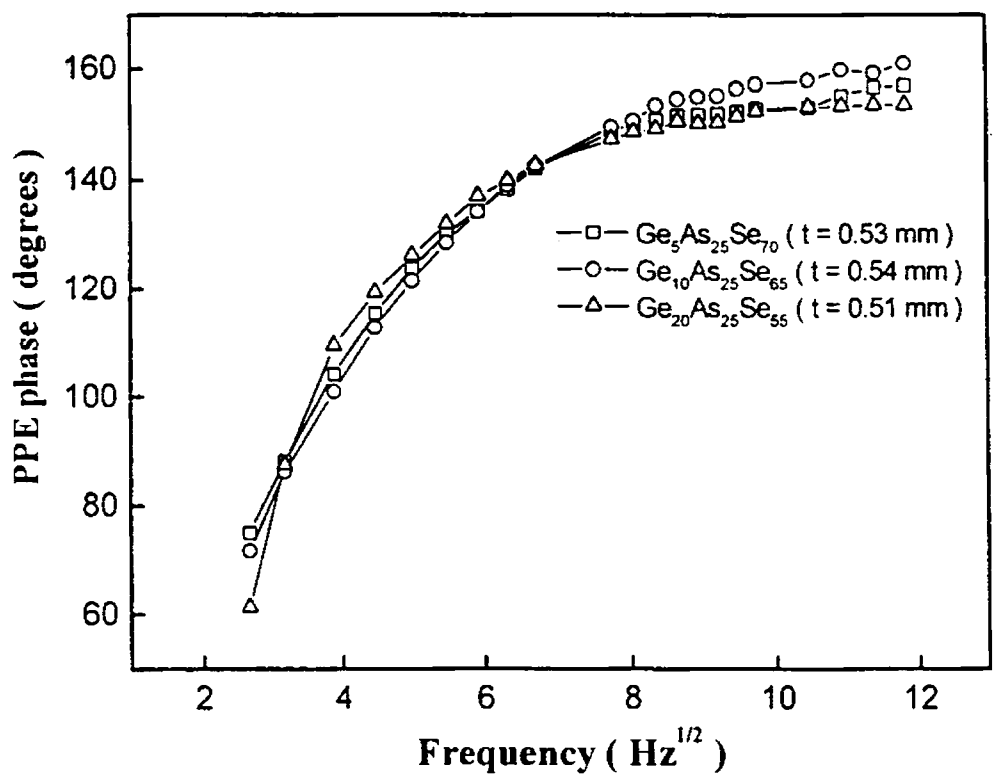

Fig. 7.2 Frequency dependence of PPE phase for different compositions of $Ge_xAs_{25}Se_{75-x}$ glasses

Thermal diffusivity (α) of the samples is determined from the corresponding PPE signal phases and thermal effusivity (e) from PPE signal amplitudes. The variations of α and e with average coordination number Z are shown in Fig. 7.3.

Sample mass densities have been determined using the Archimedean principle with liquid paraffin used as the densiometric fluid. Fig. 7.4 shows the Z dependence of density. Thermal conductivity (K) and heat capacity (c_p) of the samples can be determined using the relations,

$$K = e\sqrt{\alpha} \tag{7.6}$$

$$c_p = \frac{e}{\rho\sqrt{\alpha}} \tag{7.7}$$

Variations of K and c_p with Z are shown in Fig. 7.5.

From the composition dependence studies, it is seen that thermal diffusivity and thermal effusivity show maxima around Z = 2.67. Thermal conductivity also shows a maximum at Z = 2.67, while heat capacity shows a minimum around Z = 2.4.

The occurrence of threshold maxima in α and K values round Z = 2.67 can be explained in terms of the change in network topology and dimensionality. In Se-rich glasses of the Ge-As-Se system, the two-fold coordinated Se will form flexible chains of Se in the glass network. The addition of four-fold coordinated germanium results in branching and cross-linking of these chains. These configurational changes result in the formation of a two-dimensional structure, which is stabilized by the medium range intermolecular interactions. Thus, as the Ge concentration increases, value of Z increases and cross-linking of the Se atom chains occurs. As a result, the

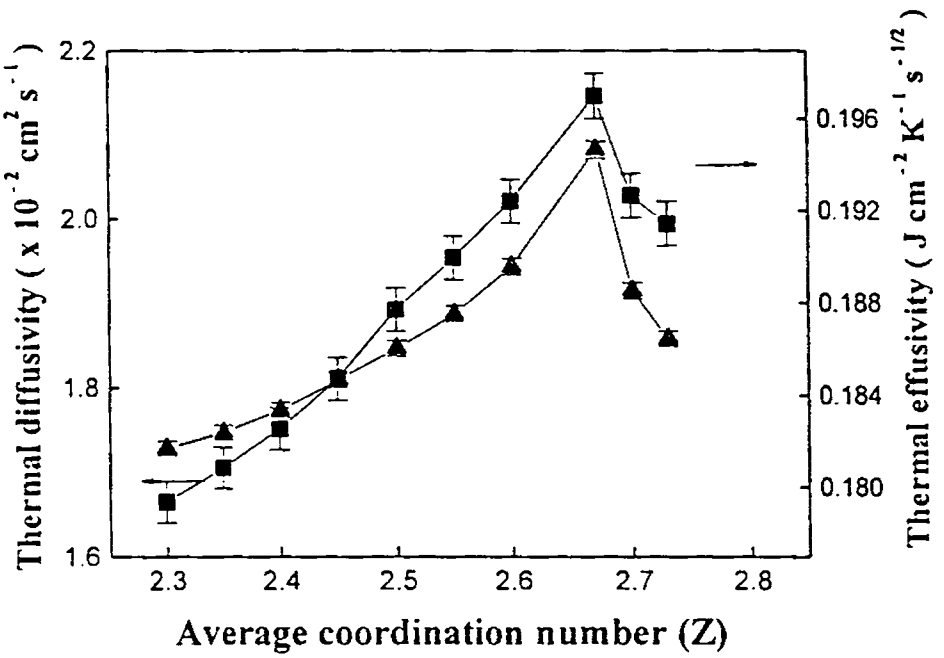

Fig. 7.3 Variation of thermal diffusivity and thermal effusivity of $Ge_xAs_{25}Se_{75-x}$ glasses with average coordination number

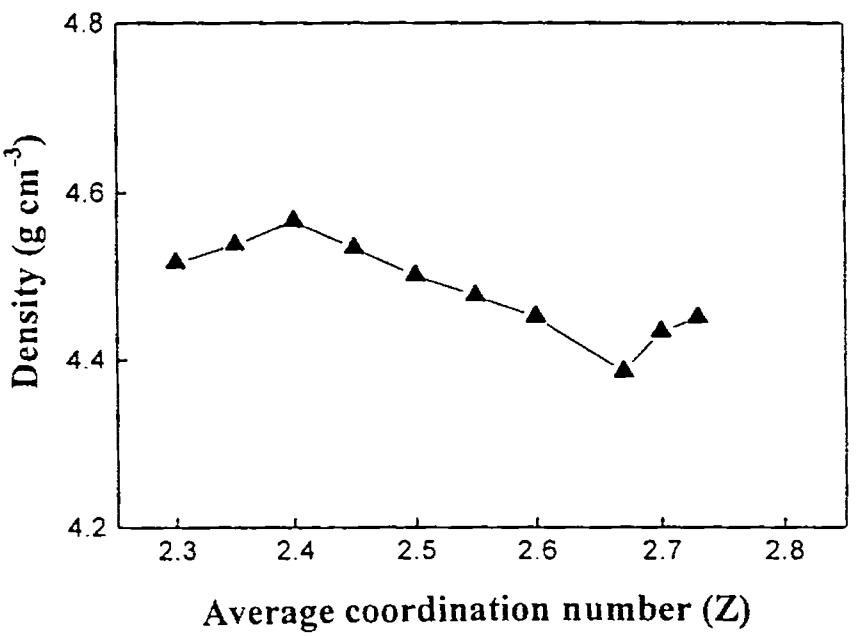

Fig. 7.4 Variation of density with average coordination number for $Ge_xAs_{25}Se_{75-x}$ glasses

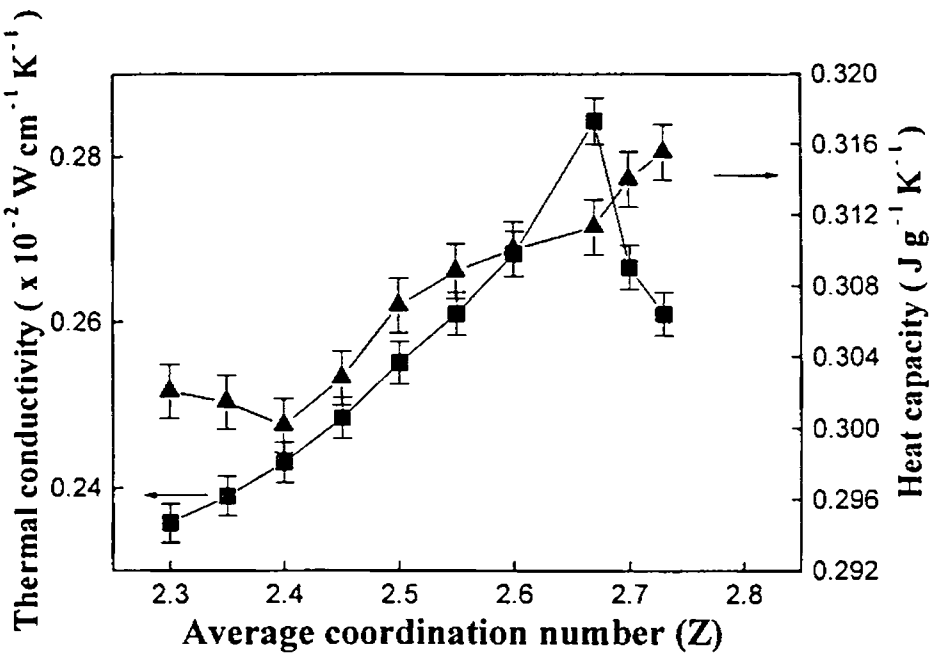

Fig. 7.5 Variation of thermal conductivity and heat capacity of $Ge_xAs_{25}Se_{75-x}$ glasses with average coordination number

flexibility of the network glass gets reduced. This results in an increase in the value of α. At Z = 2.67, the medium range order fully gets developed and a layered structure is formed. This results in a maximum value for α. At this composition, the system goes over to a rigid 3-D structure and the system will be rigid beyond this composition.

In these glassy materials, thermal conductivity depends crucially on the phonon mean free path in the system. The threshold maximum of K around Z = 2.67 can be explained on the basis of the development of a more ordered and rigid structure at this composition. The slight decrease in the value of K beyond this composition may be due to the large number of defect present in the three-dimensional structure.

7.4 Conclusions

Thermal parameters of the $Ge_xAs_{25}Se_{75-x}$ (x = 2.5-27.5) system of glasses have been measured using the photopyroelectric technique. From the average coordination number dependence studies, it is seen that anomalous variations occur at threshold compositions. The results are explained on the basis of the various structural models for chalcogenide glasses. The observed maxima in the values of α and K around Z = 2.67 indicate that medium range interactions have an important role in determining the network topology in these glasses.

References

1. D. R. Swiler, A. K. Varshneya and R. M. Callahan, J. Non-Cryst. Solids **125** (1990) 250
2. S. Mahadevan and A. Giridhar, J. Non-Cryst. Solids **110** (1989) 118
3. K. N. Madhusoodanan and J. Philip, Phys. Status. Solidi (b) **108** (1988) 77
4. A. N. Sreeram, D. R. Swiler and A. K. Varshneya, J. Non-Cryst. Solids **127** (1991) 287
5. S. Mahadevan and A. Giridhar, J. Non-Cryst. Solids **143** (1992) 52
6. A. Srinivasan, K. Ramesh, K. N. Madhusoodanan and E. S. R. Gopal, Philos. Mag. Lett. **65** (1992) 249
7. S. Mahadevan, A. Giridhar and A. K. Singh, J. Non-Cryst. Solids **169** (1994) 133
8. J. C. Phillips, J. Non-Cryst. Solids **34** (1979) 153
9. J. C. Phillips, Phys. Status. Solidi (b) **101** (1980) 473
10. K. Tanaka, J. Non-Cryst. Solids **103** (1988) 149
11. K. Tanaka, Phys. Rev. B **39** (1989) 1270
12. M. F. Thorpe, J. Non-Cryst. Solids **57** (1983) 355
13. J. C. Phillips and M. F. Thorpe, Solid State Commun. **53** (1985) 699
14. U. Borisova, *Glassy Semiconductors*, (Plennum Press, New York, 1981)
15. B. L. Halfpap and S. M. Lindsay, Phys. Rev. Lett. **57** (1986) 847
16. U. Tillie, G. H. Frishat and K. J. Leers, *4th International Conference on Physics of Non-Crystalline Solids*, Clausthal, Germany (Aedermansdorf, Switzerland and Trans. Tech. S. A., 1977) p.631

17. S. P. Love, A. J. Sievers, B. L. Halfpap and S. M. Lindsay, Phys. Rev. Lett. **65** (1990) 1792

18. K. Nandakumar and J. Philip, Indian J. Phys. **69A** (1995) 595

CHAPTER 8

Summary and conclusions

The phenomena of carrier type reversal (CTR) and electrical switching exhibited by chalcogenide glasses have attracted a great deal of scientific attention. Most of the work presented in this thesis deal with amorphous chalcogenides exhibiting these phenomena.

Bulk chalcogenide glasses, prepared by the melt quenching technique, are in general *p*-type semiconductors and their conductivity cannot be made *n*-type by the addition of impurities as in the case of their crystalline counterparts. This has been attributed to the presence of a pinned Fermi level near the middle of the gap. But, of late, it has been found that, when certain heavy elemental metallic impurities like Bi or Pb is added to certain chalcogenide glass systems, they exhibit a change in the conduction type from *p* to *n* at certain specific compositions.

In this thesis, we report the results of our measurements on $Pb_{20}Ge_xSe_{80-x}$ ($17 \le x \le 24$), $Pb_yGe_{42-y}Se_{58}$ ($0 \le y \le 20$), $Bi_xGe_{20}Se_{80-x}$ ($2 \le x \le 12$) and $Pb_xIn_{25-x}Se_{75}$ ($2 \le x \le 15$) systems of glasses, which exhibit the phenomenon of carrier type reversal. Bulk glasses were prepared by the conventional melt quenching technique. We have measured the thermal parameters of the samples as a function of composition and have found that anomalous variations occur at the critical compositions corresponding to CTR. A modified photopyroelectric (PPE) technique has been employed to determine the thermal parameters viz., thermal diffusivity (α),

thermal effusivity (e), thermal conductivity (K) and heat capacity (c_p) simultaneously. A photoacoustic (PA) phase lag technique has been used to determine α independently. The variations in thermal parameters have been explained on the basis of the enhancement in carrier concentration during carrier type reversal. Optical band gaps of the samples have been determined using a UV-Vis-NIR spectrophotometer.

Photoconductivity measurements have also been carried out on Pb-Ge-Se and Pb-In-Se systems of glasses. Composition dependences of photoconductivity and photodetectivity have been studied. It is found that CTR gets clearly reflected in these properties. Results are analyzed on the basis of existing photoconductivity models for chalcogenide glasses.

We have also studied the variations of thermal parameters during electrical switching in In_xTe_{100-x} ($20 \leq x \leq 40$) glasses. It is found that thermal conductivity shows an increase during electrical switching. It is believed that during switching, crystallization of the material occurs. The increase in thermal conductivity may be due to an increase in phonon mean free path due to crystallization.

The effect of various topological thresholds on the thermal properties of the typical ternary glass system Ge-As-Se has been investigated. We have chosen $Ge_xAs_{25}Se_{75-x}$ ($2.5 \leq x \leq 27.5$) so that the average coordination Z varies from 2.30 to 2.80. It is found that thermal conductivity shows a maximum around $Z = 2.67$. The results are explained on the basis of the Tanaka model.

The phenomenon of carrier type reversal in chalcogenide glasses has not yet fully understood. Various models have been proposed by authors to explain various experimental results obtained. More experiments have to be carried out for a better

understanding of this phenomenon. Neutron scattering and photoelectron spectroscopy experiments in glass systems exhibiting CTR can provide valuable information about the variations in bonding structure with composition. There is plenty of scope for doing further work in these areas, as several questions still remain unanswered.